POLITECNICO DI TORINO

Master of Science in Electronics Engineering

Master Thesis

Study of power dissipation in MolFCN neural structures

Supervisors
Prof. Mariagrazia Graziano
Prof. Gianluca Piccinini
Dr. Yuri Ardesi, Dr. Federico Ravera, Dr. Roberto Listo

Candidate
Elena Ferrero

December 2024

Abstract

Since 1960s, Moore's law describes the technological evolution of electronic devices through an exponential growth in computing performance. To perform increasingly complex operations, a higher energy consumption is needed, demanding energetic resources and compromising the device's performance. Moore's law is becoming difficult to be respected, thus approaching its end. New technologies must be investigated based on different principles with respect to silicon-based ones; such technologies are named beyond-CMOS.
Molecular Field-Coupled Nanocompunting (MolFCN) stands out as a promising Beyond CMOS technology thanks to its high device density and promising high-frequency operation at room temperature. MolFCN encodes binary information through charge localization in aggregation regions of molecules. The application of external electric fields, applied through the so-called molecule hosting structures, allows forcing specific charge configurations encoding (input field) or deleting (clock field) information. This currentless working principle promises low-power dissipation that must be explored to assess technology potentialities. Indeed, the current literature does not present definitive studies on MolFCN power characterization. To address such research gap, this thesis explores the potentiality of the technology, taking as a case-study a neural application.

Initially, the work focuses on realizing molecule-hosting structures. By using Synopsys Sentaurus framework, a wire has been initially explored by creating a structure that is able to host a sequence of molecules: it is a dielectric trench structure characterized by two upper electrodes and a bottom one. The project then proceeds by investigating more complex architectures, exploring the realization of angles, T connections and, finally, the majority voter, core of the technology for logic operations and for neural implementations.
Such technological structures are then verified through Sentaurus Device by means of a finite element method simulation, permitting the analysis of the electric fields with different voltage combinations applied to the electrodes. The simulations confirm theoretical predictions by showing clock fields reducing towards the center of the structure. The obtained results demonstrate that the top electrodes create overlap between the electric fields, which should be taken into account in the design of MolFCN.
Therefore, this work results in the optimization of structure geometries, bringing to an improvement of the layouts efficiency in providing correct application of the input and clock electric fields.
The thesis proceeds by verifying the correct functioning of the optimized structures by analyzing the interactions between the molecules placed in the trench. This is achieved

through the Self Consistent ElectRostatic Potential Algorithm (SCERPA), a tool capable of studying the behavior of molecular charges in an iterative manner. In this way, it is possible to fine-tune the voltages applied to the electrodes in order to achieve the correct propagation of logical information. Finally, the provided electric fields and the electrode potentials are used to evaluate the power dissipation associated with the functioning of molecule-hosting structures. In particular, the thesis considers the neural cell as a case-study device and evaluates its power consumption. It demonstrates, for the first time, the possibility of tying SCERPA to a well-established simulation toolchain like the Sentaurus one.

Acknowledgements

I would like to thank Professor Graziano and Professor Piccinini for the opportunity they have given me to pursue this thesis.

I would also like to sincerely express my gratitude to Yuri Ardesi, Roberto Listo, Fabrizio Mo and Federico Ravera. Under your guidance, I feel I have grown not only professionally but also on a personal level.

I would also like to thank my family, the safe haven of my existence: your support and constant presence are the greatest gifts life has given me. And finally, thank you Giuseppe: with you, every mountain seems reachable.

Contents

List of Tables

List of Figures

Chapter 1

Introduction

Since the 1960s, technological evolution has been characterized by an exponential increase in the computing performance of electronic devices. This trend was empirically predicted by Gordon Moore, who, in 1965, observed that the number of transistors in a chip doubled every two years [2]; in 1975 Moore's law was refined, reducing the doubling period to 1.8 years and giving precise reasons for this trend. Indeed, the growth in integration complexity can be justified by the increase in the size of the silicon die, the increased capabilities of the chips and the reduction in their size [2]. The continuous shrinking in transistor size is made possible by constant advances in manufacturing techniques, which have allowed the size of transistors to decrease from 3 µm in 1980 to 32 nm in 2009 [3]. Furthermore, reducing the size of transistors not only allowed more components to fit into an integrated circuit, thereby increasing its density, but also made transistors less energy-consuming, cheaper and characterized by higher frequencies [4], [5].
The reasons for the described phenomena are interconnected. The shrinking of MOSFETs allows for shorter interconnections, which make the devices faster. Furthermore, devices require less power supply, which leads to lower dynamic power consumption. As an addition, the increased device density allows for larger batches to be produced, lowering the cost of individual devices.

In this way, the last fifty years of electronics history have been characterized by an exponential trend, a sort of self-fulfilling prophecy that has only begun to crack in recent years. The extreme scaling undergone by MOSFETs has resulted in the emergence of non-negligible side effects, caused by the longitudinal electric fields in the pinch-off region and the transverse electric field across the gate oxide.
One example is the roll-off phenomenon, which occurs when the channel length approaches the size of depletion regions. This effect results in a significant dependency between threshold voltage and channel length, with important implications for the operation of devices operating at low voltages, where even small variations can compromise performance [6]. Another side issue that has to be taken into account in extremely small devices is the phenomenon of Drain Induced Barrier Lowering (DIBL): the proximity of the depletion regions causes the energy bands of the device to bend, thereby reducing the voltage required to activate the transistor. The reductions in the threshold voltage have

the important consequence of causing the leakage current to vary exponentially, affecting power dissipation and the correct operation of the MOSFET [7].
An additional aspect to be taken into account, as far as the dissipated power is concerned, is a consequence of the trade-off between the number of transistors per chip and the frequency of operation. Constantly increasing both parameters would lead to the creation of circuits too much energy consuming: the heat dissipated would be so intense that significant cooling systems would be required to avoid compromising the life of the devices themselves. Therefore, empirical data show that a plateau in the frequency trend occurred between 2003 and 2005: in order to be able to increase the number of transistors on a chip, it was decided not to further improve the frequency, keeping it at a constant value [8].

Overcoming these problems and creating such minute devices requires the use of increasingly expensive technologies.

The development of photolithography is a key example to understand the technological evolution required to continue to miniaturize MOSFETs and, above all, the economic demands involved. In the 1960s, optical photolithography was sufficient to create ever-smaller transistors but, as the size decreased, techniques had to be introduced to increase and improve resolution; among them, Optical Proximity Correction (OPC) and Phase Shift Masks (PSM) are of particular interest.
In the case of the Optical Proximity Correction technique, masks are designed in such a way as to compensate for unwanted optical effects: the blurry edges present in a traditional mask are thus canceled out thanks to patterns that take into account destructive and constructive interference between the optical waves. On the other hand, Phase Shifts Masks are characterized by variations in the mask thickness, allowing for a modulation of the phase of the wave passing through it: the constructive and destructive interference phenomena can thus be calibrated, obtaining a higher resolution than the one that would be obtained with a mask without enhancements. Despite the adoption of advanced techniques such as OPC and PSM, the progressive reduction of technological nodes has rendered optical photolithography a process that cannot keep up with the evolution foreseen by Moore's law. This has led to the development of new technologies, such as X-ray lithography or electron beam photolithography, that does not require the use of masks. These newer technologies have allowed for a reduction in the features of the devices created at the expense of higher production costs and increased creation requirements, such as a high vacuum condition that was not previously necessary.

Having mentioned these problems, it is possible to observe how continuously scaling MOSFETs would not be sustainable due to excessive leakages and manufacturing complications. This contextualization regarding technological evolution, dictated by performance and economic constraints, is fundamental to understand the development of devices in the coming years. In this respect, the International Roadmap for Devices and Systems (IRDS) helps the researchers to define key trends, providing estimates and forecasts on technological evolution and outlining a panorama for the coming fifteen years.

Analyzing the reports of the last few years, it was possible to appreciate the replacement of MOSFETs by devices that guaranteed better performance and continued to present ever smaller (more and more technologically challenging) dimensions: FinFETs and their evolution, GAAFETs, represented the future of silicon-based devices. These are three-dimensional structures in which the channel is a few nanometers thick fin that connects source and drain and that is built on an insulator substrate. This fin is wrapped around the gate: in this way, inversion zones are created on both sides of the channel and the electrostatic control exerted will be greater with respect to the one in planar devices. Thanks to this structure, channel lengths can be further reduced and Moore's law can continue to be fulfilled.
One consequence of the multi-gate is the increased mobility of the carriers: firstly, the absence of strong transverse electric fields, which in MOSFETs generated numerous scattering events, significantly reduces collisions between the free charges and the material structure. Secondly, the channels of FinFETs do not require as much doping as in planar FETs: this minimizes interference with impurity ions, contributing to higher carrier mobility and, consequently, to better device performance [9].
A further consequence of the structure is that the double (or triple, depending on the structure) gate strongly influences the channel potential, for example by reducing the influence of the drain and thus decreasing the effect of DIBL [10].
However, as short channel effects decrease, IRDS reports power dissipation issues that are difficult to resolve. Reducing the supply voltage, for ultra-low power applications, would decrease the dissipated power but is more and more difficult due to the subthreshold slope. FinFET devices, compared to planar technology, do not offer a substantial improvement on this front and further reductions in supply voltage would result in such a small potential difference between on and off state that even the slightest disturbances could cause malfunctions.
Furthermore, structures such as GAAFETs, in which the channel is wrapped with a gate on each side, present some difficulties regarding thermal dissipation and the increase in devices per chip creates constraints on the power consumption that can be tolerated. It must also be considered that power scaling is limited by the increase in parasitic components, which are particularly relevant in FinFETs. The configuration of these devices is such that parasitic capacitances arise between fin and source/drain zones and between fin and the epitaxial silicon layer. Parasitic resistances, which can be broken down into channel, contact and extensions region resistances, represent an important limitation on the performance of FinFETs: their unavoidable existence leads to increased delays that significantly slow down the devices. The impact of parasitic components also manifests itself in saturation current values: according to the IRDS, series resistances degrade it by 40% or more [11]. One could decrease parasitic resistance by increasing the width of the fin but this would increase the occupied area and it would be counterproductive. So, the demand for lower resistance with smaller dimensions poses a great challenge to manufacturers.

It is therefore crucial to understand how performance can be increased while keeping power consumption under control.

In the view of the above, it is interesting to think of a new technological paradigm, capable of overcoming the limitations of silicon-based devices, increasing performance and dissipating less power. The remaining of the introduction will be divided into three sections: in the first, fundamental concepts related to power will be explained, in order to better understand which technological aspects should be focused on. The second section will examine a new technological paradigm that promises to increase performance while remaining energy efficient: Molecular Field Coupled Nanocomputing (MolFCN), a particular implementation of Quantum Cellular Automaton (QCA), will be explained in detail. Finally, in the third part, a possible application of this innovative paradigm will be explored: neural networks, characterized by very high computing capabilities and frequencies, represent a particularly interesting challenge to approach and to investigate.

1.1 Brief analysis of power

The energy consumption of the electronics that permeate our lives is a crucial issue in technological development. The environmental impact of energy production exceeds that of other sectors such as industry: according to the International Energy Agency's 2024 report, CO_2 emissions from the electricity sector are almost twice as high as emissions from the transport sector [12]. Furthermore, according to the latest International Energy Agency report, electricity consumption grew by 2.2% in 2023 and this rate is expected to increase more rapidly over the next three years, growing by an average of 3.4% per year [13]. The electronics sector will also see a significant increase in energy consumption caused by artificial intelligence and data centres. The latter, while consuming 460 TWh in 2022, are estimated to reach 1000 TWh in 2026, the equivalent of Japan's energy consumption. As far as artificial intelligence is concerned, suffice it to say that if Google were to fully implement artificial intelligence, consumption per search would rise from 0.3 Wh to 2.9 Wh, (consider that daily searches are around 9 billion) [13].
In addition to this, it is important to emphasize how global energy production remains predominantly oil-based: in 2023 the consumption of fossil fuels such as oil and coal, as a proportion of total primary energy used, stood at 81.5% [14].
These figures highlight the importance of understanding the concept of power in electronics and, above all, the urgent need to minimize energy consumption. Excessive consumption is not only wasteful from both an energetic resource and an economic point of view, but also implies a decrease in the performance of a device: to avoid overheating the chip, either its frequency is reduced or cooling systems are used, which in turn require energy. To minimize power consumption, it is essential to fully understand the concept of power and its role in determining the efficiency of a system.

The instantaneous power consumed or supplied by a circuit element is the product of the current flowing through it and the voltage that can be measured at its ends (as it can be seen in Eq. 1.1).

$$P_{V_{DD}}(t) = I_{DD} \cdot V_{DD} \tag{1.1}$$

This relationship is closely related to the concept of energy, as can be seen in Eq.1.2.

$$E = \frac{P}{T} \tag{1.2}$$

There are different types of power to be distinguished:

- Active power: this is what is consumed by a chip while it is performing the functions for which it was created and is generally dominated by the power spent switching between different logical states;
- Standby power: refers to the power consumed by a chip when it is in idle state and is dominated by unwanted power consumption due to leakage;
- Sleep power: this refers to the power used by a chip when it is switched off to avoid leakages. Although power consumption in this phase is low, it must be considered that the chip requires time and energy to return to an active state once it is in sleep mode.

Furthermore, dissipated power is divided into two main components, dynamic and static one.
The former is caused, according to Eq. 1.3, by the phenomenon of charging and discharging load capacitances each time a gate switches ($P_{switching}$) and by the short circuit current that is generated when the pMOSFET and nMOSFET stacks are both partially active ($P_{short\ circuit}$).

$$P_{\text{dynamic}} = P_{\text{switching}} + P_{\text{short circuit}} \tag{1.3}$$

The switching power can be calculated as the energy stored in the load capacitor (given by the sum of gate, diffusion and wire capacitances) with respect to a certain time interval T, as seen in Eq. 1.2. Moreover, energy can be expressed as the integral of power with respect to time. Since current can be described as a function of voltage and current, equal to the time derivative of voltage multiplied by the load capacitance, Eq. 1.4 can be proven.

$$E = \int_0^\infty I(t) \cdot V_{DD}\, dt = \int_0^\infty C \cdot \frac{dV}{dt} \cdot V_{DD}\, dt = C \cdot V_{DD} \int_0^{V_{DD}} dV = C \cdot V_{DD}^2 \tag{1.4}$$

Eq. 1.4 shows a quadratic dependency of energy with respect to the power supply: one can therefore understand the reasons for wanting to reduce the supply voltage as much as possible in order to minimise the dynamic power of the device. In addition to these considerations, it must be considered that in the time interval T the gate under analysis will switch with a frequency equal to f_{SW}: the number of times the capacitance will charge and discharge is equal to $T \cdot f_{SW}$. This factor must be taken into account. This results in an expression of switching power equal to Eq. 1.5

$$P_{\text{switching}} = \frac{E}{T} = \frac{T \cdot f_{\text{sw}} \cdot C \cdot V_{DD}^2}{T} = C \cdot V_{DD}^2 \cdot f_{\text{sw}} \tag{1.5}$$

Another important clarification concerns the fact that a gate does not necessarily switch at every clock cycle. A constant (called activity factor α) must be introduced into the equation which expresses the probability that switching occurs: this is a number between 0 and 1 which takes on a unit value when switching actually occurs every clock cycle. The activity factor referring to node i is equal to the probability that the node has a value of 0 in one cycle and a value of 1 in the next cycle. Assuming that the probability between two different cycles is uncorrelated (and assuming that the variation is completely random and with probability 0.5), Eq. 1.6 is obtained.

$$\alpha_i = \bar{P}_i \cdot P_i = \left(1 - \frac{1}{2}\right) \cdot \frac{1}{2} = 0.25 \tag{1.6}$$

However, logic gates assume different switching probabilities depending on the probability that the inputs are equal to 1. For example, a two-input AND gate implemented with complementary logic MOSFET has a probability of 0.5 that input A will have a value of 1, as well for input B. The probability of the output switching to 1 equals the product of the two probabilities and will be 0.25. In the case of a two-input NAND port, the probability will be $1 - P(\text{AND})$. In general, CMOS circuits have an activity factor of about 0.1.

Dynamic power also includes a short-circuit power component. It occurs when a gate is switching and the pull-up network and the pull-down network are, for a very brief moment, both switched on. A path is therefore created for the current flowing from the supply voltage to ground, wasting it. Typically, the short-circuit power is 10% of the switching power: it is sufficient, to estimate the total dynamic power consumed by a circuit, to sum the two terms shown in Eq. 1.7.

$$P_{\text{dynamic}} = P_{\text{switching}} + 0.1 \cdot P_{\text{switching}} \tag{1.7}$$

The contribution due to static dissipation, on the other hand, represents the power consumed by a device connected to the power supply when it is not switching. In MOSFETs, up to the 90 nm technology node, this was negligible in comparison to dynamic power [15]. However, with advancing technology, characterised by reduced threshold voltages and decreased oxide thicknesses, this dissipative component has become significant, reaching around one third of the total device consumption. Static power is due to several phenomena related to leakage events: the sub-threshold current that occurs in devices that should be completely switched off, gate leakage through certain dielectrics and junction leakage caused by diffusion between different areas of the device.

$$P_{\text{static}} = (I_{\text{sub-threshold}} + I_{\text{gate}} + I_{\text{junction}}) \cdot V_{DD} \tag{1.8}$$

As far as the sub-threshold leakage current is concerned, it can be described, for $V_{DS} > 50$ mV, by Eq. 1.9.

$$I_{\text{sub-threshold}} = I_{\text{OFF}} \cdot 10^{\frac{V_{GS} + \eta \cdot (V_{DS} - V_{DD}) - k_\gamma \cdot V_{\text{substrate}}}{S}} \tag{1.9}$$

In Eq. 1.9 the following parameters that influence the final current value are highlighted:

- I_{OFF}: represents the current flowing in the device for $V_{GS} = 0$ V and $V_{DS} = V_{DD}$;

- η: it is the DIBL coefficient, a term which is multiplied by V_{DS} and which lowers the threshold voltage (since the accumulation of electrons at the drain leads to a decrease in the height of the energy barrier between source and drain). This coefficient increases exponentially as the channel length decreases [16];

- k_γ is the body effect coefficient describing the influence of the substrate on the threshold voltage.

The phenomena of gate and junction leakages are other dissipative components caused by the build-up of voltages at specific points in MOSFET devices. Gate leakage refers to the current that occurs when a voltage is applied to the gate and is strongly influenced by the thickness of the oxide separating the gate from the channel: the reduction in the geometric dimensions of devices has led to a thinning of this layer, increasing device losses. To mitigate this effect, new materials have been introduced such as hafnium dioxide (HfO_2) or aluminum oxide (Al_2O_3) [17], characterized by a higher dielectric constant than silicon dioxide. These dielectrics allow the capacitance to be maintained while increasing the thickness of the oxide layer, thus reducing the tunneling phenomena that would lead to significant leakage currents: SiO_2 thicknesses of 2 nm (equivalent to about ten atoms of silicon dioxide, [17]), associated with a supply voltage around 1.2 V, result in leakage currents of 0.1 A/cm [18].
Junction leakage, on the other hand, occurs when source or drain are at different potentials with respect to the substrate. This phenomenon has a lower contribution than the other types of leakage mentioned above.

However, in the context of device design, the mere treatment of static and dynamic power is a partial measure of a chip's overall efficiency: one could, for example, decrease dissipation by slowing down the clock frequency, causing the delay needed for a computation to be infinite. For example, inverters have been shown to operate with power supplies less than 100 mV, thus consuming low dynamic power, but they operate so slowly that dissipation due to leakages dominates, as these have more time to flow through the devices [15]. It follows, for a more complete analysis, that it is necessary to introduce figures of merit that quantify the trade-off between power consumption and performance. An important concept is the Power Delay Product (PDP), which equals the power consumed to perform an operation multiplied by the time it took the device to perform it (the propagation delay, t_{pd}): from a metric point of view, it is equivalent to a switching energy. The energy delay product is even more relevant. This figure of merit is equal to the product of PDP and delay: the quadratic dependence with respect to delay underlines the importance of operation time when considering the efficiency of a device. As for the propagation delay, defined as the time between when the input exceeds 50% of V_{DD} and when the output exceeds the same threshold, it can be calculated using the Elmore delay model. This model represents a circuit through a representation consisting solely of resistors and capacitors, and approximates the propagation delay to the sum over the different nodes of the circuit of the capacitance seen at the node multiplied by the effective resistance:

$$t_{pd} = \sum_i R_{\text{effective}_i} \cdot C_i \tag{1.10}$$

In conclusion, for an optimal and sustainable design, it is essential to consider both energy dissipation and execution time, balancing both these aspects to respect the needed requirements. Only through a full understanding of the concepts outlined in this subsection it is possible to introduce a new technology, capable of reducing power consumption without compromising performance.

1.2 A new technology: Molecular Field Coupled Nanocomputing

In order to keep up with the times and overcome the limitations of MOSFETs, new technologies, no longer based on silicon and therefore called Beyond-CMOS, have been proposed over the years. Among them, a promising candidate is Molecular Field Coupled Nanocomputing (MolFCN), which is characterized by the use of molecules in special structures created ad-hoc. This technology is based on the encoding of binary values through charge localization at precise points in the structure: the single molecule is used as a **charge container** [19] and, depending on where the charge localizes, '0' and '1' values can be represented. This information is propagated by exploiting the coulomb repulsion that occurs between the charges, which is inversely proportional to the distance between them: this technology avoids conduction phenomena, thus reducing unwanted losses and limiting power dissipation. A further advantage of MolFCN lies in the nanometric size of the molecules involved, which makes it possible to achieve integration densities that are difficult to obtain with other technologies. Moreover, this technology seems capable to operate at room temperature without the need for cryogenic cooling and promises extremely high processing speeds of up to hundreds of gigahertz [20], [21].

1.2.1 Unit cell of MolFCN

The innovation of MolFCN consists in no longer encoding binary values through voltage thresholds but instead through charge localizations; there is thus a need for a structure in which charges can be confined and in which two stable states associated with '0' and '1' can be created. On a theoretical level, it is possible to define 'structured charge containers' as cells with four possible allocations, one for each vertex of a square cell; if two negative charges are placed, they will arrange along one of the two diagonals of the cell due to the coulomb repulsion between the charges leading to the maximization of the distance. This phenomenon generates two 'lower energy configurations', which are energetically equivalent: when the system assumes one of the two configurations, it is defined as stable, requiring significant energy to overcome the energy barrier necessary to pass from one diagonal to the other. It follows that, in such a stable configuration that shows two possible states, one can associate the binary value '1' with the case in which the charges are arranged on one diagonal and the binary value '0' with the case in which the charges are arranged on the other diagonal.
In the specific case of MolFCN, the charge container is a molecule while the electron localization points are aggregation centers [19] (in the following discussion they will be also referred to as 'dots'). The charge between dots can move if sufficient energy is applied

to overcome the potential barrier. In addition to charge localization, where the state assumed by the cell is stable and not susceptible to the slightest energy fluctuations, the phenomenon of charge switching must also occur in order for information to propagate correctly. This is defined as the adaptation of the cell to the correct binary value in response to the surrounding context, as the value must change according to the input, and is in energetic contrast to charge localization: to enable the phenomenon of charge switching, the energy barriers between the stable states associated with '1' and '0' should be low, to avoid excessive consumption to vary the charge localization. In order to make both mechanisms possible, so fundamental to the proper functioning of the technology, a third possible configuration has been introduced. The 'NULL' configuration represents this third possible state in which charge can be localized: although not associated with a binary value, the 'NULL' configuration represents an energetically favourable state to position the molecule, reducing the energy barrier during switching. Furthermore, the creation of the 'NULL' state has important propagative consequences that will be explored in more detail in 1.2.3.
A representation of the unit cell, characterized by four bigger dots and by two smaller dots, defining the 'NULL' configuration, is visible in Fig. 1.1.
Several studies have been carried out to identify molecules that fit the requirements described. Among them, it is possible to distinguish between bistable molecules, which tend to place the charge naturally in two distinct positions, and mono-stable molecules, in which the charge is concentrated in a single point of the molecule under thermal equilibrium conditions. The latter are easier to synthesize and are therefore preferable. But in order to respect the characteristics of a single cell, it is necessary to place two molecules near, as it can be seen in Fig. 1.1, in order to obtain the correct number of redox centers.

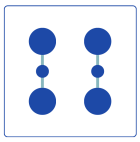

Figure 1.1: Representation of a unit cell in MolFCN technology.

In addition, according to their electrostatic nature, molecules can be classified into different categories. This classification can be made by studying the sum of the charges present on the 'active' redox centers, those encoding a binary value (Q1 and Q2), and the sum of the charges on all redox centers (Q1, Q2 and Q3, the redox center associated with the 'NULL' state):

- Neutral molecule: both the sum of the charges in the active dots and the sum of all charges is 0;
- Oxidized molecule: both the sum of the charges in the active dots and the sum of all charges is +1;
- Reduced molecule: both the sum of the charges in the active dots and the sum of all charges is -1;

- Zwitterionic molecule: the sum of the charges in the active dots is +1 but the sum of all charges is 0.

Historically, one of the first molecules proposed for MolFCN implementation was 1,4-diallyl butane, consisting of two allyl groups connected by a butyl bridge [19]: simulative studies have shown how the application of electric fields allows good charge localization on the two active dots, making the molecule an interesting candidate for forming half of a unit cell [20].
Another molecule that has been extensively studied is Bis-Ferrocene, composed of two ferrocene groups, where the two active dots are located, connected by a carbazole that hosts the dot encoding the 'NULL' state.
Bis-ferrocene, generally used in its oxidized form [20], is particularly interesting in that, by adding an alkyl chain with a thiol group (-SH), it is possible to form a Self Assembled Monolayer (SAM) of molecules on a gold substrate [22], thus facilitating the practical implementation of the technology. A MolFCN unit cell is thus represented by two molecules, placed close together, and takes on a binary value depending on the polarization assumed by the charges [23], according to Eq. 1.11.

$$P = \frac{(Q_2 + Q_3) - (Q_1 + Q_4)}{Q_1 + Q_2 + Q_3 + Q_4} \tag{1.11}$$

Having seen the implementation of a single cell, more and more complex structures can be studied, with the aim of arriving to a technology that implements all the functions of digital electronics.

1.2.2 Propagation of information in MolFCN

In order to propagate binary information, several unit cells can be placed close together, thus creating a wire, which is the simplest structure to realize [24]. When the polarization of one of the cells is set to '1' or '-1', due to the coulomb repulsion established between the charges, the neighbouring cells will assume a polarization such that the distance between the localized electrons is maximized. Consequently, they will tend to copy the polarization of the neighbouring cell, creating a stable state only when the charges are arranged in the dots of the same diagonal as the reference cell, whose values has been externally fixed, which is called the 'driver cell'.
Note how, in the case of mono-stable molecules where a unit cell consists of two molecules, the behaviour of one molecule will be inverted with respect to the adjacent molecule. This configuration allows the combined cell to act as a buffer, since inversion is neutralized by the presence of the second molecule.
A few important considerations must also be considered: the influence of a cell extends within a certain radius, and therefore two very distant cells will not exert any particular influence on each other. Furthermore, this range will extend over both the cells on the left and those on the right: the propagation mechanism will not be unidirectional, as is usually in traditional electronics.

However, by combining unit cells in different ways, more complex functions can be implemented than the wire: the fundamental layouts of the MolFCN are the inverter and

the majority voter (MV). In the case of the inverter (Fig.1.2a), a bifurcated structure is used to make charge reversal stable, whereas in the case of the MV (Fig. 1.2b), three wires carrying three different inputs meet in a central cell; this is polarized according to the binary value carried by the majority of the inputs. The MV is particularly important due to one of its functions: from its truth table, it can be seen that by fixing the binary value of one of the three inputs, AND or OR logic gates can be implemented. In fact, fixing A = 1 we can obtain the logical function OUT = B x C, typical of an AND gate, while fixing A = 0 it is derived the function OUT = B + C, typical of an OR gate [25].

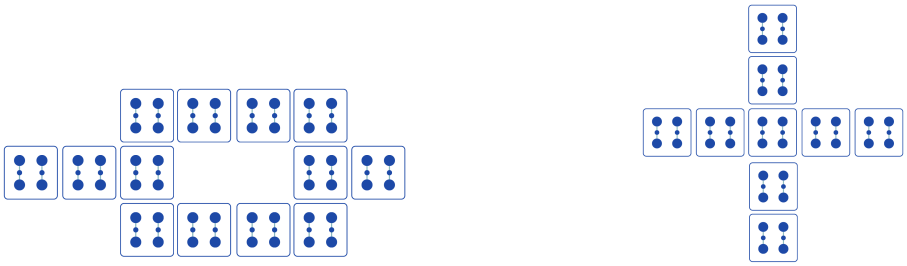

(a) Inverter representation. (b) Majority voter representation.

Figure 1.2: Pictorial representation of the most important structures in MolFCN technology.

It follows that inverters and MVs are sufficient to implement everything that can be created by MOSFETs. The only remaining elements to be able to create a circuit are, for the purposes of design optimization, the various types of connections. These include: L connections, capable of varying the direction of propagation of a wire by 90°, T connections, capable of dividing the information into two distinct wires, and finally the realization of cross-wires through the use of unit cells placed in a diagonal orientation with respect to the others. All these types of structures are united by their operating principle, which is based on the principle of repulsion between charges.

(a) L connection representation. (b) T connection representation.

Figure 1.3: Pictorial representation of connections.

1.2.3 Enhancing propagation: clock mechanism in MolFCN

The construction of long wires, composed of numerous molecules arranged close together, can generate problems in the correct propagation of information. If, for any metastability

problem, one of the intermediate cells in the wire were to assume a random binary value without waiting for the correct propagation given by the driver cells, incorrect information would be propagated. In order to avoid this situation, a clock mechanism was created to guide the propagation of information and avoid problems due to incorrect charge localization. It therefore has the objective of varying the height of the energy barriers to be overcome in order to localize the charge in the various dots of the molecules: lowering or raising this barrier can inhibit or favour the localization of electrons.
In MolFCN it is implemented by applying an electric field, which localizes the charges either in the dot associated with the *NULL* state or in the part of the molecule where the two active dots are present. In fact, applying an electric field generates a coulomb force that is able to influence the position of the charges within the system.

Thus, when the charges are localized in the *NULL* state, they cannot take on any binary value but are destined to wait until the clock electric field allows them to take on a binary value. Conversely, locating the charges at the top of the molecules, where the active dots are located, will limit the electrons located on the dot associated with the *NULL* state. Most of the charge will be located on one of the two active dots, depending on the adjacent molecules, allowing a better representation of the binary value and improving the polarization value. In reality, the circuits are then divided into different clock zones, depending on the type of electric field applied [26]:

1. Switch phase: the molecules switch from a *NULL* to an active state by the application of an appropriate electric clock field;

2. Hold phase: the clock electric field is kept constant after the transient in the switch phase. The energy barriers between states are thus kept high and, in theory, no change in charge localization within a molecule is permitted: the stable states assumed in the switch phase are maintained and the binary information that the cells encode is preserved;

3. Release phase: through a change in the electric clock field, the energy potential barriers between states are lowered, so that the molecules' charge is localized in the zone associated with the *NULL* state. The cells in this phase show no binary value;

4. Reset phase: the clock electric field is kept constant after the transient performed in the release phase. The charge remains localized in the dot associated with the *NULL* state without encoding any binary value.

In order for the technology to function properly, the four clock phases must be applied to the structure in a coordinated and sequential manner. With this in mind, the circuit can be divided into four different zones that repeat periodically, to allow the electric field of each phase to be applied only to specific areas of the structure at specific times. This approach ensures the alternation of the various clock phases and a phase shift of $\pi/2$ between the hold and reset phases, which allows for proper localization of the electrons in the unit cells. A crucial aspect is the maximum limit of molecules that can be positioned in each region. This constraint is intended to avoid propagation errors: a molecule, as already mentioned, if it waited for an input for a long time, could locate the charge on a random dot, without waiting for the input of previous cells. Furthermore, if a region

were too large, the information might not reach the end of the region at the start of the next clock period, thus compromising the correct timing of the signal along the entire circuit.
The application of the electric clock field, in addition to ensuring correct propagation within the circuit, has the important function of enabling pipelining, increasing the flow of information that can be processed by the created logic gates. Whenever the first region of the circuit is in the switching phase, it can receive information from the driver cells to begin propagating new inputs, without waiting until the previous inputs have already been fully processed by the circuit. This allows the rate of processed data to be increased, thereby increasing the performance of the device.

1.3 From a neuron to neuromorphic computation

In recent decades, in addition to a constant optimization of individual devices in agreement with Moore's Law, there has been an increasing complication of the operations to be performed. The advent of artificial intelligence, visual recognition or language processing are pushing the limits of what traditional technology can offer: the constant increase in the number of operations to be performed at increasing frequencies brings the traditional paradigm to which electronics had become accustomed [11]. Consequently, not only do individual devices have to change, but also systems composed of several devices have to be renewed in order to keep up with the current requirements. And so, by studying the model in place since 1945 [27], the von Neumann architecture, it is possible to understand its effectiveness but also its inherent limitations. Only in this way can it can be understood how overcome tradition

Von Neumann's architecture imposes a physical separation between central processing units (CPUs) and program and data memories [28]. The two components are linked to allow the exchange of information, but it must be considered how the CPU, capable of much higher speeds than the memory access speed, is often forced into an idle state, dissipating energy uselessly while it waits to receive information [29]. This phenomenon, known as the von Neumann bottleneck, has important consequences on the throughput, that is the number of data processed by the circuit in a certain amount of time: it is small compared to the amount of information that the CPU could actually process.
Possible solutions include the addition of hierarchical memories inside the CPU, in order to avoid delays for the most used data, but the energy consumption of a cache memory is directly proportional to its size [29]: this solution mitigates the problems of the von Neumann architecture but does not fully overcome them.

Neuromorphic computing represents one of the emerging paradigms that promises to overcome the aforementioned limitations. This model is inspired by the architectures of the human brain, recreating structures that emulate the functions and performance of neurons and synapses. The paradigm stems from the observation of the incredible performance of the human brain, where each neuron receives signals from 10^4 other neurons while the total dissipation of the brain is around 20 W [30]). However, the aim of

neuromorphic computing is not to reproduce a human brain in its full functionality but instead to create a circuit capable of processing a large number of inputs quickly. Not only that, but the system must also be able to *learn* specific operations while remaining robust with respect to the randomness of inputs, ensuring reliability and efficiency, as well as independence in performing precise functions.

1.3.1 Biological neuron

Neurons represent the basic units of the human brain, responsible for processing data. They are divided into three main parts, illustrated in Fig. 1.4: soma, dendrites and axons. The soma is the most important part of the neuron: it is the cell body, containing all

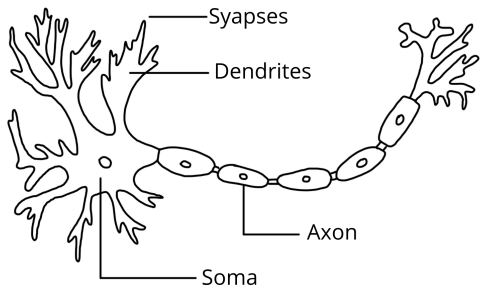

Figure 1.4: Representation of a biological neuron.

the organelles responsible for the functioning of the system and responsible for processing the signals received. On its sides are extended the dendrites and axons, branches with different functions: the dendrites receive signals from other neurons and transmit them to the soma while the axons transfer what has been processed by the soma to the next neuron.
Communication between neurons occurs through synapses, microscopic gaps between two neurons, which are responsible for the exchange of chemical signals. Synaptic transmission occurs through the opening of calcium ion channels, allowing these ions to bind with receptors located in the dendrites of the pre-synaptic neuron, the one before the neuron under analysis. This interaction causes a change in the membrane potential, that is the voltage difference between the inside and the outside of the cell.

> "When an axon of cell A is near enough to excite a cell B and repeatedly or persistently takes part in firing it, some growth process or metabolic change takes place in one or both cells such that A's efficiency, as one of the cells firing B, is increased" [31].

This mechanism implies that the various inputs received by a neuron may have different weights, determined by the past history of the stimuli received: the efficacy and influence of each input will vary according to its activation history. In particular, the weights will be higher in the case of excitatory signals and lower in the case of inhibitory signals, thus influencing the neuron's final response. Synaptic plasticity can be considered one of the bases of learning and memory [32]. Therefore, by modulating the weights, specific outputs can be obtained: this phase, performed by algorithms, is called the training phase of the network[33].

1.3.2 Artificial neurons and neural networks

By abstracting from what has been seen from a biological point of view, it is possible to implement the functions seen in the section 1.3 from an engineering point of view. Hence, the inputs of a circuit can be identified with the potentials in the dendrites. The soma will then be the computational part that takes care of performing a weighted sum of the inputs while the output will be the potentials transmitted to the axon. The connections between the neurons are the correspondent of the biological synapses, which are responsible for encoding the weights, amplifying or reducing the effect of the inputs.
Considering a mathematical modeling point of view, Hodgkin and Huxley's model provides the most detailed description of biological phenomena by using differential equations that describe the trends in membrane potential and currents of ion channels. While this model provides a deep understanding of biological mechanisms, it is not necessary from an engineering point of view. Depending on the aspects to be investigated, different representations describing the union of several neurons can be used, leading to rather complex systems. In this way, one can create neural networks, systems made up of interconnected nodes organized on several levels, capable of processing information in an innovative and adaptive manner.
The two most important macrocategories of neural networks are deep neural network (DNN) and spiking neural network (SNN).

Deep neural networks are based on the weighted sum of inputs. Mathematically, the neuron-system is initially described by a weighted sum of N inputs, whereby each input is multiplied by its own weight. The output of the neuron is then calculated through a non-linear activation function, dependent on the result of the summation and an activation threshold. The key aspects of this model are the weight given to each input and the activation function. In particular, the latter adds complexity to the structure created: if it was not present, the output signal would be a linear function of the inputs. This would result in a linear regression model, unable to handle the complexity required by applications such as image recognition, where the output must be able to represent intricate relationships [34]. Among the most common and used activation functions there is the binary step function, which has the merit of being one of the simplest functions and which well represents the threshold mechanism that inputs must overcome for the neuron to give an output signal. Other historically implemented activation functions are sigmoid, rectified linear unit (ReLU) and Softmax functions [35], [36], [34].

Spiking neural networks, on the other hand, focus on emulating the potentials of biological neurons. The exchange of information takes place through the frequency of voltage spikes that are created: this type of communication is called event-based processing [33]. At the circuit level, one of the most commonly used models is the Leaky - integrated and fire (LIF). In such a representation, the membrane potential V(t) is described through differential equations that model the voltage evolution as a function of a time-varying input current. This current charges a capacitor: when the voltage at its terminals exceeds a certain threshold a switch closes, discharging the capacitor and generating a very fast voltage variation at the output. The presence of a resistor in parallel with the capacitance

provides a dissipative path for the current: the result is a non-linear voltage trend, as it would occur in the presence of the capacitor alone, but a spike behaviour [37].
SNNs are quite efficient from an energy point of view: the neurons, being active only when receiving and sending spikes, present a reduced energy consumption when in idle state [33]. However, it must be considered how the power consumption of such neural networks, being related to the number of spikes created, increases as the throughput increases: this makes SNNs not always preferable to DNNs from an energetic point of view. Furthermore, SNNs do not have the same abundance of usable datasets as DNNs: their training is more difficult. Lastly, the discontinuous characterisation of SNNs cannot be differentiated: hence it is difficult to apply back-propagation algorithms that establish a feedback system between input and output and that are of a particular technological interest due to their operation capabilities. [33].

1.3.3 Implementation of neural networks: state of the art

In 1943, W.S. McCulloch and W. Pitts proposed one of the first neural models, creating a system characterised by fixed thresholds and the absence of weights. Their work was the basis for later studies and played an important role in the creation of neural networks [38]. However, it was not until 1989 that M. Mahowald and R. Douglas distinguished themselves by developing a silicon neuron, a circuit designed to simulate the physiological behaviour of a biological neuron and based on MOSFET technology. The design exploits the sigmoidal trend of the current voltage relationship of a differential pair of mosfets, a trend similar to the one shown by the voltage-dependent conductances of cell membranes. The basic principle of the circuit is that this differential pair compares the membrane voltage with a threshold voltage value. The outcome of this comparison, if the membrane voltage exceeds the threshold voltage, will be a current, known as an activation current, which will drive a transistor referred to as a conductance transistor. This transistor, representing the conductance of a membrane, will control an activation and an inactivation circuit part, therefore emulating the biological functions of a neuron.

Over time, the development of technology has enabled the creation of increasingly sophisticated devices. And so, since 1989, many attempts have been made to reproduce a neural structure. This leads to CMOS-based circuits in which the synapses can be implemented through registers containing the input weights while the multiplication and summation (MAC) operations are performed by the neurons [39]. In other approaches, the MAC operations are instead performed in the circuit part that expresses the synapses while the neuron's role is to sum the results and to apply the activation function [40].
But the literature also reports various neural networks based on beyond CMOS devices. Among these, magnetic technologies are of particular relevance: thanks to their non-volatility they promise excellent performance and are able to perform DNN operations efficiently. Neural networks based on Magnetic Tunnel Juctions (MTJ), which encode binary values through the variation of magnetisation in one of the two magnetic layers, separated by dielectrics, that make up the device are therefore highlighted. In the circuit shown in [41] an example of such an implementation can be appreciated: MTJs store the input weights while an XNOR network implemented by Carbon nanotube field-effect

transistors (CNTFETs) produces the logical result. The output of this network will reflect the majority of the results of XOR operations between the inputs and their respective weights, in a manner similar to a majority voter.

Other studies mention the use of in plane nano magnetic logic (i-NML) or domain walls to implement the role of synapses. The latter technology involves the use of boundaries, called domain walls, between two differently magentization domains. Domain walls exist to balance energies and can be moved along a magnetic nano-strip by applying a magnetic field or injecting current.
In [42] a DNN created through this magnetic technology is analyzed. In the illustrated approach, the weight of the synapses is modified depending on the position of the domain wall at one of the end of the nano-strip, allowing the creation of a neural network with binary weights, which is particularly appreciated in the field of pattern recognition [42]. The study therefore explores the use of notches along the nano-strip to discretize and increase the possible positions in which domain walls can be located. The system arranges the stripes in such a way as to form a majority voter, whose central part is an MTJ. In one of its ferromagnetic layers, the one with variable magnetization (and for this reason called the free layer), there is a different magnetic orientation depending on the input given by the synapses. If this orientation is parallel to that of the second ferromagnetic layer, whose magnetization is fixed, there will be a binary value, otherwise there will be a different binary value. It is interesting to notice in [42], in order to reduce the currents to move the domain walls and so reduce energy consumption, the Bennet-clocking system: by introducing instability phases in the magnetic polarization of the devices used in the circuit, it is possible to reduce the energy required to make them stably encode a binary value.

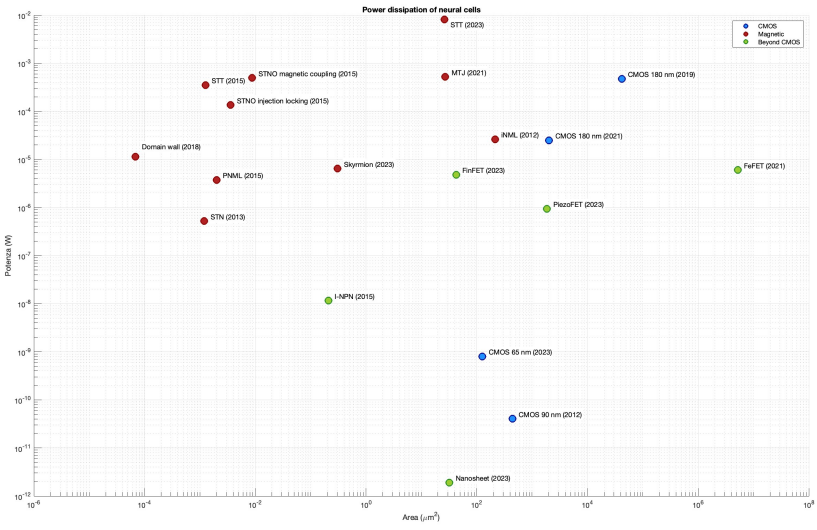

Figure 1.5: Power comparison with respect to the occupied area.

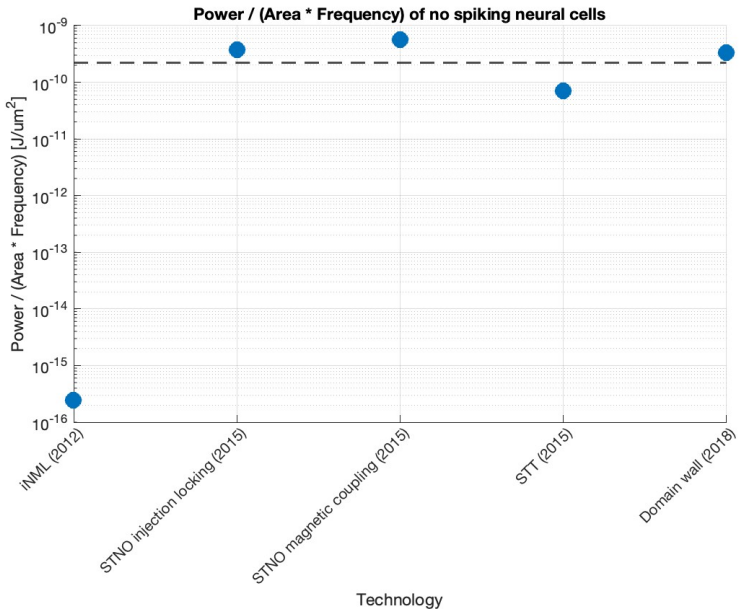

Figure 1.6: Power comparison with respect to the occupied area and the clock frequency, focusing on Deep Neural Networks. The black line refers to the average value.

Fig. 1.5 shows the results obtained by analyzing the literature on neural cell implementations, relating the power consumption to the device area. Fig. 1.5 does not distinguish between DNN and SNN: this can be seen as a preliminary analysis. The works referred to are: [49], [50], [51], [52], [53], [54], [55], [56], [57], [58], [59], [60].

Fig. 1.6 shows the results obtained by analyzing the literature on neural cell implementations, highlighting the energy consumption in relation to the area occupied and the clock frequency. It is important to bear in mind how the characteristics of the different devices make a quantitative comparison difficult: the easier production, because it is well established, of CMOS or the non-volatility of magnetic devices are elements that cannot be represented on a graph but which complicate a direct comparison.
Nine devices are depicted in Fig. 1.6: the average value of dissipated energy per unitary area is equal to $1.9188 \times 10^{-10}\,\mathrm{J/\mu m^2}$.

Of particular note it's the magnetic device previously discussed in this chapter, which presents the lowest dissipation value of $2.44 \times 10^{-16}\,\mathrm{J/\mu m^2}$. This value takes into account the detection unit used to convert the coding from the neuron's spin-mode information to a charge-mode coding that is more compatible with the technologies used to interpret the data. The detection unit also performs the important function of the axon since the spin diffusion length (that is the characteristic length at each material that describes the spatial decay of spin polarization) is rather small: the distance between two neurons would not be sufficient to allow for proper propagation of information. The study hence uses a CMOS latch to connect the MTJ of one neural cell to a synapse of the next cell.

The latch, created using 45 nm technology, compares the resistance of the neural cell with that of a reference MTJ and will output the current required to vary the domain wall of the next neuron's synapse. This device is therefore the benchmark for future discussions related to power dissipation, offering a comparison for the neural cell that is the subject of this thesis, implemented through MolFCN technology.

1.3.4 Implementation of neural networks: MolFCN

In this subsection, the key principles for implementing neural networks through MolFCN technology will be discussed. Due to the advantages previously described such as increased processing frequencies and reduced size through the use of molecules, this technology is a promising candidate for implementing complex functions. Furthermore, as MolFCN technology does not rely on conductive phenomena, leakages are minimized, promising low energy dissipation.

MolFCN technology can effectively implement a DNN-type neural network, whose basic principle of function is based on the weighted sum of different inputs. From a modeling point of view, the action of the neural network can be defined as shown in Eq. 1.12 and in Eq. 1.13.

$$s = \sum_{i=1}^{N=3} w_i \cdot x_i \tag{1.12}$$

$$y = f(s - \theta) \tag{1.13}$$

MolFCN performs the summing operation through the majority voter [43], whose output value depends on the superposition of the electric fields of the three inputs, defined as the voltages Vi (with i ranging from 1 to N=3) at the interfaces of the input wires of the MV preceding its central cell, as can be appreciated in Fig. 4.7. These potential differences are created due to the different charge arrangements between the active dots of the molecule; the fact that they are even defined between dots of two different molecules does not negatively influence the propagation of information (note the configuration of Vx and Vx in Fig. 4.7). Thanks to the superposition of the electric fields and to the coulombic repulsion between the charges, there is a precise charge distribution within the first molecule of the MV center. Its potential (called Vs), taking all inputs into account, takes on the role of s in Eq.4.7.
Depending on the value given by the drivers, different charge aggregations will occur in the active dots of the molecules. A trend can be identified in the behaviour of these distributions with respect to the input voltages: this will be referred to as Vin-aggregated charge trans-characteristic, VACT. For applied voltages below a certain threshold, there will be a change in the aggregated charge that is linear to the changes in the applied input voltage. For applied voltages above this threshold, which is referred to as V_{sat}, the charge aggregation will settle to a constant value on one of the two active dots. This means that, if for $V_{in} = 0$ V one expects half of the charge aggregated on dot 1 of the molecule and the other half of the charge aggregated on dot 2, for values of V_{in} above 0 V the charge aggregation will start to be increasingly unbalanced, accumulating more and more on one of the two dots. This will occur until a value of V_{in} equal to the threshold

value V_{sat} is reached: at that point the aggregated charge will be almost exclusively on one of the two dots and the polarization will assume a constant value, peculiar to each molecule [44]. An example of the VACT is reported in Fig. 1.7, depicting the behaviour of bis-ferrocene when no external input is sensed by the molecule.

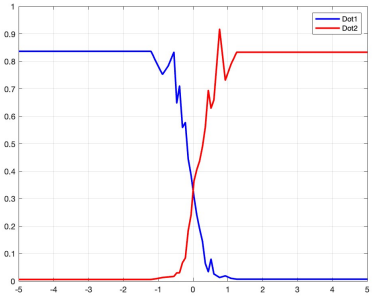

Figure 1.7: VACT of bis-ferrocene.

The increase or decrease of the effect of an input signal, so the weight wi, can be adjusted depending on the molecule that is inserted into the circuit. It is defined as the ratio of the polarization in the molecule at the control unit (Pc) with respect to the voltage in the molecule at the interface under study(Vint), minus a sign **??**, as can be seen in Eq. 4.7. The weight is therefore a negative numerical value since it must be remembered that, in MolFCN technology, two neighbouring molecules have opposite charge aggregations due to coulombic repulsion. From a practical point of view, the weight of an input is encoded in the slope of the linear region of the VACT. It is therefore crucial, in order to make the most of MolFCN technology, to understand the value of Vsat, which determines the behaviour of the charge transition between the two active dots.

$$w_i = \frac{P_{\mathrm{c}}}{V_{\mathrm{int}_i}} \quad \text{with } i = 1, 2, 3 \tag{1.14}$$

After having analyzed the terms of Eq. 1.12, those of Eq.1.13 can be studied. The link between the two equations is the voltage between the two active dots in the molecule of the central cell of the majority voter: its value will be transformed, through an activation function (f in Eq. 1.13), into the output (y) of the system, so into the polarization assumed by the central cell of the MV. The activation functions that can be implemented include step-like functions [23] and tan-sigmoid functions [43], depending on the complexity required by the neural cell. Both, as already stated, have the objective of transforming the voltage value Vs into a polarization state, which can be associated with one of the two binary values. This polarization may not have a value large enough to be attributed with absolute precision to a binary value, leading to possible logical errors. To this end, a key role is played by the application of clock and driver fields and the choice of molecule, which should ideally have a small saturation voltage, resulting in a very steep transient behaviour where the charge tends to aggregate at precise points in the molecule. A second critical issue of MolFCN technology concerns the phenomenon of information fading that occurs as the binary value is transmitted from one cell to another: this is due to a

weakening of the polarization assumed by the molecules due to border effects when the kinetic energies exceed the Coulomb terms [44]. This attenuation event results in loss of information along the wire responsible for the propagation of the neural cell output (the axon of the system). To solve this problem, the insertion of molecules with a very small Vsat of 0.1 V was proposed in [43]. These, called charge saturators, are meant to improve propagation and avoid polarization fading. However, the polarization may not be sufficient to be encoded in a binary value, so the codification shown in Eq. 1.15 is adopted.

$$P_{\text{out}} = \begin{cases} -1 & P < 0 \\ 0 & P = 0 \\ 1 & P > 0 \end{cases} \tag{1.15}$$

Finally, regarding the threshold mechanism, present in Eq. 1.13 under the symbol of *theta*, it can be implemented through a shifting of the activation function, obtained through the use of different molecules with respect to bis-ferrocene in the central cell of the MV [43].

Chapter 2

Structure simulation

The aim of this thesis is to calculate the power dissipated by a neural cell implemented using MolFCN technology. In the chapter 4.7 it was seen that, in order to ensure the correct propagation of information, it is essential a precise application of the electric field to vary the localization of the charge in the chosen molecule. Since the technology has negligible consumption due to leakages, it follows that the main component of power dissipation is caused by the creation of electric fields. So, studying how to optimally apply these fields is crucial to evaluate the performance of the implemented neural network.
This chapter will illustrate the simulative creation of a structure suitable for hosting the molecules of MolFCN technology, a *molecule-hosting structure*. The chapter is divided into five sections that explore the processes to arrive at the creation of a correctly functioning construction: first, the design criteria will be defined; in the second part different types of structure will be created using the TCAD Synopsys Sentaurus Structure Editor tool followed, in the third part, by the use of TCAD Synopsys Sentaurus Process. The electrical simulations, performed through Sentaurus Device, will be then explained. Finally, the MATLAB code created to parametrize the simulations is reported.

2.1 Technological creation of MolFCN

MolFCN technology requires precise electric field application to function properly. Furthermore, the structure must also permit the molecules to be close enough to influence with each other, propagating the correct binary information.
To implement MolFCN, a dielectric structure is therefore designed [**?**], [**?**]: a trench is created to accommodate the molecules that meet the needed characteristics, for example bis-ferrocene molecules. Two electrodes are placed on either side of the trench and a third electrode is placed at the bottom of the trench. By establishing voltages between these electrodes, the arrangement of charge in the molecules can vary, encoding different binary values. The reason for this lies in the uniform electric field that is created when a potential difference is established between two conductors separated by a dielectric. The field, reported in **??**, is directly proportional to the potential difference and inversely proportional to the distance separating the conductors. The Coulomb force thus generated is able of displacing the free charges of a molecule between the two conductors, inducing

a localization in the molecule itself.

The voltage application between the upper electrodes creates a transversal electric field with respect to the molecule, localizing charges in one of the two active dots and therefore forming a driver cell. On the other hand, by applying a potential difference between the upper electrodes and the bottom one (the trench electrode), a vertical electric field is established. This field, according to its verse, directs charges by placing them in the lower part of the molecule (where the NULL dot can be found) or in the upper half, where the two active dots can encode a binary value, constituting half of the unit cell of MolFCN technology. In this way the clock electric field is generated, capable either to encode a binary value defined by the driver either to place the molecule in an idle state. To ensure the effectiveness of the electric fields, the geometrical dimensions of the trench must be chosen in an accurate way: its height and width must consent the electric field to be intense enough in order to vary the charge arrangement within the molecule.

To create several clock zones, it is necessary to apply electric fields with different signs depending on the phase that has to be applied. Therefore the upper electrodes of the different regions of the circuit can be separated by a nanometer spacing: this makes it possible to apply different voltages and obtain clock fields consistent with the theoretical requirements. The spacing results in a partial overlap between the fields at the points between two different regions: this effect must be taken into account but does not prevent the propagation of information. On the other hand, the trench electrode must be kept continuous to ensure that the molecules are close enough to not lose the information they are propagating. In order for the structure to work properly, given the different voltages applied in the various clock regions, the trench electrode is connected to ground, remaining a constant reference point throughout the operation of the circuit.

From a manufacturing point of view, the deposition of the molecules on the electrode, given the geometric dimensions involved, is a technological challenge. The idea is to create the structure through nanometric deposition techniques such as PVD or CVD and then insert the molecules into the circuit by creating a self-assembled monolayer (SAM): by exploiting the spontaneous creation of chemical bonds between certain molecules, layers with an ordered pattern of molecules can be obtained, creating organic thin films.
The molecules that form a SAM can be divided into two parts: the head group, the component capable of chemically bonding to the substrate, and the functional group, whose properties influence the nature of the created film. In the specific case of MolFCN, the bis-ferrocene plays the role of the functional group while thiol (R-SH) is used as the head group, which spontaneously bonds to both the bis-ferrocene and the the trench electrode made of gold. There are several techniques to obtain a SAM, the main ones being the Langmuir process and the Langmuir-Blodgett process.
The Langmuir process is a method applicable if the molecule has an ambiphilic character: it should show a hydrophylic part and a hydrophobic one. The deposition environment is a tank filled with water with two mobile barriers. By adding the molecules to be

deposited to the bath in a certain concentration and starting to reduce the distance between the two mobile barriers, a compact film of molecules will be formed at the interface between air and water. By adding a substrate to the bath, the Langmuir-Blodgett process is achieved: the thin organic film will no longer be obtained on the surface of the liquid contained in the tank, but instead on the surface of the substrate. The moving barriers will also force the molecules to compact on the substrate, which will be raised in the meantime: the molecules will stick to it in an ordered pattern. The procedure to obtain an ordered pattern of molecules on the electrode of the MolFCN technology trench consists of two steps: first, a SAM of sulphur atoms (the head group of thiol) is created thanks to the fact that it only spontaneously locates between four gold atoms. Binding at precise points in the metal, a very ordered structure can be created, ignoring the variations in the crystal structure of gold, like different crystallographic orientations. The thiol groups are then functionalized with the bis-ferrocene carbazoles, exploiting the hindrance of the molecule, which is the space that is spontaneously created between the molecules to remain in a minimum energy condition. An extremely ordered molecular pattern is therefore obtained: the technology is highly reproducible.

2.2 Simulative creation of MolFCN with Sentaurus Structure Editor

Sentaurus Structure Editor is a tool intended for the creation of 2D and 3D structures through the use of a graphical user interface or by writing a script, making the process iterative. This tool is mainly based on the creation of primitive geometric bodies (rectangles, cubes, ellipsoids,...) but also includes finer functions such as patterning, creation of rounded corners or polishing operations.
The creation of the structure containing the molecules of the MolFCN therefore begins with this tool in order to explore the possible geometric variations in an immediate and intuitive manner.

The Sentaurus Structure editor file is divided into a first part for the definition of geometric variables using the command:

```
(sde:define-parameter "z_EndFirstZone" 0.010 )
```

In which the round brackets enclose the command, `sde:define parameter` is used to specify the type of command, between the quote marks there is the name assigned to the variable and then there is the numerical value expressed by default in micrometers.
The axes have been chosen in such a way to be consistent with the structures later created on Sentaurus Process. For this, the x-axis expresses the height of the device along which there is the alternation between dielectric, titanium and gold. Along the y-direction there is the width (in this direction it can be appreciated the alternation between elevated parts and trench) and z the length, along which the different clock regions toggle. The origin of the axes is the extreme left of the structure, coinciding with the beginning of the first clock region.

The second part of the Sentaurus Structure Editor concerns the creation of volumes in different materials. The structure of the command is:

```
(sdegeo:create-cuboid (position 0 0 0)
(position x_BottomTrench y_End z_LengthWire) "SiO2")
```

In which the command `sdegeo` specifies the creation of a figure, followed by the typology (`cuboid`). In the next two pairs of round brackets are specified the extremes of the volume: first the (x,y,z) referring to the point that indicates the minimum of the body, then the (x,y,z) corresponding to the point at the antipodes of the structure, indicating the superior extreme of the volume. Finally, the material is specified in quote marks and it is present in a library of Sentaurus materials.

The first structure created is a wire, so a sequence of unit cells, assuming the geometrical parameters from [**?**]. In the study, a wire divided into several clock regions 10 nm long and spaced 2 nm apart is proposed. By placing the molecules 1 nm apart, there will be approximately ten molecules per clock region. The trench height is set at 6 nm, the electrodes, made of gold, are volumes 2 nm wide and 4 nm high. Given the lattice constant of gold, this thickness is equivalent to approximately 10 molecules. The trench electrode is placed in the bottom of the created trench, 3 nm wide, with 0.5 nm between the start of the trench electrode and the elevated dielectric part. With respect to [**?**, **?**] it is introduced an adhesion layer made of Titanium, with the aim of improve the adhesion between gold and dielectric. The thickness of such adhesion layer is set to 2 nm [**?**]. The initial structure consists of a SiO_2 substrate of 2 nm thickness, 9 nm width and 22 nm length. Two dielectric volumes are deposited on it in order to obtain two elevated structures on which to place the upper electrodes. The adhesion layers are then deposited, followed by the gold electrodes.

Next, a more complicated structure, which included pi/2 angles in order to optimize the occupied area is created. This design is named L connection, from the top view of the geometry of this architecture. A first hypothesis was to create a curved structure, consisting of several clock regions. However, this solution is not efficient: the molecules would be inclined one with respect to the other, so that the active dots of two neighbouring molecules would not be placed at the same distance. In addition, the introduction of more clock regions to maintain the correct electric fields would result in a slowing down of the structure and a greater occupation of the area.
The second proposed structure avoids these problems and it is much more efficient. The idea is to create a modular structure, taking into account that the structures to be created are MV, L connections and T connections (structures where the binary information is splitted into two orthogonal branches). The idea is therefore to create a basic structure, named the transition region, from which all the necessary structures could be created. The transition region has a square shape at the vertices of which there are four electrodes, separated by the trench, which assumes a cross-shaped configuration. The creation of such electrodes allows better control over the molecules due to the superposition effect of the created electric fields. In addition, the redundancy of molecules, especially in the

case of the L connection for which a cross-shaped structure in the trench would not be necessary, has the important effect of decreasing the fading effect of the terminations. This makes the propagation of binary information much more stable.
These considerations are confirmed by the paper [**?**], in which aggregate charge trends are analyzed using SCERPA (Self-Consistent Electrostatic Potential Algorithm), a fundamental algorithm for dealing with MolFCN technology. The article demonstrates the importance of additional 'stabs', which do not have the transport of logical value as the main objective, but rather have the important purpose of avoiding the weakening of propagation in the wire due to border effects. The cross structure of the trench also allows the desired modular structure to be achieved: it is sufficient to create output wires to obtain the desired configuration and easily vary between MV, L connection or T connection. From the point of view of technological production, the existence of the cross structure allows the connection between wire and transition region without further etching. In this way, the following were created: an L connection, adding one output wire, a T connection, adding two, and finally a MV, adding three output wires and so obtaining the desired neural cell. These structures can be seen in Fig. 2.1, 2.2 and 2.3.

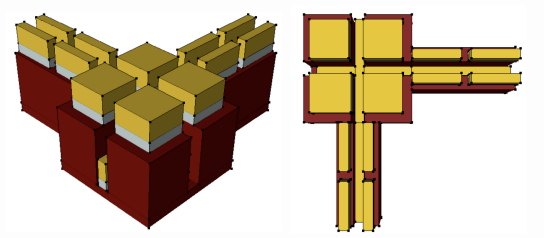

Figure 2.1: L-connection obtained through Sentaurus Structure editor.

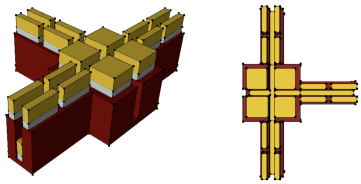

Figure 2.2: T-connection obtained through Sentaurus Structure editor.

Once the basic logic gate are created, the simulation is then extended to include driver structures in the system. The structure of a driver cell is analogous to that of a clock region, with the trench surrounded by two elevated dielectric zones. In this area the voltage will be applied in such a way as to create a potential difference between the two upper electrodes: the resulting electric field will localize the charge in one of the two active dots, varying the encoded binary input. It is then expected that the inverting pattern between molecules will not be present in the driver region: the applied electric field will overcome the coulomb repulsion, locating the charge in the same active dots of different molecules. The first unit cell after the driver region will assume the inverting behaviour that allows the polarization of the two-molecule system to be encoded in a binary value, creating the

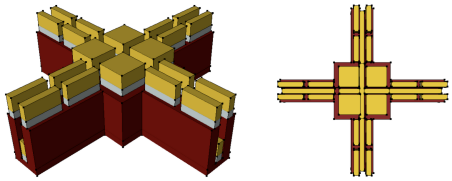

Figure 2.3: MV obtained through Sentaurus Structure editor.

first unit cell of the wire.
The length of the driver region does not need to be as long as a clock region of a wire: the redundancy of molecules with the aggregate charge on just one of the active dots is only necessary in order to obtain a stable signal and in order to avoid errors due to fluctuations. The upper electrodes in the simulation were therefore kept at a thickness of 4 nm gold to which the 2 nm titanium adhesion layer must be added. The distance between the upper electrodes of the drivre region and the upper electrodes of the first clock region of a wire has been maintained to 2 nm. The result of the simulation, which displays the so defined structure, is reported in Fig. 4.7.

The simulations proceed by investigating the creation of a trench with a larger width, capable of hosting two lines of molecules and so creating a 2-line bus structure. The creation of this type of trench has several advantages, explored by [**?**]. The larger number of molecules makes it possible to localize the charge on the correct active dot, since the coulomb repulsion is greater: this decreases coding errors and decreases the fading phenomenon that occurs at the terminations of the structures, giving a more robust structure. An additional advantage of the bus consists in the easier experimental implementation: increasing the size of the trench allows for more feasible patterns from the point of view of deposition and etching techniques.

Finally, the simulations continue by exploring the possibility of concatenating multiple MVs, and thus multiple neurons, by having the output of one (the axon of the neuron) become the input of the second (the synapse of the neuron). The results of the simulations can be seen in Fig 2.4.

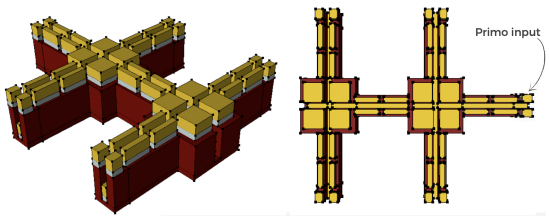

Figure 2.4: Two concatenated MV obtained through Sentaurus Structure editor.

2.3 Simulative creation of MolFCN with Sentaurus Process

The structures are then deepened through Sentaurus Process. This tool was chosen for its ability to model various device creation processes, such as deposition, etching or oxidation, so offering a more realistic modeling than Sentaurus Structure Editor.

In the simulation with Sentaurus Process, the command file (.cmd) plays a central role since it contains the commands needed to manage the entire creation flow. At first it is necessary to specify the coordinate system, which is used to define the mesh, the central element of any simulation: the mesh consists of the decomposition of the simulated structure into smaller volumes in such a way that the system can be represented through finite elements.
Therefore, the first line of .cmd file specifies the use of unified coordinate systems (UCS).

```
math coord.ucs
```

The x-axis points down into the wafer, along the y-direction there is a radial direction relative to the wafer, the same for the direction along z. It is also important to specify how, unlike in Sentaurus Structure Editor, the origin of the axes is placed exactly in the center of the structure with respect to the y-axis, at the height of the end of the upper electrodes and at the beginning of the first clock region. This is due to the method of creation that is used: with the aim of reducing simulation time, one can create half of the structure and then reflect it with respect to the plane of symmetry. Therefore, in the first part of the code, only the coordinates related to half of the trench and to one of the two upper electrodes will be defined and then reflected to obtain a complete structure.

The command file of the structure continues by the definition of variables in order to obtain a parametrizable file. Notice that comments are preceded by a `#` symbol. In addition, the units of measurement are by default expressed in micrometers: to set nanometric values, one must insert in the code the `<nm>` key-word.

```
# ------------------------------------
# Desired Thicknesses
# ------------------------------------
set ThicknessOxideArms 0.003
set ThicknessGold 0.004

# ------------------------------------
# First Vertical wire
# ------------------------------------
set z_StartZone1_VerticalWire 0.000
set z_EndZone1_VerticalWire 0.010
set z_StartZone2_VerticalWire 0.012
set z_EndZone2_VerticalWire 0.022
set z_StartZone3_VerticalWire 0.024
set z_EndZone3_VerticalWire 0.034
```

```
set y_Mid 0.000
set y_EndTrench_VerticalWire 0.006
set y_EndElectrode_VerticalWire 0.016
set y_EndRight_VerticalWire 0.018

set x_TopElectrode 0.000
set x_TopOxide 0.004
set x_TopTrenchElectrode 0.007
set x_TopTrenchOxide 0.011
set x_Bottom 0.013
```

The nomenclature of the variables follows a convention in order to easily interpret the code. Each variable begins with the prefix `x_`, `y_` or `z_`, which specifies the axis to which the coordinate refers. The main structure from which each simulation starts is called the vertical wire and represents the wire that occupies the origin point (0,0,0). The wire extends along a vertical axis, the z-axis, and includes several clock regions, each one separated by a nanometric distance. The .cmd file contains the coordinates where a clock region begins and where the same region ends, with each region identified by a numerical value. The length of the upper electrodes can be appreciated through the difference between `z_StartZone1_VerticalWire` (the stating point of the first clock region) and `z_EndZone1_VerticalWire` (the end of the same first clock region): in this case the length is equal to 10 nm.
Along the y-axis, the width of the structure is defined, permitting a distinction between the trench and the areas occupied by the upper electrodes. Recalling the specularity of the structure, the first coordinate along y that is specified is `Mid`, identifying the origin of the axes. The trench extends for positive y and, due to the reflection of the structure, for specular negative y. `y_EndTrench_VerticalWire` indicates where the trench ends, from which a dielectric raised section is located. On the dielectric the upper electrodes are placed, starting from the point where the trench ends and ending at `y_EndElectrode_VerticalWire`. `y_EndRight_VerticalWire` finally indicates the maximum position of y assumed by the dielectric, which extends beyond the electrode.
The coordinates therefore refer to the extremes furthest from the origin and are distinguished according to the presence or absence of the term 'Trench', hence distinguishing the coordinates related to the trench from those related to the dielectric overhead.
Concerning the x-axis, all coordinates refer to the tops of the various elements of the architecture. The exception is `Bottom`, which indicates the point of maximum extension of the structure reached by the dielectric substrate. Similarly to the other coordinates, the presence or absence of the term 'Trench' specifies which region of the structure is being observed. The summit of the top electrode (`x_TopElectrode`) can thus be distinguished from the one of the trench electrode (`x_TopTrenchElectrode`).

In addition to `VerticalWire`, different denominations are used in order to distinguish between various basic architectures.

The modular zone characterized by the four electrodes at the vertices is called the transition region. Its functionality is to compose L connections, T connections or MVs depending on the number of wires connected to it. It is therefore a fundamental architecture for achieving efficient designs through MolFCN technology.
The electrodes closest to the axis origin are referred to as the bottom, while those furthest away are referred to as the top. Considering `Mid`'s position, the electrodes in the transition region will be named as right if they occupy positive y, left if they occupy negative y.

Output region represents the wire parallel to the vertical wire that extends outside the modular region, indicating the signal output area. In addition, there are two horizontal wires, perpendicular to both the vertical wire and the output wire: the first is the horizontal wire, originally created, while the second is the horizontal reflected wire, which is generated by reflecting the structure. Thanks to their presence, a T connection, a L connection or a MV are achieved. Hence, the vertical wire, the output wire, the horizontal one and the reflected horizontal one are subdivided in more clock regions, each distinguished by a numerical value, like in the vertical wire case.

Having defined the variables to be used in the simulation, the initial grid section is then added to the command file. Indeed, Sentaurus Process needs a geometric grid to subdivide the structure into finite elements. In this way the software solves more accurately the equations describing the structure behaviour: each finite element will be treated as an independent region where the physical properties are calculated. Only after the individual resolutions the results are combined with the ones of other elements, thus obtaining a global picture of the system. It follows that the size of the finite elements influences not only the simulation time but also the accuracy of the simulation results.
The definition of the lines therefore determines the key points for generating the basic mesh. Each line is characterized by a `spacing` value that represents the minimum dimensions of the mesh elements in the area delimited by the parameter specified through the `location` command. In order to make the command file parametric, the variables previously defined have been used, preceding the `$` symbol to recall them.

```
# ------------------------------------------
# Initial grid (half structure)
# ------------------------------------------

line x location= $TopElectrode spacing=0.05<nm>
   tag=TopElectrode
line x location= $TopTrenchSiO2     spacing=0.05<nm>
   tag=TopTrenchSiO2
line x location= $Bottom spacing=50<nm>      tag=Bottom
line y location= $Mid        spacing=0.05<nm> tag=Mid
line y location= $EndTrench spacing=0.05<nm> tag=EndTrench
line y location= $End spacing=50<nm>         tag=End
line z location= $StartFirstZone     spacing=0.05<nm>
   tag=StartFirstZone
```

```
line z location= $LengthWire          spacing=50<nm>
   tag=LengthWire
```

Along the y axis and z axis, only the lines referring to the extremes of the figure are reported: for the sake of the creation of the structure, it is not necessary a fine mesh. The `line` commands are therefore used mainly to define the initial substrate region that will be successively created. A mesh refinement will be next defined for assure correct simulations in the Sentaurus Device environment. So, through the reported commands, a rough mesh structure is defined: the numerical values reported refer to the smallest dimension of a mesh element but don't specify maximum dimension. Sentaurus Process automatically adapts the finite elements to the structure created, increasing or maintaining them at the minimum size in order to optimize the simulation time. Since the x-axis corresponds to the direction along which different materials alternate, more `line` commands are defined, resulting in a finer mesh. In this way, the finite elements well reproduce the changes between the different materials, such as those between the top electrode (`TopElectrode`) and the trench material (`TopTrenchSiO2`). The initial grid will then have much larger mesh values at the base of the structure, identified by the parameter `Bottom`: setting the spacing value several orders of magnitude larger than the other coordinates reduces the complexity of the mesh at the points of least interest. Indeed, it is not necessary to maintain a high resolution in the farthest area from the more interesting regions (in this case, the trench and the electrodes). Therefore, this approach reduces the total number of elements in the mesh, optimizing calculation time without compromising accuracy in the areas of interest.

At this point in the simulation, a section is defined to specify the masks used in later deposition processes. Masks are required to define a model and thus to limit a deposition or etching action to a precise window of the structure: they mimic the pattern that can be obtained with a lithographic action. Below there is an example of a mask definition:

```
mask name=mask_first_electrode left= $EndTrench right=
   $EndElectrode
front=-1 back= $EndFirstZone negative
```

After naming the mask so that it can be recalled and used in next code lines, there are the minimum and maximum points along y and along z that delineate the window through which it will be or it won't be performed the deposition. The value `-1` refers to a point that extends beyond the origin of the axis: the action of the masks assures to include the borders of the structure. At the end of the command the key-word `negative` is specified iin order to reverse or not reverse the polarity of the mask. This imitates the behaviour of polarity in positive or negative photoresists, the core of the lithography operation. The photoresist are light-sensitive substances used to coat a device surface during its creation. Through a mask, the photoresist is then partially exposed to a radiation: its polymers have a chemical composition that varies the solubility of the material according to the exposition. Introducing the `negative` command, Sentaurus Process mimics the presence of a photoresist whose polymers increase cross-linking in the irradiated areas, therefore decreasing the solubility of the exposed regions of the device.

In the simulative environment, in order to create more complex masks the `polygon` command can be used by specifying pairs of coordinates along y and z axes. Each pair of coordinates represents a vertex and, by connecting them, a geometrical figure is created. The shape can be used to define the boundaries of the mask. The choice to use the `polygon` command lies in the necessity to delineate a parametrizable trench structure. Indeed, the definition of this mask exploits the crossed-type trench structure that L connections, T connections and MV share: by varying the vertices of the crossed-shape figure, different logic structures can therefore be generated. An example of the mask for the trench of a MV, composed by three phase wires as inputs and by a three phase wire as an output, is subsequently shown:

```
polygon name= pol segments= {$Mid $StartFirstZone \
$EndTrench $StartFirstZone \
$EndTrench $StartTrenchHorizontal \
$RightTransition $StartTrenchHorizontal \
$RightTransition $EndTrenchHorizontal \
$EndTrench $EndTrenchHorizontal \
$EndTrench $EndTopTransition \
$Mid $EndTopTransition }
mask name=mask_trench polygons = { pol }
```

Having defined the masks, the simulation continues by creating the structure. At first the dielectric substrate is defined by specifying its material and its lower and upper limits of the coordinates along each axis. In this way the volume occupying the region on which the structure will be created is delimited.

```
region HfO2 xlo=x_TopTrenchOxide xhi=x_Bottom ylo=y_Mid
   yhi=y_EndZone3_HorizontalWire
   zlo=z_StartZone1_VerticalWire zhi=z_EndZone3_OutputWire
```

The simulation is then initialized through the command `init`. The deposition steps are performed by specifying the correct mask, the material that has to be deposited and the desired thickness.

```
# Deposition of gold everywhere on the substrate
deposit thickness=$ThicknessGold Gold
# Deposition of dielectric to obtain the arms
deposit thickness= $ThicknessOxideArms HfO2 mask=mask_trench
# Deposition of electrodes on the arms, vertical wire
deposit thickness= $ThicknessGold Gold
   mask=mask_1_electrode_verticalwire
deposit thickness= $ThicknessGold Gold
   mask=mask_2_electrode_verticalwire
deposit thickness= $ThicknessGold Gold
   mask=mask_3_electrode_verticalwire
```

The employed materials belong to the datexcodes.txt, a database provided by Synopys. This file contains a table specifying the names of the materials, their colour in graphical representations and a series of identifiers useful for visualization and post-processing of the data. For example, a material such as SiO_2 will be associated with a label equal to 'Oxide' and a unique colouring, simplifying the interpretation of results. During the simulation, Sentaurus refers to dataexcodes.txt to assign materials to the different regions of the structure that has to be created. Physical properties are not included in the .txt file but they are managed through parameter files that include, for each name appearing in dataexcodes.txt, variables such as bandgap, carrier mobility, thermal properties and dielectric constants. A new material can be added by updating the dataexcodes.txt file and by creating a new .par file. As an alternative, it is possible to use a pre-existing and generic file .par: by overwriting its content, a new material can be added to the simulation. The generic files .par are named Anyinsulator, Anymaterial and Anyseminconductor and, in order to correctly use them in Sentaurus Process, it must be specified the likeness of the used material to another one present in the library of predefined materials:

```
mater add name = Anyinsulator new.like = Oxide
```

In this way, through the keyword `new.like`, the properties of a pre-existing material are specified: the new material inherits the existing properties. In the example case, all physical parameters of SiO2 are adopted by a generic material, named Anyinsulator. Later, during the use of Sentaurus Device, its variables will be redefined, so that a material distinct from oxide will be taken into account. However, for the purposes of constructing the structure, this approximation is for the time being sufficient for a correct implementation of the deposition commands.

Reaching the conclusion of the .cmd file, the following lines are defined:

```
grid remesh
# Reflection
transform reflect left
```

To recreate the grid that subdivides the whole structure in finite elements, `grid remesh` is declared: the command adopts the specified refinements. Then, the structure is reflected with respect to its y-axis: if half of the structure had been created so far, its specularity is exploited, reflecting what has been created and obtaining a trench as required in MolFCN technology.

The rougher initial mesh results in a geometrically accurate representation of the structure in a reduced time, since it is not necessary to adopt an extremely fine mesh for the deposition steps. However, refinement becomes necessary during electrical simulations, which will be executed through Sentaurus Device and which require a much more detailed mesh to guarantee accurate results. Hence, once the structure has been created, the `refinebox` command is used to obtain finite elements with smaller dimensions. Through this remesh strategy, simulation times are shortened as the structure creation steps have already been completed and the more detailed mesh is only applied where

strictly necessary for electrical analysis.

```
refinebox mask=mask_refinement_trench
    extrusion.min=$x_TopElectrode
    extrusion.max=$x_TopTrenchOxide xrefine= { 0.002 0.002
    0.002} yrefine= {0.002 0.002 0.002} zrefine= {0.002
    0.002 0.002} extend= 0.010
```

The refinement is performed in the area exposed to the mask of the whole trench previously defined. It is important to use a different mask from the one implemented during the structure creation: given the reflection that must be performed, the mask used in the deposition steps represent half of the actual trench. The refinement strategy must be nevertheless applied to the whole structure, so a different mask must be used.
`extrusion.min` and `extrusion.max` refer to the coordinates along the x-axis in which the refinement must be performed, since the mask utilization define the coordinates along y and z-axis. `xrefine`, `yrefine` and`zrefine` clarify the mesh dimensions on the different axes at the beginning, in the middle and at the end of the specified region where the remesh must be performed. In order to obtain a fine mesh in every point of the structure, a constant value is chosen equal to 2 nm. Finally, the `extend` key-word extends the mask over its borders by the metric specified afterwards. In this case, the extension is set to 10 nm in order to include in the remesh strategy the upper gold electrodes, whose width is here set equal to 10 nm.

Next, contacts are added by adopting the `contact` key-word. A side-analysis is then performed to compare two possible contact definitions: the box-type contact and the point-type one. In the box-type, the contact is declared as a volume of specified material. In the point-type the contact is defined through a point inside a region. The interfaces of that region take the role of the planar contact while the region it-self is removed: this typology of contact is easily spotted through the graphic interface since the material disappears and gas replaces the region. To explore the two concepts, a brief simulation is performed by defining two conductors, separated by a dielectric box. The choice of contact type in Sentaurus, whether contact box type or point contact are used, is of little significance for electrical simulations. This anticipation concerning electrical simulations, which will be discussed in more detail in the following chapters, is necessary to understand the motivation behind the definition of contacts. The results show that there are no relevant differences from the point of view of either capacitance or electric fields. Therefore, the influence of the contact definition on the behaviour of the device is negligible. Therefore, it is chosen to define the contact through the `box` command, keeping the properties of the metal electrode unchanged and assuring an intuitive visualization of the structure, closer to reality.

Each contact is given a name that represents a link between the structure created through Sentaurus Process and the electrical simulations performed in Sentaurus Device: in the first Synopsys tool, the contact is assigned to a physical region of the simulated architecture, while in the second one the contact will be associated to specific voltage values.

So, it is important to maintain consistency between the used nomenclature in the two Synopsys tools. Therefore, the contacts have been named recursively to reflect their position and function in the structure. The name of each contact defines the part of the structure to which it belongs, in order to clarify whether it is part of the vertical wire, the horizontal wire, the horizontal wire reflected due to the use of structure symmetry, the output region or the transition region. The contact `name` includes too the number of the clock region to which the electrode belongs. There is also a specification that distinguishes the right electrode from the left one. In the wires parallel to the z-axis, the right term refers to the electrodes that extend themselves for the positive y coordinates. For the horizontal wires, perpendicular to the z-axis, the right electrodes are the ones closer to the origin of the axes. This convention allows each contact to be identified clearly. An example is here reported; notice that the material specification must too be declared.

```
contact box xlo=$x_TopElectrode
   ylo=$y_EndTrench_VerticalWire
   zlo=$z_StartZone1_VerticalWire xhi=$x_TopOxide
   yhi=$y_EndElectrode_VerticalWire
   zhi=$z_EndZone1_VerticalWire
   name=Electrode_VerticalWire_1_Right Gold
```

Finally, the command file is concluded by specifying the output file where the structure must be saved.

```
struct tdr= n@node@_presimulation;
```

The keyword `tdr` specifies the format used to save the geometry of the device and the mesh information, necessary for the following electrical simulations.

2.4 Electrical simulations with Sentaurus Device

Once the molecule-hosting structures have been created, the next step consists in their electrical simulation. The goal is to understand the influence of geometrical parameters on the establishment of the electrical clock and driver fields necessary for the functioning of the technology.
Sentaurus Device, a tool from Cadence Synopsys, is therefore employed in order to study the electrical behaviour of the created structures. It receives in input a `.tdr` file containing information on the geometry and on the mesh of the architecture produced by Sentaurus Process. As an ouput, another `.tdr` file is cretaed, containing the results of the electrical simulations.

The simulation flow is managed in the Sentaurus Device command file, which is divided into several sections that define various aspects of the electrical simulation.

The File section specifies the input files needed for the sake of the simulation and the output ones that will be produced. The simulation receives a `.tdr` file containing the geometrical definitions of the structure and a .par file that specifies the physical

parameters of the used materials. The output files are also declared: an ulterior tdr file that will contain the solutions obtained from the physical models adopted (defined through the command `Plot = '<string>'`) and a file indicating output electrical data, such as currents, voltages and charge at the electrodes (specified through the command `Current = '<string>'`) and having the `.plt` extension.

```
    File {
        * Input files
        Grid ="n1_presimulation_fps.tdr"
        Parameter ="@parameter@"

        * Output files
        Plot ="n@node@_des.tdr"
        Current ="n@node@_des.plt"
}
```

Having loaded the device structure into Sentaurus Device, the Device section is declared. It contains the electrode definition and the physics specification, describing the basic properties of the architecture. First, there is the electrode definition, linking the geometrical contacts of Sentaurus Process to the electrical ones of Sentaurus Device. The nomenclature, consistent between the two Synopsys tools, creates an ideal Ohmic contact, where charge neutrality is assumed. Hence, the thermal-equilibrium concentrations of positive charges and the negative charges in the valence and conduction band (the energy levels closer to the Fermi level) are balanced. Therefore, each contact exhibits a resistive behaviour, as required by Sentaurus Device. The following commands ensure that the nodes of the resulting circuit that comes up from the electrical simulation (where every node is associated to each electrode) present a resistance behaviour, by default equal to 0.001 Ω.

```
    Electrode  {
        { Name="TrenchElectrode" Voltage=0.00000
          Material="Gold"}
        { Name="Electrode_VerticalWire_1_Right" Voltage=0.0
          Material="Gold"}
        { Name="Electrode_VerticalWire_1_Left" Voltage=0.0
          Material="Gold"}
}
```

In addition to the names of the contacts and their materials, the initial biases are declared.

In the Physics section, the physical models that will be applied during the simulation are specified, as follows:

```
    Physics {
    Mobility(DopingDependence, HighFieldSaturation, Enormal)
    Fermi
```

```
}
```

The mobility model (`Mobility`) includes the phenomenon of velocity saturation which occurs when charges, due to the presence of a high electric field, reach a maximum value of velocity (`HighFieldSaturation`). Furthermore, the dependence of mobility on the transverse field (`Enormal`) is considered. Finally, the Fermi-Dirac statistic is taken into account (`Fermi`) in the simulation to best describe the behaviour of electrons in the band structure, thus replacing the default model using the Boltzmann statistic.

In the Plot section, the output variables that are needed to be plotted are specified. According to the Physics specifications, the `.tdr` output file will contain the reported parameters (the `/Vector` key-word plots the vector components of the variable instead of only its magnitude):

```
    Plot {
    *--Density and Currents
        eDensity hDensity
        TotalCurrent/Vector eCurrent/Vector hCurrent/Vector
        eMobility/Element hMobility/Element
        eVelocity hVelocity
        *--Band structure
    BandGap
        ConductionBandEnergy
        ValenceBandEnergy
    *--Fields
        ElectricField/Vector Potential
}
```

The Math section contains the needed specifications in order to solve the partial differential equations in an iterative way. For each iteration, a solution is calculated: the simulation ends with the convergence of its results.

```
Math {
        Extrapolate
        Derivatives
        RelErrControl
        Digits=5
        Iterations=100
        Wallclock
        ExitOnFailure
        }
```

With the `Extrapolate` command, Sentaurus Device uses the linear interpolation of the last two solutions that it has obtained in order to find a third solution. This method is adopted when, in the Solve section, two or more `Transient` commands that solve the system are implemented and the ending time of the first `Transient` is the starting time

of the second `Transient`.
The following parameters define the conditions for the approach that is used by Sentaurus to solve the requested physical models. The adopted algorithm, known as Newton's method, finds approximate solutions of non-linear equations in an iterative manner [**?**]. Given the initial guess x_0, the function whose solutions are to be found is approximated by its derivative at the point x_0. This tangent line to the function intercepts the x-axis at the point x_1, resulting in Eq.**??**.

$$f'(x_0) = \frac{f(x_0) - 0}{x_0 - x_1} \tag{2.1}$$

From which it is obtained:

$$x_1 = x_0 - \frac{f(x_0)}{f'(x_0)}. \tag{2.2}$$

The process is repeated over and over, up to a maximum number of iterations (defined by `Iterations` key-word) and until the relative error in Eq.2.3 becomes less than 10^k where k takes the value specified by the variable `Digits`.

$$\varepsilon_r = \frac{|x_{n+1} - x_n|}{|x_{n+1}|} \tag{2.3}$$

Two more settings are present in the Math section: the visualization of the total time needed by Sentaurus to solve the equations (instead of displaying CPU time) by the `Wallclock` command and the `ExitOnFailure` command that terminates the simulation when it can't be found a solution of the physical models.

The structure is then defined at the circuit level in the System section, where the connections between the different nodes are specified, in a SPICE-like way. Each electrode is paired to a node, whose name is now defined. The nodes are named in a similar way as the electrodes but by adding the prefix 'n'. They will be recalled later on, when the `Plot "nodes.plt"` is employed. In this way, the output files `.plt` will contain the information related to each contact. Furthermore, the applied voltages can be declared through the `Vsource_pset` key-word by assuming a voltage source attached to each electrode. In this command, after naming the voltage, the nodes at whose ends the voltage is measured are specified. In the brackets, the voltage typology is declared. As the nodes, the voltages are named in a similar way to the electrodes but with the addition of the prefix 'V'.
Several different definitions of voltages can be implemented: the most simple one is composed by the DC definition of a constant voltage source attached to the contacts. To obtain more complex simulations, a pulse type voltage can be provided: by specifying rising times, falling times and the period, a swinging voltage source, dependent on time, is implemented. Furthermore, Sentaurus Device gives the option to create a voltage source that follows a piece wise linear function: by specifying pairs of times and voltages, great freedom can be achieved in the tensions provided.
In the reported example, the voltages are implemented either by providing a constant value (as in the case of `VTrench`, the voltage supplied to the electrode of the trench) or

by creating a piece-wise linear function.
Indeed, `VVerticalWire_1_Right` and `VVerticalWire_1_Left` display the same behaviour: from the bias condition, the voltage source goes to 3 V at 0.1 ns, maintaining the voltage value until 0.5 ns, when it varies to -3 V with a transient that endures 0.1 ns.

```
    System{
        GHz "GHz" ("TrenchElectrode"=ntrench
        "Electrode_VerticalWire_1_Left"=nvertical1left
        "Electrode_VerticalWire_1_Right"=nvertical1right
)
        Set (ref=0.00)
        Vsource_pset "vtrench" (ntrench ref) {dc=0}
        Vsource_pset "VVerticalWire_1_Right" (nvertical1right
           ref) {pwl= (
                1.000e-10 3.00
                5.000e-10 3.00
                6.000e-10 6.00
                1.000e-09 6.00
)}
        Vsource_pset "VVerticalWire_1_Left" (nvertical1left
           ref) {pwl= (
                1.000e-10 3.00
                5.000e-10 3.00
                6.000e-10 6.00
                1.000e-09 6.00
)}

Plot "nodes.plt" (time() ntrench nvertical1left nvertical1right
   )

}
```

The Solve section is composed by the steps of the electrical simulations, specified in a sequential order. Indeed, each command in the section corresponds to a specific simulation step, such as applying a voltage bias, increasing a parameter or performing a transient simulation. Furthermore, the order by which the steps are defined is important, unlikely in the other sections of the .cmd file.

```
   Solve{
   * EQUILIBRIUM
        Coupled(Iterations=100){ Poisson }
        Coupled{ Poisson Electron Hole Contact Circuit }
        Plot()
```

The base command, `Coupled`, is used to solve a set of equations, specified in the brackets. This is the base command that solves the defined system in an equilibrium situation, by adopting a Newton-like solver. By specifying `Poisson`, the Poisson equation is therefore solved, in order to define the electrostatic potential ϕ of the system, as reported in Eq. 2.4

$$\nabla \cdot (\varepsilon \nabla \phi) = -q\,(p - n) - \rho_{\text{trap}} \tag{2.4}$$

The parameters in the Poisson equation are:

- ε is the electrical permittivity, given by the multiplication of the vacuum permittivity ε_0 ($8.8541878 \times 10^{-12}\,\text{F} \cdot \text{m}^{-1}$) and the relative one ε_r, characteristic proper to each material;
- q is the elementary charge, associated to the electric charge of a single proton. Its value is equal to $1.602176634 \times 10^{-19}\,\text{C}$;
- p and n are the electron and hole densities;
- ρ_{trap} is the charge density associated to the traps (hence the energy levels in the band gap) that could arise due to deposition defects.

The importance of the electrostatic potential equation lies in its linking to the electric field (refer to Eq. 2.5, which determination is the goal of the electrical simulation performed in Sentaurus Device.

$$E = -\nabla \phi \tag{2.5}$$

Next, in the `Coupled` statement, the carrier continuity equations for electrons and holes are solved thanks to `{Electron Hole}` instance. The electronic densities are then computed, following Eq. 2.6 and Eq. 2.7. The Fermi-Dirac statistics is implemented, instead of the Boltzmann one, in order to obtain more accurate physical results: the Fermi-Dirac approach includes the Pauli exclusion principle, which is essential for the fermionic nature of the carriers involved.

$$n = \gamma_n \int_{E_C}^{+\infty} \frac{\sqrt{E - E_C}}{1 + \exp\left(\frac{E - E_F}{k_B T}\right)}\, dE \tag{2.6}$$

$$p = \gamma_p \int_{-\infty}^{E_V} \frac{\sqrt{E_V - E}}{1 + \exp\left(-\frac{E - E_F}{k_B T}\right)}\, dE \tag{2.7}$$

Where $E_{F,n}$ and $E_{F,p}$ are the quasi Fermi energies for electrons and holes and $k_B T$ is the product of the Boltzmann constant ($1.380649 \times 10^{-23}\,\text{J} \cdot \text{K}^{-1}$) and the temperature expressed in kelvin. The γ parameters are constants linked to the Planck constant and the effective mass of electrons and holes. The concept of effective mass is a simplification of the band structure, introduced to describe the variations a particle shows when it is surrounded by other particles: it is the multiplication of the rest mass by a numerical values. To define E_C and E_V, so the energies associated to the extremes of the conduction and the valence bands, Eq. 2.8 and 2.9 are used.

$$E_C = -\chi - q\,(\phi - \phi_{\text{ref}}) \tag{2.8}$$

$$E_V = -\chi - E_{\text{gap}} - q\,(\phi - \phi_{\text{ref}}) \tag{2.9}$$

Where χ is the electron affinity, equal to the difference between the conduction band and the vacuum level (the energy of an electron outside the material) , E_{gap} is the band gap energy (so the difference between the conduction band and the valence band). Finally, ϕ_{ref} is the intrinsic Fermi level of the material with the smallest bang gap, automatically selected by Sentaurus Device. The solutions of the densities n and p are stored in the `eDensity` and `hDensity` variables, defined in the Plot Section.

In the Solve section, after defining the equilibrium solution, the `Transient` command is employed, obtaining a time-dependent solution of the system.
By specifying the starting time and the ending time, the differential equations specified into the Math section are solved taken the specified time constraints. The time-step simulation is performed by declaring the step size, so the minimum (`MinStep`) and the maximum (`MaxStep` extension in time that steps can present. Actual step sizes are determined internally, in agreement with the convergence of the obtained results. The procedure is iterative; if a computation at a time step fails, the duration of the step is reduced until the system can solve successfully the equation.

```
*ANALYSIS IN TIME
    Transient (
            InitialTime=0 FinalTime=2.50e-09
               InitialStep=1.00e-10 MaxStep=2.50e-10
               MinStep=1.00e-10
            Increment = 1)
            { Coupled {Poisson Electron Hole Contact
               Circuit}
            Plot(FilePrefix = "OnePhaseWire_" Time =
               (2.50e-10; 7.50e-10; 1.25e-09; 1.75e-09;
               2.25e-09 ) NoOverwrite )
            CurrentPlot()}
```

The example shows a transient simulation that endures 2.5 ns (as specified by `FinalTime`), where the Poisson equation and the carrier continuity equations are solved. Through the `Plot` command, specifications about the output `.tdr` files are given: the files will have the prefix `OnePhaseWire_` and will be generated at the time instants declared within the parentheses. The `NoOverwrite` option ensures that each time step generates a separate output file, which will not overwrite previous results. These files are distinguished by an increasing numeric value added to the `FilePrefix`.

In the end of the `.cmd` file, a small signal analysis is performed. A file with the extension `.plt` will be generated, containing the terms of the complex admittance matrix. For each term, it is specified the current response (`j`) that a node presents when a small voltage signal (`v`) is applied to another node of the circuit. The relation can be seen in Eq. 2.10, where `Y` is the complex admittance matrix.

$$j = Y \cdot v = A \cdot v + i \cdot \omega \cdot C \cdot v \tag{2.10}$$

The equation is composed of two terms: the first term, $A \cdot v$, represents the conductance response, where A is the real-valued conductance matrix. The second term, $i \cdot \omega \cdot C \cdot v$, stands for the capacitive response, where C is the capacitance matrix. Thanks to these components, it its possible to construct the small signal equivalent circuit, which models the behaviour of the circuit that represents the simulated structure. Indeed, the matrices contains important relations between the nodes of the circuital representation, listed in the brackets of the `Node` command.
Therefore, a `ACCoupled` command, is employed by specifying the range of frequencies at which the simulation must be performed. In the reference example, `NumberOfPoints` is set equal to one: the simulation will be performed at a single frequency, equal to 1 GHz, as it can be seen from `StartFreequency` and `EndFrequency`. The denomination of the output file is declared through `ACExtract` command: the file will contain the frequency, the voltages at the nodes, the entries of the matrices A and C.

Sentaurus Device therefore plays a key role in understanding the physical parameters in the simulated structures. Indeed, the output files generated ensure a good comprehension on how electric fields form and interact with the different regions of the created device, providing crucial information on the design optimization of MolFCN technology. Furthermore, important characteristics such as the band diagram, the carrier densities and the currents can be appreciated through graphical files. Quantitative data can be further extracted, resulting in a comprehensive understanding of the physical phenomena behind the designed structures.

2.5 MATLAB code to parametrize the simulations

After obtaining the results of the equations describing the physical models, it is necessary to think about the optimization of the geometric parameters and the stresses applied to the structures. In order to make the simulations on Sentaurus Process and on Sentaurus Device effective and easily variable, it was therefore thought to parameterize the management files of the simulations, characterized by the extension .cmd. To do this, three MATLAB codes were created, visible in Appendix. Two of them produce the process flow through which Sentauru Process creates different structures, the third one is dedicated to the creation of electrical simulations through Sentaurus Device.

The two files relating to Sentaurus Process differ in the type of geometry that can be created. In the first, a wire can be created that has the upper electrodes shifted with respect to the edges of the dielectric. In this way, the electrodes do not lie on the edges of the structure and the electric fields created by them do not include edge effects that could alter the results. The second MATLAB code, on the other hand, is designed to create modular structures, varying from the single wire to the T connection and up to the Majority voter. In this section, which is more focused on creating complex layouts, the upper electrodes coincide with the beginning of the dielectric region afferent to the wires.
The two MATLAB files are united by their structure: at the beginning of each file is a

section in which the various desired geometric parameters can be set, such as the width of the trench, the height of the electrodes, the spacing between the various clock regions. Each variable is subdivided according to the region to which it belongs (whether it pertains to a vertical wire or a horizontal one) and according to the reference axis. In the file intended for the creation of more complex structures than the single wire, there is also an identifier to select the type of structure to be created. Further degrees of freedom are assumed by the materials used in the simulation and the presence or absence of an adhesion layer between the dielectric structure and the metal electrodes. Materials such as SiO_2, HfO_2 and Al_2O_3 can be implementes. The latter, along with all materials not directly supported by the previously mentioned dataexcodes.txt, requires a customized configuration, introducing in the simulation the generic material named 'Anyinsulator'.
In both MATLAB codes, there are parts where the sums of various coordinates are performed, creating the various sections required for the simulation. The outcome of the MATLAB codes is an output file that is fully functional on Sentaurus Process, given also to the creation of MATLAB functions that implement repetitive parts of the Synopsys code while simplifying the structure of the MATLAB code. An example it is writeParamsToFile, which converts the geometric parameters obtained into commands that can be understood by the Senataurus framework.

To parameterize the electrical simulations, the third MATLAB file was created. By specifying certain parameters in a similar way to what was done in the first two MATLAB codes, it is possible to automatically vary the number of electrodes involved in the electrical simulation, set different voltage values and change the frequency at which the small signal analysis is to be carried out. The result is an output file compatible with Sentaurus Device and capable of correctly analyzing the electric fields required by MolFCN technology.

In summary, the parametrization achieved through the MATLAB codes ensures a high level of flexibility and efficiency, facilitating the research of optimized parameters to make MolFCN technology works correctly.

Chapter 3

One phase wire: single-line

This chapter presents several simulations aimed at analyzing the electrical behaviour of the structure under study, a one-phase wire. Using Sentaurus Process, a basic structure is created: a 14 nm-long wire characterized by a single region of upper electrodes, 12 nm long and located at the center of the structure. A depiction can be seen in Fig. 3.1, 3.2a and 3.2b.
Electrical simulations are carried out using Sentaurus Device to understand how geometric and material variations influence the electric field distribution.

The chapter begins with an analysis of the global electric field, conducted by identifying a representative point within the trench. Afterwards, two types of structures are compared in order to identify the design configuration that best meets the technological requirements in terms of electric field distribution.
Once the most promising structure has been selected, the analysis is deepened by introducing variations in geometric parameters and materials. The results obtained through Sentaurus Device will be complemented by SCERPA, an important algorithm for establishing the functioning of MolFCN technology.

This approach guarantees a complete view of the behaviour of the device and the physical phenomena governing it, establishing a connection between the Synopsys framework and SCERPA and verifying the functioning of the created structure.

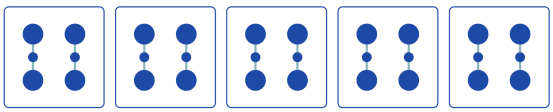

Figure 3.1: Schematic of a single-line wire composed by five unit cells, each characterized by two molecules. The bigger dots correspond to the 'active dots', the smaller ones refer to the Dot 3.

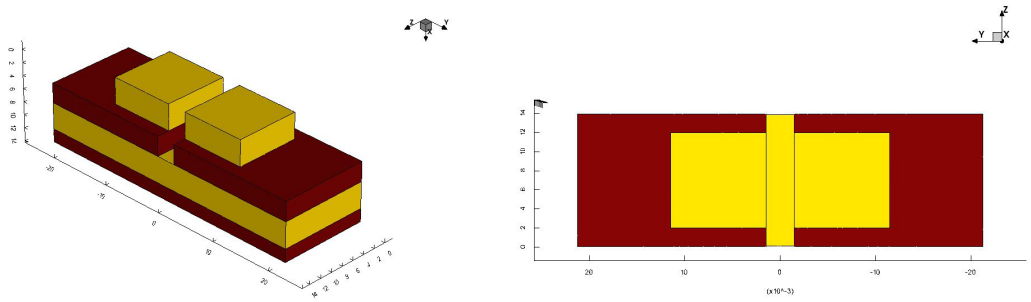

(a) Three-dimensional side view.

(b) Top view.

Figure 3.2: Visualization of an example of single-phase wire, obtained through Sentaurus Process.

3.1 Field analysis at various heights of the trench

The examination of the electric field at different points in the trench provides a comprehensive overview of the spatial variations of the field and an understanding of how it evolves as a function of distance from the electrodes. This subchapter therefore explores the field variations at different heights along the x-axis, identifying the zone where the field reaches an average value, representative of the entire distribution. This mid-value provides an indicator of the overall behaviour of the field in the structure, which will be useful for subsequent analyses that will be performed at this coordinate.

On a theoretical level, a simplified model of the structure can initially be used: the parallel plate capacitor model. According to this model, a uniform behaviour of the field lines can be theorized: the modulus of the field is equal to the ratio of the potential difference between the electrodes to the distance separating them. This situation occurs exactly at the beginning of the trench, where the upper electrode ends and the trench one begins: there, a field value similar to the ideal one will be obtained. Given the difference with respect to the ideal model, it is estimated the the field far from the electrodes won't present the exact same behaviour of the model. Therefore, to begin to study the geometrical variations and their influences on the field sensed in the trench, it is necessary to conduct an analysis where the behaviour of the fields is expected to be as close as possible to the ideal model: at the points of the trench nearer to the electrodes.

The structure chosen as a case study has a 3 nm wide and 3 nm high trench, the electrodes are made of gold while the dielectric structure is made of silicon dioxide. The applied voltage to the upper electrodes is set to -3 V, while the trench electrode is connected to ground. Through Sentaurus Device, the structure is first divided into sections parallel and transverse to the main axes of the reference system. The architecture is initially sectioned for y = -1.4 nm, resulting in a plane spanning the x and z axes. The y-coordinate is chosen in such a way as to analyze the field at points where the trench electrode is almost parallel to the upper electrode. In those points, the ideal parallel-plate capacitor model can be used to estimate the field values, ensuring the correctness of the results.

The upper left electrode extending on the negative y is taken as a reference. Since the two upper electrodes will present a symmetric behaviour, it is not necessary to study both points.

The left electrode spans from y = -1.5 nm to y = -11.5 nm, while the trench extends from y = -1.5 nm to y = 1.5 nm: the point where the structure is sectioned is in the trench but near its borders. A representation of the section performed is highlighted in green in Fig. 3.3.

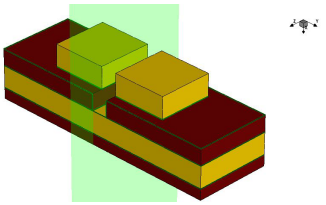

Figure 3.3: Representation of the first cross-section performed at y = -1.4 nm.

The structure is then dissected again to extract the electric field values at various heights of the trench (Fig. 3.4).

The trench extends from x = 4 nm, given the 4 nanometers thick upper electrodes, to x = 7 nm. Forty cuts are therefore made between these two coordinates, excluding the extremes: the sections span from x = 4.1 nm to x = 6.9 nm. In this way, the surface of the trench electrode is not included in the analysis since the interesting region is above. Furthermore, by excluding the point located at x = 4 nm, the area that divides the two upper electrodes is ignored.

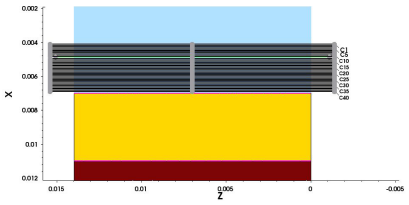

Figure 3.4: Representation of the forty cross-sections performed along the x-axis.

In Fig. 3.4 the forty sections at different heights can be appreciated in the region highlighted by the light blue color: the air that fills the trench is the medium where the electric fields must be studied. The gold and dark red colours refer to the trench electrode and the substrate beneath it, which can be seen from the section.

The obtained electric fields describe the clock fields along the z of the structure, characterized by 10 nm of electrodes placed in the center of a 14 nm long dielectric structure. Fig. 3.5 represents the clock field data at different specific heights in order to capture the local variations induced by the proximity of the electrodes. At different values of the trench height, the electric fields reported in Fig. 3.5 show a good consistency in their behaviour: the decrease in the field at the ends of the structure is caused by the distance from the studied points of the upper electrodes, which extend from z = 2 nm to z = 12 nm. At these coordinates the field transitions rather quickly to constant values, the modulus of which varies according to x. The spikes that can be seen at z = 2 nm and z = 12 nm, so at the extremes of the upper electrodes, are imputable to edge effects. Two important deviations from this pattern are the clock field at x = 4.10 nm (the darkest

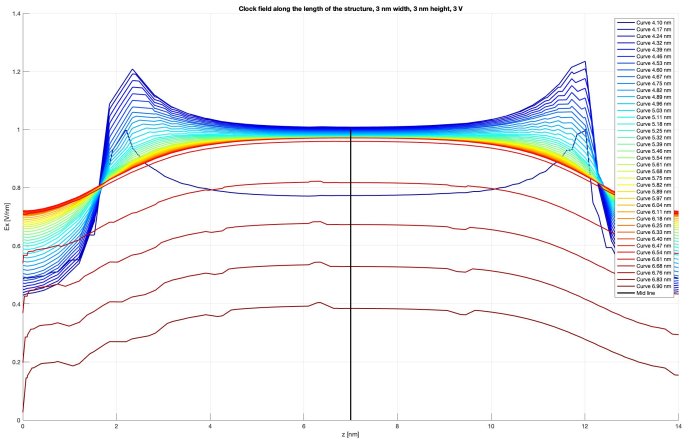

Figure 3.5: Electric field distribution along the z-axis at different heights of the trench.

blue curve) and the clock fields from x = 6.61 nm to x = 6.9 nm (the darkest red curves). The curves, clearly distinguished from the others, refer to the extremes of the trench: they are respectively the points nearer to the upper electrode and to the trench one. Their values are due to the vicinance to the electrodes.
In order to explore these electric field variations along the height of the trench, the section is sectioned at the center of the wire, at z = 7 nm. In this way, the analysis moves away from the ends of the upper electrodes where, due to the absence of electrodes, the electric field does not show uniform values but spikes. The black line in Fig. 3.5 emphasizes where the wire is sectioned, resulting in an analysis that correlates clock field values to various x values. Confirming the theoretical expectations, Fig. 3.6 shows that, at points away from the electrodes, the electric field is uniform and almost exactly coincident with what is predicted by the model of the parallel plate capacitor, recalled in Eq. 3.1.

$$E = \frac{V}{d} = \frac{3\ V}{3\ nm} = 1\frac{V}{nm} \tag{3.1}$$

The average value that the electric field assumes between x = 4.1 nm, where the upper electrodes end, and x = 6.9 nm, where the trench electrode then starts, is equal to 0.9759 V/nm, validating the theoretical results. Approaching the trench electrode, the clock field in Fig.3.6 exhibits a steep decrease, until its minimum value, exhibited at x = 6.9 nm, equal to 0.384 05 V/nm. Approaching the upper electrode: at x = 4.1 nm, the clock field reaches 0.7728 V/nm, reducing by nearly 30% with respect to the maximum values. To explain these field decreases, it must be considered how electric fields on the surface of metals vanish due to the balance of charges in them. Given this constraint, an electric field gradient is expected in the proximity of the electrodes. This phenomenon could be intensified by the discretization of the structure studied by Sentaurus Device, which solves the equations through a finite element characterization. The obtained results show two distinct regimes, one uniform, characterized by electric field uniformity, and one

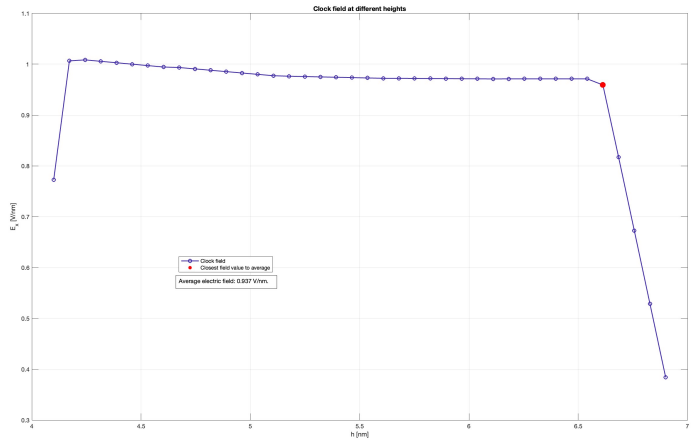

Figure 3.6: Electric field values sensed at different heights of the trench. The studied range spans between x = 4.1 nm and x = 6.9 nm, 0.1 nm from the electrodes. The red point refers to the coordinate at which the average electric field can be measured.

of decay. The mean value of the electric fields is affected, reducing to 0.937 V/nm. The height for which a field value close to the mean value is experienced is at x = 6.613 nm, 0.387 nm from the trench electrode.
A further analysis is then carried out by sectioning the structure in a similar manner as did before but restricting it to a spatial analysis between x = 5.9 nm and x = 6.9 nm. The motivation behind this choice lies in the size of the molecules that will be placed in the trench: being characterized by a height of approximately one nanometer, the region immediately above the trench electrode will be the one of greatest interest. The results are depicted in Fig. 3.7. The obtained values, referring to forty different heights, present an average value of 0.888 V/nm. The important conclusion is that the height at which the clock field is closer to its average value is at x = 6.644 nm, hence 0.3560 nm from the trench electrode. In conclusion, it can be affirmed that the height that best represents the development of the electric clock fields in the trench electrode is 0.4 nm above the trench electrode. It therefore follows that successive electrical simulations will be performed at this coordinate, which can provide an overview of the trend of the entire trench.
This value is also consistent with the height of approximately one nanometer of the molecules that will be placed in the trench: analyzing the electric fields at half their height permits a representative study of their behaviour when influenced by a field.

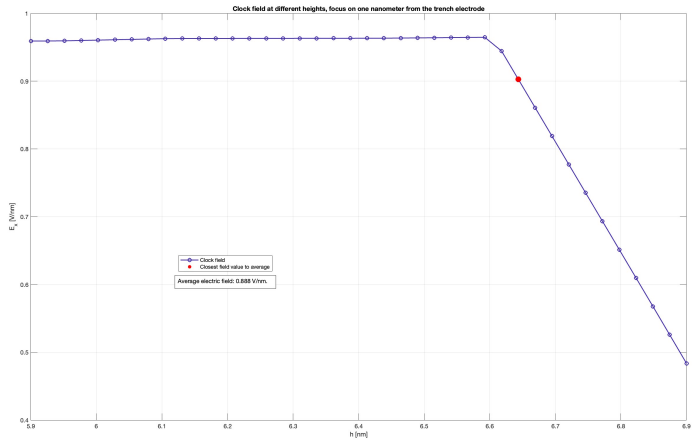

Figure 3.7: Electric field values sensed at different heights of the trench, zooming on the nanometer above the trench electrode. The studied range spans between x = 5.9 nm and x = 6.9 nm, 0.1 nm from the electrodes. The red point refers to the coordinate at which the average electric field can be measured.

3.2 Effects of trench electrode geometry on field distribution

Once the x-coordinate at which to perform the analysis concerning electric fields was found, the analysis continues by trying to understand how electrodes influence electric fields. This study is not only theoretical but also looks to the future, considering the practical realization of the devices. Indeed, it is essential to consider, already at the design stage, the influences of geometric variations and the feasibility of the proposed structures.

The work therefore begins with the single-line wire proposed by F. Ravera et al. (2024) [45], which introduces a molecule-hosting structure characterized by precise geometrical parameters. This structure, with a trench at whose sides two electrodes are located, has a lower electrode that fills the trench it-self. The idea of taking this structure as a reference is not random, since it represents an already theoretically validated basis and it is therefore an excellent starting point.

The structure, denoted from now on as *Structure A*, is then created through Sentaurus Device, initially performing a dielectric substrate deposition and then an etching operation to create the trench. The creation of the device is then finished by deposition of the gold electrodes by properly defined masks. In this way, the structure visible in Fig. 3.8a is obtained. 3.8a is obtained. However, considering the practical aspects of fabrication, *Structure A* presents significant limitations. In particular, the etching operation required to define the trench demands an extremely high level of resolution, which

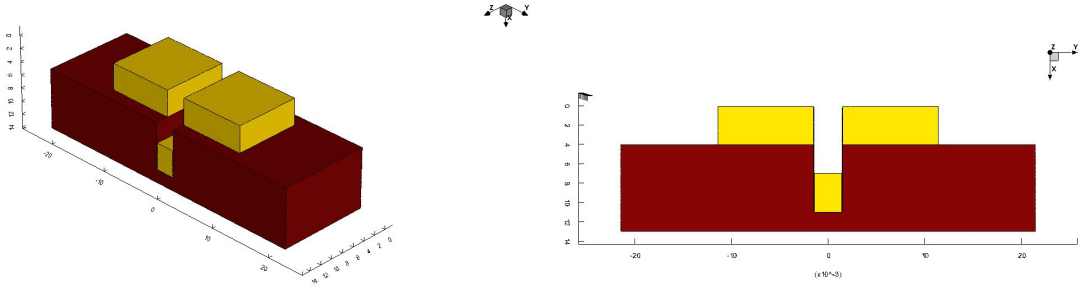

(a) Three-dimensional side view. (b) Lateral side view.

Figure 3.8: Single-line one-phase wire, structure A.

may be difficult to achieve with currently available fabrication technologies. This critical aspect has led to the proposal of an alternative structure, which can be realized without etching steps.

The new structure, from now on referred to as *Structure B*, is fabricated by starting with a dielectric substrate. A layer of gold is then deposited over the entire surface of the substrate: the whole layer will take the role of the trench electrode. At this point, using appropriate masks, two dielectric structures are deposited, leaving an area of separation that constitutes the trench. The creation of the structure is then concluded by the deposition of the upper electrodes. A representation is shown in Fig. 3.9a and Fig. 3.9b. This approach greatly simplifies the required fabrication steps, avoiding etching operations: structure B is therefore the most promising solution for implementing MolFCN technology. To conduct a more precise comparison of the two structures, their functionality

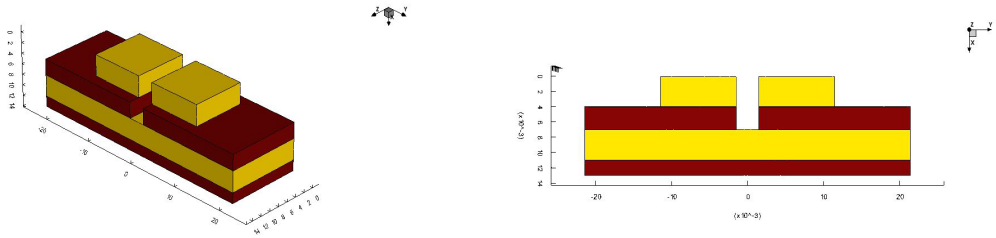

(a) Three-dimensional side view. (b) Lateral side view.

Figure 3.9: Single-line one-phase wire, structure B.

is then analyzed. The two structures are therefore studied in exactly the same way to examine in detail the electric fields generated by the electrodes.

To ensure a fair comparison between *structure A* and *structure B*, most of the geometrical parameters are kept the same, with the exception of the size of the trench electrode. As a result, both one phase wires have a trench that is 14 nm long, 3 nm wide and 3 nm high. The top electrodes in both cases are 10 nm long, positioned centrally with respect

to the length of the dielectric structure. The voltage applied to the top electrodes is -3 V while the trench electrode, regardless of its size, remains connected to ground.
In this manner, the variations in the analyzed electric fields cannot be attributed to any other effect than the geometry of the trench electrode.

The structures are the sectioned in the same points: at first, a cut is performed at the height identified in the subchapter 3.1, hence at x = 6.6 nm, 0.4 nm from the trench electrode. Next, ten cuts are applied along the y-axis, varying from y = -1.5 nm to y = 0 nm, therefore varying from the left end of the trench to its center.

The analysis is conducted by considering only one half of the trench since the structure, being symmetrical, exhibits a similar behaviour in the half of the trench not considered. This choice reduces the complexity of the analysis, facilitating the interpretation of the results.

Fig. 3.10 and Fig. 3.11 show the trend in the two structures of the electric fields in the direction of the x-axis, named **clock fields**. The electric fields show in both wires a reduction in their value in the regions where the upper electrodes terminate, between z = 0 nm and z = 2 nm and between z = 12 nm and z = 14 nm. However, the behaviour of the fields in the two structures, apart from this similarity, are significantly different.

In *structure A* (Fig. 3.10) no perfectly parallel electrode zones are observed. Furthermore, the size of the trench electrode causes a greater proximity between trench and trench electrode edges. This aspect affects the distribution of the electric field along the x-axis: Fig. 3.12a, in which the electric field lines can be distinguished, confirms this phenomenon. At the edges of the electrodes the distribution of the field lines that connect the conductive surfaces creates a non-uniform field, not directed parallel to the x-axis. In fact, Fig. 3.12a shows a diagonal field behaviour with respect to the direction connecting trench and upper electrodes. This phenomenon, named fringe effect, is also clearly visible in Fig. 3.10 which shows the trend of the clock fields, the fields along the x-axis, in the ten sections of the structure. The values at the borders of trench are lower than expected by the parallel-plate capacitor model.
The electric fields in *structure A* are reduced for the y-coordinates near the ends of the trench (the dark blue curves visible in Fig. 3.10) and this phenomenon is imputable to fringe effects. As the center of the trench is approached, the values of the electric fields increase as the fringe effects become less persistent. However, the electric field values decrease again as the distance between the electrodes in the center of the trench is maximized.

On the other hand, in *structure B* (Fig. 3.11) the bottom electrode, occupying the entire structure, has regions that are parallel to the upper electrodes: in these areas the structure can be approximated through the model of the parallel plate capacitor. Consequently, the electric field in these regions is uniform and consistent with what the theoretical model predicts. This is further confirmed by the field lines shown in Fig. 3.12b

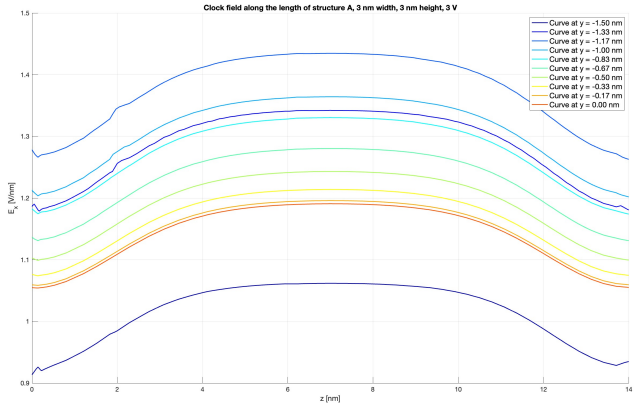

Figure 3.10: Clock fields along the length of structure A.

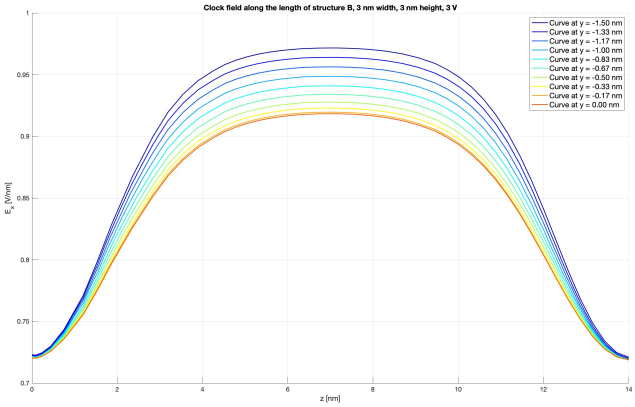

Figure 3.11: Clock fields along the length of structure B.

(the number of vectors shown in the figure does not correspond to the total number: the density is deliberately decreased manually in order to obtain more easily interpretable results). It follows that the points closest to the boundaries of the trench, where the upper and lower electrodes are closest to being parallel, present an electric field similar to the field obtained from the equation of the parallel plate capacitor (Eq. 3.1 given in the sub-chapter 3.1 where the electric field is given by the ratio between the potential difference between their electrodes and the distance between the electrodes). As the center of the trench is approached, the distance between the upper and lower electrodes increases, causing a decrease in the electric field value. This phenomenon is consistent with the inverse relationship between electric field and electrode distance. At the center of the length of the structure, specifically at z = 7 nm, the maximum value of the field is equal to 0.975 V/nm. At the same point, the minimum clock field measures 0.918 V/nm: the field reduction is equal to 0.0570 V/nm, so the reduction with respect to the maximum value is equal to 5.85%, an acceptable difference.

A further element of analysis concerns the **transverse fields** (the field components

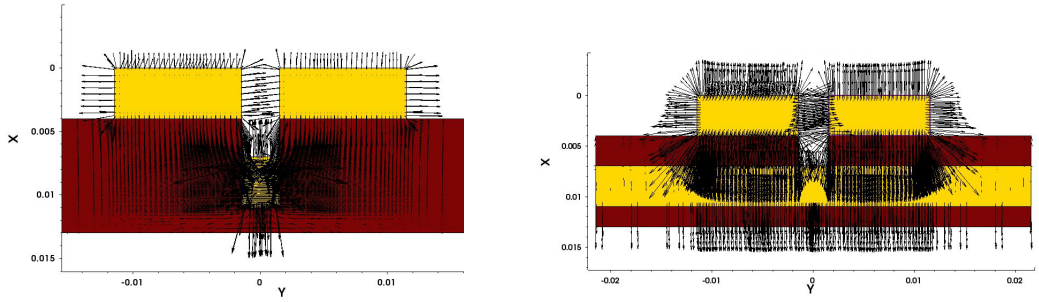

(a) Visualization of electric field lines in structure A.

(b) Visualization of electric field lines in structure B.

Figure 3.12: Visualization of electric field lines, representing their direction and intensity. Their density has been reduced in order to obtain more interpretable results.

parallel to the y-axis, referring to the width of the structure). Fig.3.14, referred to structure B (the architecture characterized by an entire layer of trench electrode) shows the reduced values that the transverse fields present. This phenomenon is due to the strong vertical directionality that the capacitor model with parallel plates well describes. In addition, the symmetry of the structure allows an overlap of the fields produced by the electrodes so that, at the center of the trench, the transverse fields add up and cancel each other out. The two pair of electrodes (the right upper one paired with the trench one and the left upper one paired with the trench one) in fact generate fields that, at the central point of the trench, have the same modulus (since the distance between the electrodes and the applied voltage is equal) but opposite direction. Consequently, the transverse field value for $y = 0$ is zero.

In *structure A* the transverse fields too cancel themselves in the center of the trench, as it can be noticed in Fig. 3.13. But, unlike in structure B, the transverse fields far from $y = 0$ are now not negligible: the blue curves reach $1\,V/nm$ too.
In fact, the electrodes in *structure A* are displaced one from the other and they are no longer parallel: there is a shift in their horizontal coordinates (along the y-axis). This shift induce the creation of field components along y. This phenomenon is critical in MolFCN technology, since it leads to a localization of the charge on a precise part of the molecules placed in the trench. The force applied by the transverse electric field, favouring one binary encoding over another, could result in the wrong propagation of information in the one phase wire. This situation must therefore be avoided.

In conclusion, the fact that *structure B* has very low field values along the y-coordinate is an enormous advantage over *structure A*. This aspect is even more relevant if the geometrical parameters of the trench are varied: by increasing the width of the trench, it is possible to create multi-line systems where each wire accommodates more than one

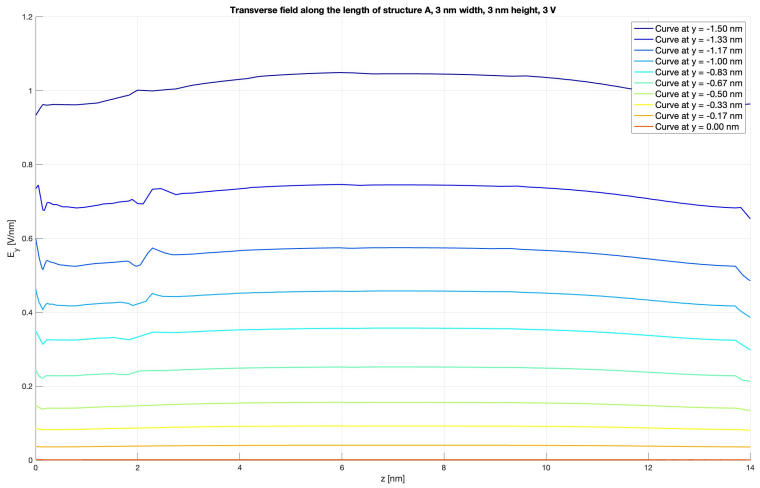

Figure 3.13: Transverse fields along the length of structure A.

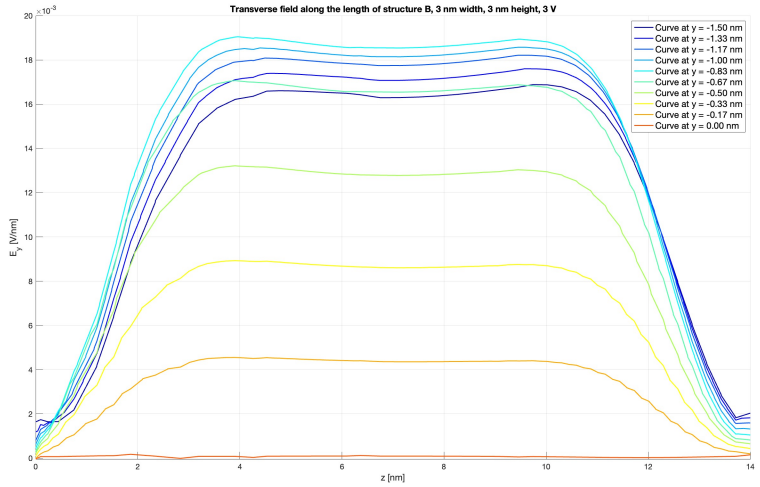

Figure 3.14: Transverse fields along the length of structure B.

molecule along the y-axis. This aspect will be discussed in the next sub-chapters.

The analysis conducted in this sub-chapter shows how the geometry of the trench electrode significantly influences the electric field distribution in the trench.
Structure B, due to the presence of parallel regions between the electrodes, ensures a uniform field distribution in which transverse fields are reduced. The minimization of the transverse fields avoids undesired charge localization in the molecules that will be placed in the trench to implement MolFCN technology.
Furthermore, *structure A* exhibits significant edge effects and stronger transverse fields

that could compromise the device operations.
In addition to these results, the feasibility of the practical realization of the structures must be considered. In this aspect too, *structure B* is better than *structure A*, avoiding etching operations with very high resolutions. Consequently, *structure B* emerges as the most promising solution for the technological implementation of MolFCN. In the remaining part of this thesis, the analysis will therefore focus on *structure B*.

3.3 Single line: geometrical variations

Once the structure promising to efficiently implement MolFCN technology has been identified, the next step consists in the understanding how the structure works when varying its geometrical parameters. The aim, considering a future practical realization of the devices, is to analyze the electric fields in the trench and understand how they vary depending on the applied geometrical parameters. This work therefore provides an overview of how it is possible to create functioning and efficient systems with good production feasibility.

In the present chapter, it is studied how the height of the trench affects the distribution of electric fields along the x-axis (**clock field**) and along the y-axis (**transverse field**). The trench width is kept at 3 nm for the time being. This parameter is deliberately kept very small to ensure that the molecules are arranged in the most orderly configuration possible, avoiding misalignments. Hence, a wire must present molecules arranged in an orderly line, always maintaining -ideally- the distance between them: in this way, there will be no points on the molecules where it will be more likely to find localized charges than others.
Therefore, the control of the molecular position is a task as complex as it is fundamental to ensure the correct propagation of information.
Keeping the trench width fixed, the variation of another degree of freedom is explored: the trench height. The expected result is that, by varying the distance between the upper electrodes and the trench electrode, the electric fields will vary in a inversely proportional way.
The geometrical parameters, with the exception of the trench height, remain constant to the ones set in Chapter 3.1. The single-phase wire is 14 nm long, the upper gold electrodes present a width of 10 nm. Along the z-axis, the electrodes are 10 nm long, 4 nm thick; they are placed in the center of the dielectric structure. The upper electrodes extend from z = 2 nm to z = 12 nm. The dielectric, SiO_2, extends 10 nm beyond the electrodes. Along the y-axis, therefore, there is an overall structure 43 nm wide, the center of which is exactly in the middle of the trench.

In order to carry out the analysis, the electrical simulations performed through Sentaurus Device are supported by the use of Self-Consistent ElectRostatic Potential Algorithm (SCERPA), a powerful tool that analyzes charge localization in MolFCN-based circuits in an iterative manner. SCERPA is implemented through a set of MATLAB scripts that, based on results from ab-initio simulations, establish the electrostatic potentials present

between the system's charges, the key principle responsible for the different charge localizations in the molecules of the system. In this way, complex systems are precisely analyzed, avoiding the computational burden that would characterize a system's resolution based solely on ab-initio simulations.

The electric fields obtained by solving the Poisson equations in Sentaurus Device are then entered into SCERPA. In this way, it is possible to verify whether the field distributions obtained are sufficient to localize the charges in the molecules in the desired manner, ensuring a correct propagation of the information.
This work therefore for the first time offers the possibility of linking a simulation of a physical structure to the analysis of the molecular behaviour of the MolFCN technology.

The height of the one phase wire taken as a case study is varied, analyzing the electric field behaviour at a trench height of 3 nm, 6 nm and 9 nm. In this way, it is possible to understand not only the connection between physical structure and molecules, but also to identify a trend that relates geometric variations to electric field distributions.

3.3.1 The approach to the analysis: introduction to SCERPA

The structure analyzed in Chapter 3.1 is here reported. This time, the analysis focuses on the electric field values at the center of the trench. The structure is then sectioned at a height of 0.4 nm from the trench electrode. A second section is carried out perpendicular to the other, for y = 0, resulting in a graph showing the clock electric fields (along the x-axis) as the length of the device (extending along the z-axis) varies. The obtained field presents minimum values at the extremes of the structure, where the absence of the upper electrodes exerts its influence.

The clock field values are then sampled in order to obtain a value every nanometer of the structure. In this way, a clock field value is assigned to each molecule in the wire, placed approximately one nanometer apart one from the other. Sampled point corresponding to the extremes of the structure (whose extension is equal to 14 nm) are excluded, resulting in thirteen electric field values. These values are then introduced into the SCERPA environment.

In SCERPA, the clock field values are introduced in a matrix form: each value is associated with a molecule in the circuit, so that each component receives information about the field that is affected by. In addition to importing the values obtained from Sentaurus Device, certain parameters must be selected for SCERPA in order to be able to calculate the interactions between the molecules. First of all, the type of circuit must be defined, specifying the width of the trench taken into account and declaring whether it is single-line or multi-line (a trench that can host several molecules side by side, along the y-axis). In addition, it is necessary to specify the number of molecules in the circuit, at which it must be added the contribution given by the initial driver molecules, capable of providing a binary value to subsequent MolFCN cells. In addition, it is possible to select the type of molecule that is included into the circuit. In this case, oxidized Bis-ferrocene

is implemented, characterized by a counter-ion to preserve the charge neutrality of the molecule. The oxidation event of the molecule is achieved through the removal of an electron by a process of electrochemistry [**?**].
Once the structure-related parameters have been defined, SCERPA iteratively establishes the electrostatic potentials between the molecules, localizing the free charge in each molecule depending on its surroundings. The charge will concentrate more on one of the two dots to maximize its distance from charges located on other molecules. The electric clock field has the important role of enhancing binary propagation by concentrating the charge at the top of the molecule where the two active dots are located.

To verify that the system set up on SCERPA works correctly, initial simulations are performed by imposing constant electric field values in the structure.

Five separate simulations are carried out, applying electric fields ranging from $-2\,\mathrm{V/nm}$ to $2\,\mathrm{V/nm}$, with $1\,\mathrm{V/nm}$ increments. The results are shown in Fig. 3.15, 3.18, 3.19, 3.20 and 3.21. For each voltage value, a representation of the wire is reported, where each bright dot corresponds to a localized charge in a molecule. Hence, to identify a MolFCN cell, a pair of neighbouring bright dots must be considered. Furthermore, the figures include a depiction of the charge separation in each molecule (identified by a numerical value) for the system. If this graph reports an high value it means a precise positive charge localization on the active dots is occurring; on the contrary, if the value is low, the active dot taken into account has almost no charge at all and a dark spot will be reported in the wire representation.

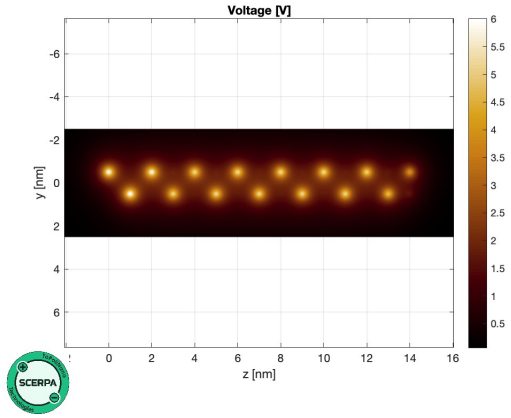

(a) Visual representation obtained by SCERPA of the localization of positive charges in the wire.

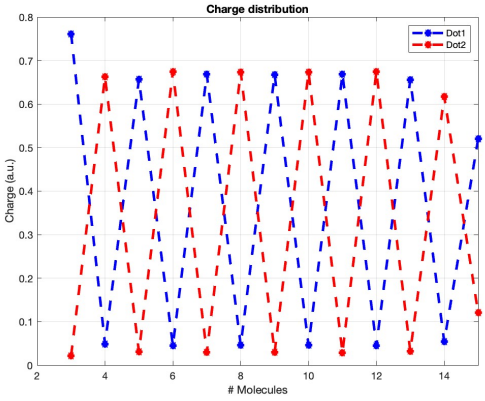

(b) Charge distribution along Dot 1 and Dot 2, the active dots, for each molecule of the wire.

Figure 3.15: Charge distribution along a single-line one-phase wire when no clock field is applied.

Fig. 3.15 shows that the logic information is propagated through an alternating sequence of bright spots, indicating where the positive aggregated charge is located in each

molecule, in response to the influence of the driver and the charge placed nearby. By grouping the molecules in pairs, starting with the driver (identified on the left of the wire by the brightest spots), the unit cell characteristic of MolFCN technology is obtained, encoding a binary value. Notice that, given the configuration of the geometry, the number of molecules in the one phase wire is odd: the geometry of the structure creates an **inverter** gate.
Figure 3.15 shows the values of the aggregate charges at the two active dots, the sum of which should give the unit value. The amount of charge missing from the unitary value is located in Dot 3, not shown in the figure. Since no electric field is applied, the charge is not exiled in the upper part of the molecule where the two active dots are located. Instead, charges tend to partially redistribute on Dot 3 in order to maximize their spatial separation as much as possible (due to columb repulsion). It follows that, if no clock field is applied, an active dot on which the charge is localized does not have values close to unity but settles at 0.7 a.u.: the charge separation between the dots of a molecule is sufficient to guarantee propagation of information but it is not maximized. In addition, the last molecule has a lower charge separation. This phenomenon, known as **fading effect**, is caused by the absence of two first neighbours at the last molecule in the wire which, being affected by only one first neighbour, will exhibit a reduced charge separation. The coulomb repulsion will not be sufficient to induce a separation as occurs in the molecules of the central portion of the wire.

Hence, the one phase wire is capable of correctly propagating binary information even in the absence of a clock field. This behaviour is due to the intrinsic properties of the chosen molecule, bis-ferrocene: its trans-characteristic is particularly favourable for achieving a correct charge localization thanks to coulomb repulsion. However, it must be emphasized that, by increasing the length of the wire, molecules further away from the driver molecules could spontaneously assume an improper charge localization, without waiting for the correct polarization to propagate in the circuit in a certain time. If the length of the wire is increased, therefore, the operation of the wire without applied clock fields could be compromised.
This would particularly occur if the driver molecules were polarized in such a way as to assume the binary value '1'. Observing the Voltage Aggregated Charge Trans-characteristic (VACT) of bis-ferrocene in the case of zero clock applied (Fig. 3.16), it is indeed reported that one of the two active dots is slightly favoured in terms of localization. In the absence of input voltage, the charge distribution between the two dots is not perfectly symmetrical: dot 1 shows an aggregate charge of 0.4959 a.u., while dot 2 shows a value that settles at 0.4423 a.u..
Input voltage is evaluated by integrating the electric field that influences the molecule.

This slight asymmetry implies that, under conditions of no external input, the molecule tends to stabilize by localizing the charge on dot 1. This unbalance implies that, under conditions of no external input, the molecule tends to stabilize by localizing the charge on dot 1.
Neighbouring molecules will accordingly arrange themselves in such a way as to minimize electrostatic potentials, creating a cell containing a binary information. However, as one configuration is more likely, the cell will more often spontaneously represent the binary value '0'. Having a wire in which one of its cells spontaneously polarizes without waiting for driver information, if a '0' has to be propagated, the information contained in the wire will not be compromised, given that the terminal molecules will assume spontaneously the same binary value.

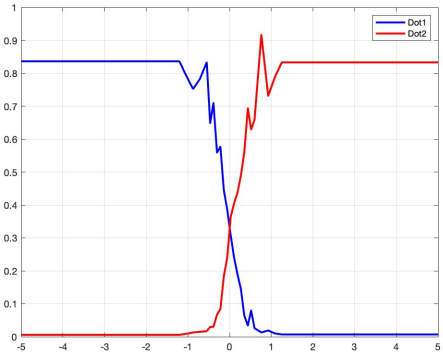

Figure 3.16: Voltage Aggregated Charge Trans-characteristic (VACT) of the oxidized bis-ferrocene with no clock field applied.

On the contrary, if the driver value is set to '1', the cell encoding the binary value '0' would be an obstacle to the propagation of the information, interrupting it.

The phenomenon of **spontaneous polarization** occurs more frequently in systems characterized by a lot of molecules, where the propagation time from the driver to the other extreme of the wire becomes considerable. It occurs more likely at the ends of the wire, where the border effect is more important. There, the final molecule is not affected by two surrounding molecules but only by one molecule. Hence, the charge separation is reduced, negatively affecting the end portion of the wire.

The solution to this problem lies in the application of a **negative clock field**. Indeed, by subdividing the system in more clock regions and applying a negative clock field at the farthest zones from the driver, the molecules at the end of wire are inhibited from localizing the charge in one of the two active dots. Therefore, the binary information can propagate in the wire without spontaneous polarization phenomena occurring.
Once the binary value has reached the zone where the negative clock field is applied, the field is removed and the charge is able to move from the lower part of the molecule, where it was confined by the negative clock field, to the upper part, where the two active dots are. This phenomenon is depicted in the VACT of the bis-ferrocene molecule in the case of the application of a negative clock field. Particularly, Fig. 3.17 shows the behaviour of the aggregated charge when $-2\,\mathrm{V/nm}$ are applied. Notice that, even by exerting on the molecule a considerable input, the maximum value of aggregated charge corresponds to 0.07 a.u.. According to the value of the negative clock field, different situations can occur. If the applied electric field is equal to $-1\,\mathrm{V/nm}$, its influence is not negligible. However the driver molecules still succeed to localize correctly the charge up to the first molecule

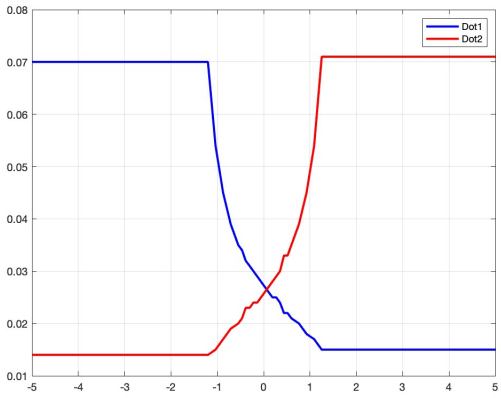

Figure 3.17: VACT of oxidized bis-ferrocene at a clock field equal to -2 V/nm.

of the wire, as it can be seen in Fig. 3.18. From there on, the reduced influence of the driver is not sufficient to counteract the clock field. Even in the first molecule, most of the charge is found in the non-active dot, referred to as Dot 3. Indeed, even in the first molecule, more than 60% of the total charge is located on Dot 3. This value is found by adding up the charges found on Dot 1 and Dot 2 and considering that the total sum of the charges on the three dots of each molecule must give a unit value. The propagation in the wire is therefore inhibited: this phenomenon is depicted through the absence of bright spots in Fig. 3.18. The charge is not localized only on one of the two active dots and two lightly bright spots are present for each molecule: this phenomenon is referred as aberration.

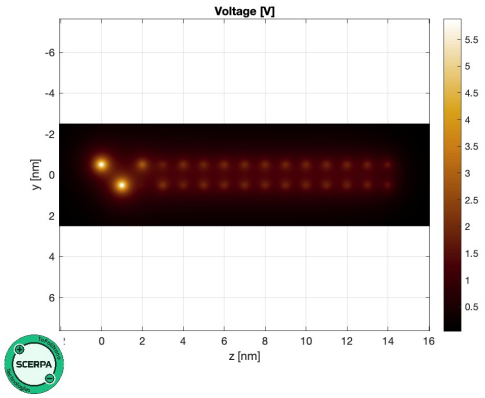

(a) Visual representation obtained by SCERPA of the localization of positive charges in the wire.

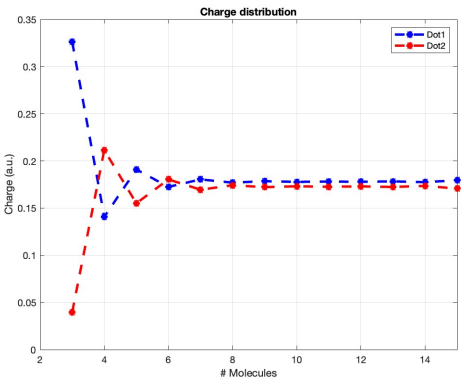

(b) Charge distribution along Dot 1 and Dot 2, the active dots, for each molecule of the wire.

Figure 3.18: Charge distribution along a single-line one-phase wire when every molecule senses a clock field equal to -1 V/nm.

The application of an electric field with a higher absolute value (−2 V/nm, Fig. 3.19) accentuates this phenomenon: the localization of the charge is quite exclusively on the third dot, preventing the information propagation. The absence of bright spots in Fig. 3.21 depicts a scenario where the active dots present no positive charge at all, since it is located on the inferior part of the molecule, where the third dot lies. By exiling the charge on Dot 3, the charge alternation on Dot 1 and Dot 2 can't occur.

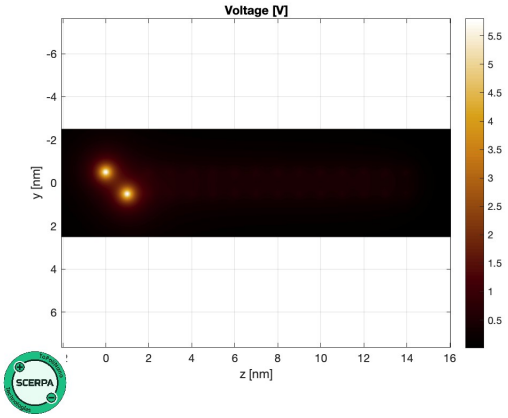

(a) Visual representation obtained by SCERPA of the localization of positive charges in the wire.

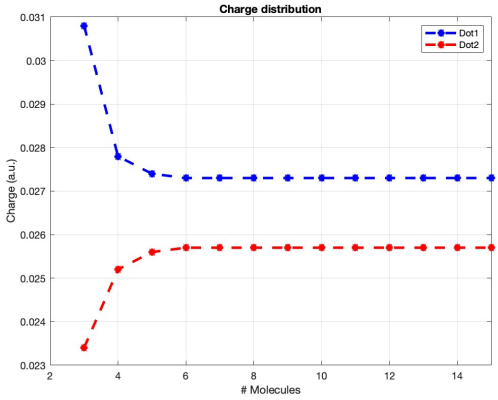

(b) Charge distribution along Dot 1 and Dot 2, the active dots, for each molecule of the wire.

Figure 3.19: Charge distribution along a single-line one-phase wire when every molecule senses a clock field equal to -2 V/nm.

On the contrary, the application of a positive clock field (1 V/nm, reported in Fig. 3.20 or, even better, 2 V/nm, in Fig. 3.21) helps to obtain greater charge separations, easing the information propagation. Under these conditions, the aggregate charge on Dot 1 and Dot 2 approaches the unit value: the distribution is well defined along the entire wire. The fading effect can't be avoided since it is a natural occurring phenomenon, but a visible difference can be appreciated between Fig. 3.20, where 1 V/nm is applied and the charge localization is not uniform along the molecules of the wire, and Fig. 3.21. There, 2 V/nm are applied, and the charge behaviour is more constant along the wire.

The described phenomenon is in agreement with the VACT in the case of a positive clock field applied to the system. In the absence of applied voltage, the charge distribution between Dot 1 and Dot 2 is still not perfectly symmetrical. This behaviour is intrinsic to the chemical properties of the molecule itself, deriving from its electronic structure, and it can't be therefore avoided, event by applying an intense clock field. Nevertheless, the aggregated charge reports a good separation between the two active dots, providing a stable information propagation in the wire.

The importance of the clock field thus emerges from these results. While it might initially appear to be an unnecessary element for the propagation of information, it turns out to be the very heart of the structure, capable of enabling the technology to function, especially in the case of complex systems.

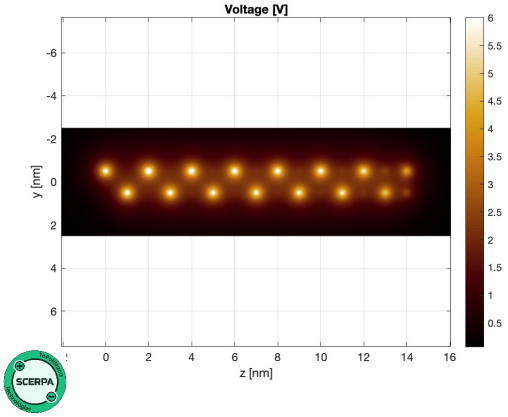

(a) Visual representation obtained by SCERPA of the localization of positive charges in the wire.

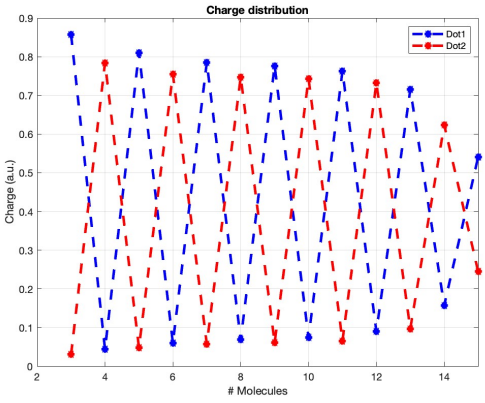

(b) Charge distribution along Dot 1 and Dot 2, the active dots, for each molecule of the wire.

Figure 3.20: Charge distribution along a single-line one-phase wire when every molecule senses a clock field equal to 1 V/nm.

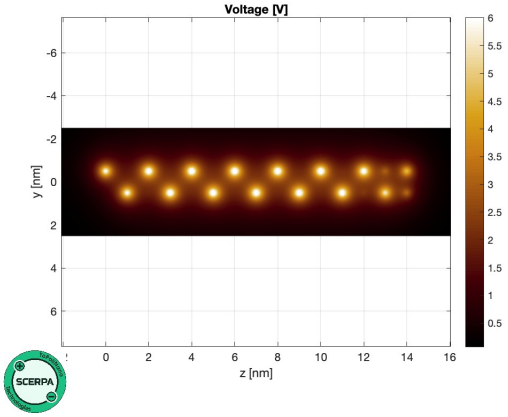

(a) Visual representation obtained by SCERPA of the localization of positive charges in the wire.

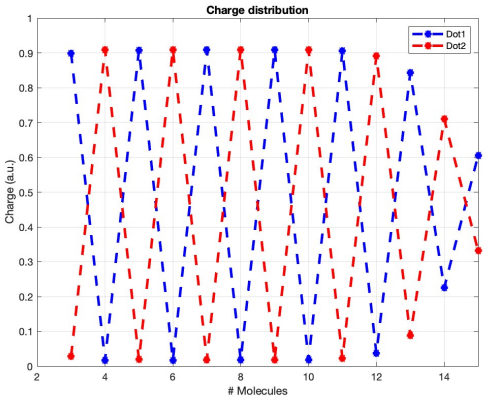

(b) Charge distribution along Dot 1 and Dot 2, the active dots, for each molecule of the wire.

Figure 3.21: Charge distribution along a single-line one-phase wire when every molecule senses a clock field equal to 2 V/nm.

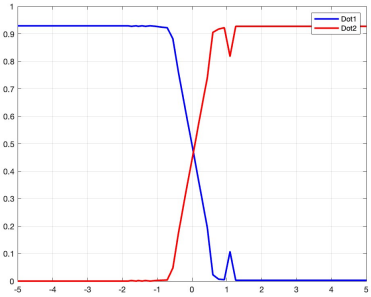

Figure 3.22: VACT of oxidized bis-ferrocene at a clock field equal to 2 V/nm.

3.3.2 Analysis of single-phase wire with 3 nm high trench

Following the previously described procedure, the analysis of the one phase wire characterized by a 3 nm wide and 3 nm high trench is performed. While the trench electrode is connected to ground, the upper electrodes are set to -3 V.
The minimum values of the clock field are obtained at the extremes of the structure: 0.747 V/nm at z = 1 nm (associated to the first molecule of the wire after the driver region) and 0.745 V/nm at z = 13 (referred to the thirteenth molecule of the wire). On the contrary, the maximum field value is obtained at the center of the structure (0.918 V/nm at z = 7 nm). The average clock field value is 0.6860 V/nm. These values, given the simulation conditions such as the length of the wire and the applied voltages at the electrodes, result in a correct propagation of the information. The charge separation permits a sufficient localization of the charge. Indeed, the field values lie between 0 V/nm and 1 V/nm and are coherent with the behaviour described in the previous subchapter.

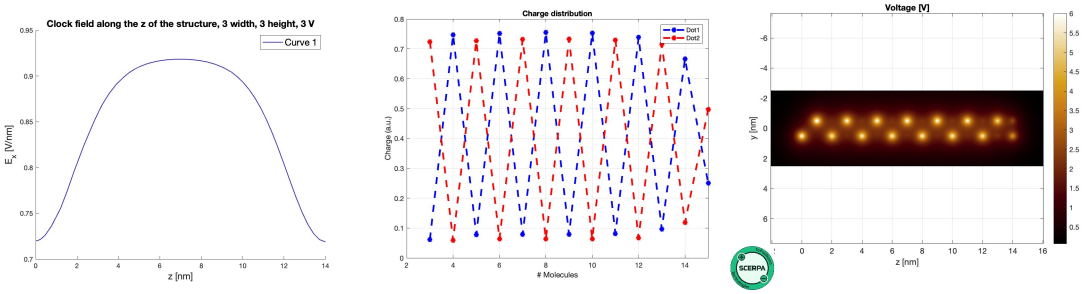

(a) Clock field. (b) Charge separation. (c) Binary propagation.

Figure 3.23: Analysis of the single-phase wire characterized by 3 nm high and 3 nm wide trench. The applied voltage on the upper electrodes is equal to -3 V.

Furthermore, the transverse electric fields are studied through Sentaurus Device.

Since the structure is perfectly symmetrical, the transverse electric fields along the y-axis add up and cancel each other out. The graphical representation of the phenomenon is here not reported, for sake of shortness.

The same simulation is then conducted by increasing the applied voltage to the upper electrodes: by setting them at -6 V, an increase in the clock field values is expected. This phenomenon is proved by the values displayed in Fig. 3.24a and by the higher separation of the charges reported in Fig. 3.24b. On the contrary, the transverse field won't change, since at the center of the trench there is a perfect overlap of the field given by the left upper electrode and the one given by the right upper electrode. The graph is not provided again for the sake of brevity. The increase in the fields sensed by the molecules of the wire locate more charge on the active dots. The simulation conducted through SCERPA proves that the wire still functions properly: the information propagation can be seen in Fig. 3.24c. The results are not surprising, given that the average field values sensed by the molecules at the center of the trench is equal to 1.719 V/nm: in agreement with the theoretical study conducted on SCERPA (where every molecule was set in an environment with constant field values), such values succeed again to help the propagation of the information in the wire.

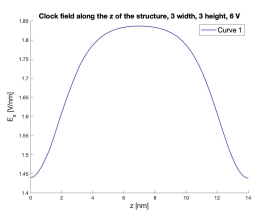

(a) Clock field.

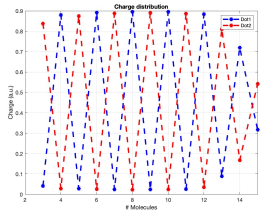

(b) Charge separation.

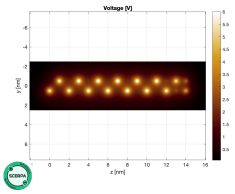

(c) Binary propagation.

Figure 3.24: Analysis of the single-phase wire characterized by 3 nm high and 3 nm wide trench. The applied voltage on the upper electrodes is equal to -6 V.

3.3.3 Analysis of single-phase wire with 6 nm high trench

The increased height of the trench results in lower clock fields. Indeed, the distance between the trench electrode and the upper ones is doubled while the voltage of the upper electrodes is set to 3 V. According to the plate capacitor model, the clock field should present 0.5 V/nm. Given the point of study, that is at the center of the trench, the expected results would be lower, since the ideal model can't be really applied at y = 0. The minimum value is 0.454 V/nm, reported at z = nm and z = 13 nm. Instead the maximum value is equal to 0.484 V/nm, at the center of the wire, a decrease of 0.016 V/nm with respect to the ideal parallel plate capacitor model. The here reported one phase wire still works: the fields that each molecule feels are sufficient to help the charge to localize correctly, according to the input values. The same simulation is then

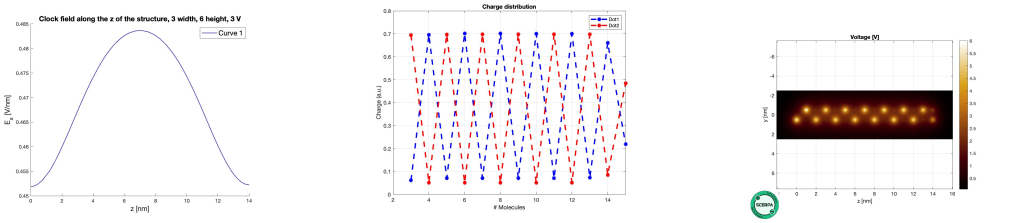

(a) Clock field. (b) Charge separation. (c) Binary propagation.

Figure 3.25: Analysis of the single-phase wire characterized by 6 nm high and 3 nm wide trench. The applied voltage on the upper electrodes is equal to -3 V.

conducted by increasing the applied voltage to the upper electrodes: by setting them at 6 V, an increasing in the clock field values is depicted in Fig. 3.26a. The transverse field maintains a null value, while the charge separation (Fig. 3.26b, as happened in the structure 3 nm high, increases since less charge is located on the third non active dot. The clock values sensed by the molecules at the center of the structure reach even 0.967 V/nm, ensuring a correct propagation of the information along the wire. The wire continues to work correctly, as it can be appreciated in Fig. 3.26c.

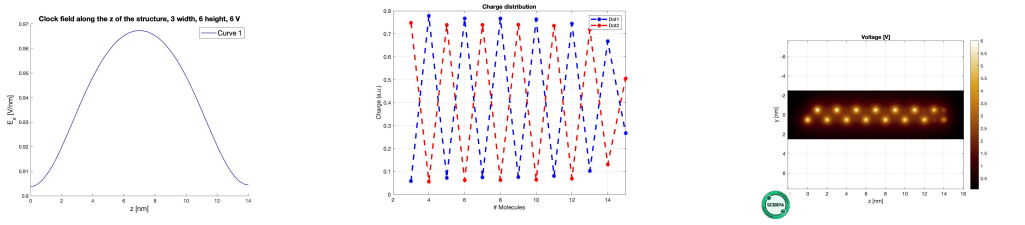

(a) Clock field. (b) Charge separation. (c) Binary propagation.

Figure 3.26: Analysis of the single-phase wire characterized by 6 nm high and 3 nm wide trench. The applied voltage on the upper electrodes is equal to -6 V.

3.3.4 Analysis of single-phase wire with 9 nm high trench

A further increase of the trench height to 9 nm results in an additional reduction of the clock field along the wire, given the upper electrodes' voltages set to 3 V. The minimum and maximum values are confirmed at the ends and at the center of the structure, respectively. For increasing z-coordinates, therefore, these values are: 0.312 V/nm, 0.318 V/nm. Despite the reduction, the clock field values remain above the threshold required to ensure a proper charge separation, hence it assumes values greater than zero. The wire works: despite having tripled the trench height, the system stability maintains a good information propagation. The technology therefore proves to be robust.

The simulation is then conducted by applying 6 V to the upper electrodes. The clock field values increase, reaching 0.624 V/nm as the maximum values, and so the charge separation increases as well: the wire still works. The greater the height of the trench, the more equally distributed the electric fields along the structure, hence the reduced separation between minimum and maximum values. Fig. 3.28 proves these statements.

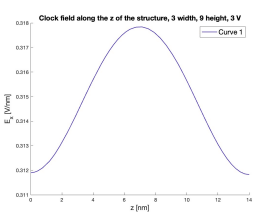

(a) Clock field.

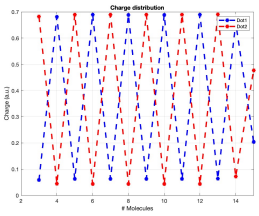

(b) Charge separation.

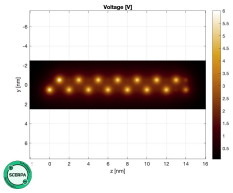

(c) Binary propagation.

Figure 3.27: Analysis of the single-phase wire characterized by 9 nm high and 3 nm wide trench. The applied voltage on the upper electrodes is equal to -3 V.

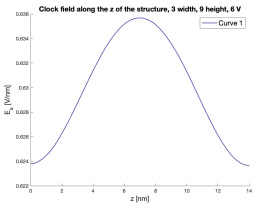

(a) Clock field.

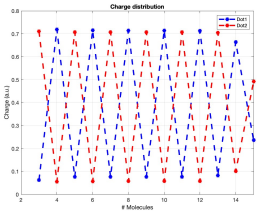

(b) Charge separation.

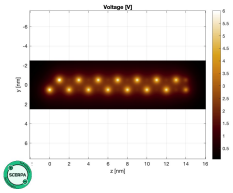

(c) Binary propagation.

Figure 3.28: Analysis of the single-phase wire characterized by 9 nm high and 3 nm wide trench. The applied voltage on the upper electrodes is equal to -6 V.

3.4 Variation of materials

The fabrication of structures suitable for hosting MolFCN molecules requires extremely high fabrication resolutions. Therefore, the selection of materials used for the dielectric structure becomes an extremely important choice: the properties of the insulator influence not only the performance of the device but also the fabrication process. Regarding device performance, the choice of dielectric influences the parasitic capacitances established between the electrodes of the system, since varying material corresponds to a change in the dielectric constant. This parameter directly influences the capacitance values, according to Eq. 3.2.

$$C = \varepsilon_0 \varepsilon_r \frac{A}{d} \tag{3.2}$$

Where ε_0 and ε_r are the vacuum permittivity and the relative permittivity of the dielectric that separates the electrode, respectively. A and d, instead, are the geometrical parameters referring to the area occupied by the electrodes and the distance between them.
These values will later be analyzed in great extent as they are related to the power consumption associated with the created devices: the application of a voltage to the electrodes charges the capacitances that spontaneously arise due to the alternation of metals and dielectrics. This phenomenon therefore represents the contribution of power switching, the main dissipative term since the technology does not involve conduction phenomena that would lead to higher power consumption values.

Regarding the manufacturing process, the very high resolution required during the creation of the trench structures has to be considered. While silicon dioxide has been widely used in semiconductor technology due to its high compatibility with silicon, the reduction in device size has introduced the possibility, sometimes the need, to use new materials. Valid alternatives to silicon dioxide are hafnium dioxide and aluminium oxide (HfO_2 and Al_2O_3). Through advanced deposition techniques, devices with very high resolutions have been created. For example, [**?**] and [**?**] report the creation of sub-3 nm trenches made by Al_2O_3. The best deposition technique is the atomic layer deposition (ALD), a self-limiting technique that, through the use of one or more precursors, creates chemical bonds between the surface to be coated and the molecules to be deposited. This technique is characterized by the high control with which the materials can be deposited and the very thin layers obtained, realized with molecular thicknesses. HfO_2 ($\varepsilon_r = 25$) is an excellent candidate to replace SiO_2 due to its low conductivity and excellent thermal stability. Al_2O_3, on the other hand, is characterized by a dielectric constant that assumes a value somewhere between SiO_2 and HfO_2: $\varepsilon_r = 9$. It is a very good insulator (its band gap is very large, between 7-8.8 eV [46] but has lower breakdown strength values than HfO_2 (5.78 MV/cm with respect to the value referred to HfO_2: 16.64 MV/cm, [47]): lower electric fields can be applied before irreparably damaging the atomic structure of the device. Analyses concerning the geometrical variations of the single-line one phase wire are therefore conducted, now varying the dielectric from the SiO_2 used in the previous chapters. As expected, since the medium where the fields are studied is the unchanged air, the electric field values measured in the trench do not vary. Instead, the capacitance

values register a shift, but these changes will be investigated in the following chapters.

3.4.1 HfO_2 simulation results

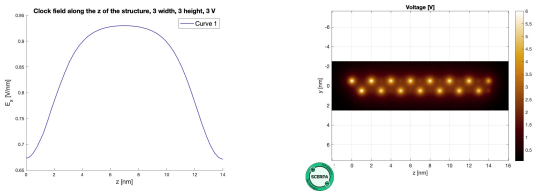

Figure 3.29: 3 nm high trench, 3 V applied voltage.

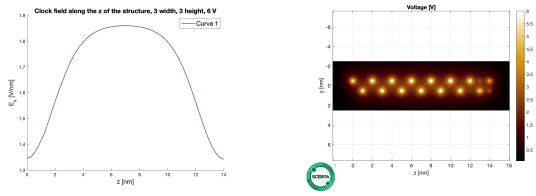

Figure 3.30: 3 nm high trench, 6 V applied voltage.

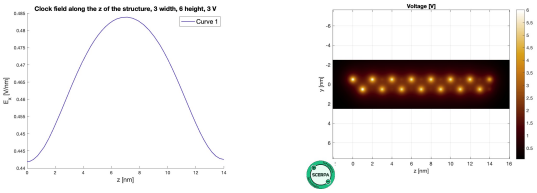

Figure 3.31: 6 nm high trench, 3 V applied voltage.

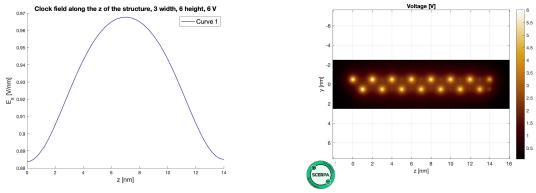

Figure 3.32: 6 nm high trench, 6 V applied voltage.

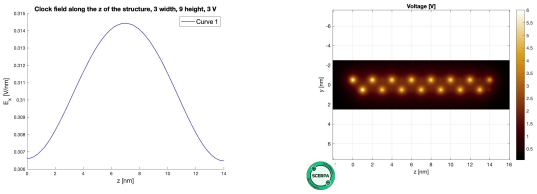

Figure 3.33: 9 nm high trench, 3 V applied voltage.

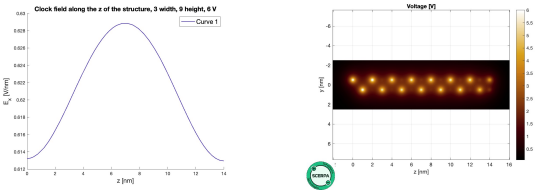

Figure 3.34: 9 nm high trench, 6 V applied voltage.

3.4.2 Al_2O_3 simulation results

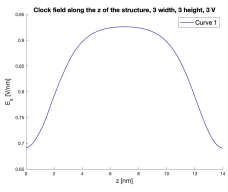

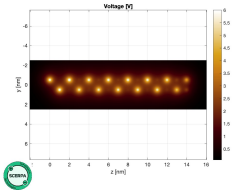

Figure 3.35: 3 nm high trench, 3 V applied voltage.

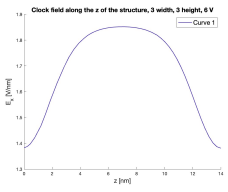

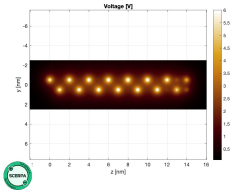

Figure 3.36: 3 nm high trench, 6 V applied voltage.

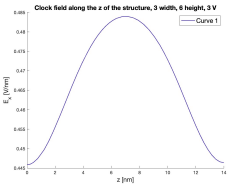

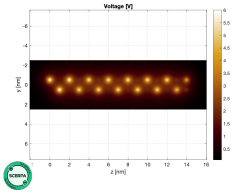

Figure 3.37: 6 nm high trench, 3 V applied voltage.

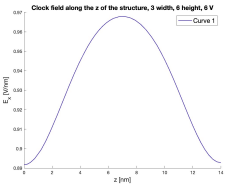

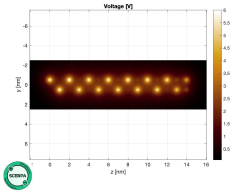

Figure 3.38: 6 nm high trench, 6 V applied voltage.

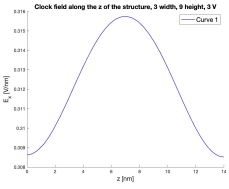

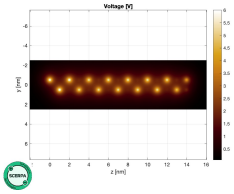

Figure 3.39: 9 nm high trench, 3 V applied voltage.

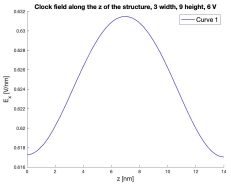

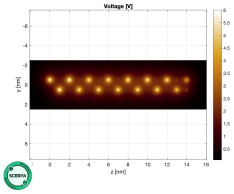

Figure 3.40: 9 nm high trench, 6 V applied voltage.

Chapter 4

One phase wire: multi-line

Once the impact of the height of the trench on the functioning of the MolFCN technology has been analyzed, it can be considered to vary the second crucial geometrical parameter of the trench: its width. Reducing this variable would be complicated from a technological point of view. Increasing the size of the trench, on the other hand, would be possible and would have the advantage of requiring lower manufacturing resolutions. However, the greater feasibility is accompanied by a higher difficulty in keeping the molecules aligned. If it is already difficult to maintain a constant intermolecular distance in a space that forces the molecules in a line, having more area in which to place the molecules would increase the degrees of freedom and possible manufacturing variations. Consequently, molecules could be more or less far apart, affecting the charge localization in the active dots.

This apparent increased complexity can be exploited to the point of turning it into an advantage: widening the trench allows more lines to be placed side by side within the same layout. The resulting system, called multi-line or bus structure, has a binary propagation no longer assigned to a single cell but shared by several logical unit cells arranged along the same z-coordinate (Fig. 4.1).
In fact, a central molecule surrounded by a higher number of neighbouring primes should more precisely localize the aggregate charge on its dots, since the coulomb repulsion it would feel would be greater. Increasing the number of charges has the advantage of increasing the stability of the charge localization, which is less susceptible to fluctuations, and of reducing the fading effect in areas further away from the driver regions.

This chapter therefore addresses this geometrical variation, exploring the connection between the applied voltages at the electrodes and the electric fields felt by the molecules at various points in the structure. The structure explored in this section is therefore a system characterized by four molecular lines, distributed in an 8 nm wide trench. The total number of molecules amounts to fifty-two, to which eight driver molecules must be added, two for each line defined in the bus. The length of the structure is maintained at 14 nm. The height of the structure is varied in the range of 3 nm, 6 nm and 9 nm. The simulated structures, obtained trough the Sentaurus framework, are depicted in Fig. 4.2.

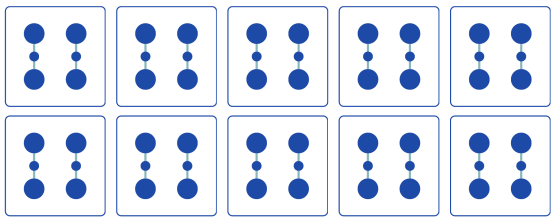

Figure 4.1: Pictorial representation of a multi-line structure composed by two lines of molecules made by five unit cells.

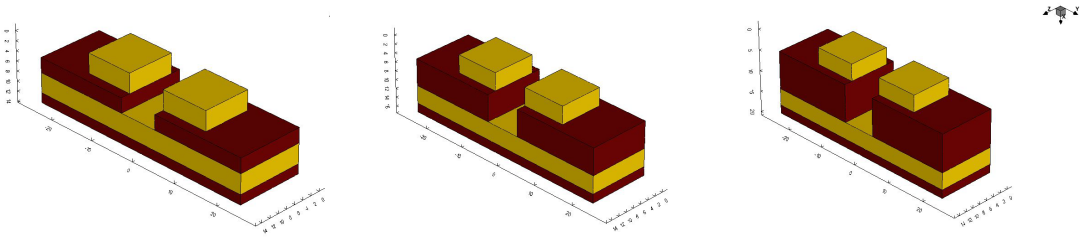

(a) 3 nm high trench. (b) 6 nm high trench. (c) 9 nm high trench.

Figure 4.2: Three-dimensional view of the one-phase multi-line wire by varying the height of the trench.

4.1 Geometrical variation

4.1.1 Approach to the analysis

Initially, and similarly to what have been done with the single line system, uniform electric field values are entered on SCERPA. In this way, the wire behaviour is explored by varying the fields associated to each molecule in the circuit. Hence, five distinct simulations are performed, in which five different field values are applied to the system, spanning in the range between -2 V and 2 V, with 1 V increments. The objective of this first phase is to verify the robustness of the propagation of binary information and to identify possible side effects caused by interactions between the lines. Subsequently, fields with non-uniform distributions along the length of the circuit will be introduced to simulate more realistic scenarios.

Initially, the behaviour of the multi-line system in the absence of an electric field is analyzed. The aim of this analysis is to understand how the system behaves spontaneously, without any external input. The analysis requires analyzing the behaviour of the bus depending on the input provided by the driver. If in the single line, in fact, no differences were experienced in the propagation of information depending on the value being propagated, in the case of the bus, the behaviour of the structure changes.

At first, by assigning the driver molecules the binary value '0', the propagation along the bus seems correct. This result might suggest that, similarly to what was observed in the previous chapter, the coulomb repulsion between the charges is sufficient to correctly localize the charge in the molecules, even in the absence of an external electric field.

Fig. 4.3 indeed shows a coherent propagation of information within the structure. There is a slight skin effect caused by the crosstalk between the adjacent lines: the molecules at the borders of the wire have the positive charge distributed over both active dots. The propagation of the information is not obstructed, despite this skin phenomenon: the logical information seems to reach correctly the end of the wire. Furthermore, the fading effect is attenuated given the interactions between more molecules: the binary encoded value proves to be stable in such system.

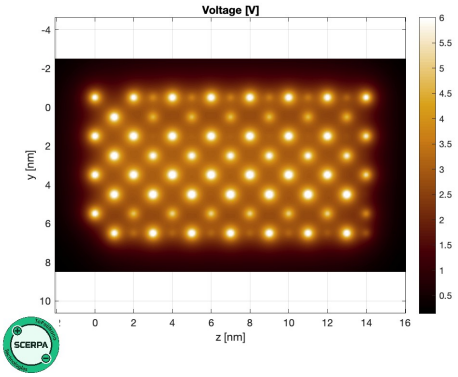

Figure 4.3: Propagation along the multi-line structure in the presence of driver molecules set to '0' with no clock field applied. The binary value reaches correctly the end of the wire.

However, by assigning the driver molecules the binary value '1', a different behaviour is observed in the same structure: the propagation of information fails to reach the end of the wire, as it can be seen in Fig. 4.4. Towards the end of the bus, in fact, the molecules spontaneously assume the binary state '0'. The reasons for this are related to the previously analyzed asymmetric VACT of bis-ferrocene (stability reasons). As a conclusion, in the case of '0' input, the logical propagation seems to happen correctly but a closer analysis reveals how propagation does not actually occur.

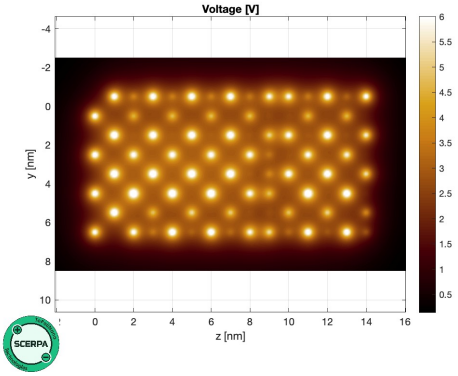

Figure 4.4: Propagation along the multi-line structure in the presence of driver molecules set to '1' with no clock field applied. This configuration shows the malfunctioning of the structure: the binary value does not reach the end of the wire.

This phenomenon highlights the limitations of the multi-line system which requires high electric fields to function properly. Consequently, the impact of a clock field on the circuit is explored. The input driver is kept equal to '1', the unfavourable case that needs to be focused on in order to understand whether the bus functions correctly.

Fig. 4.5a and 4.5b show how, despite applying clock fields of 1 V/nm and 2 V/nm respectively in such a way that every molecule in the circuit is affected by the same electric field value. The propagation of the binary information cannot sustain itself.

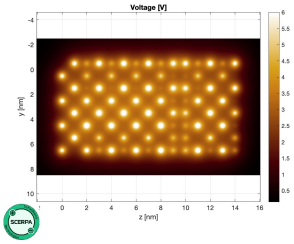

(a) Erroneous propagation along the multi-line structure when 1 V/nm clock field is applied.

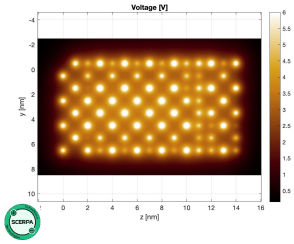

(b) Erroneous propagation along the multi-line structure when 2 V/nm clock field is applied.

Figure 4.5: Various positive clock field values applied to the multi-line system. The information does not reach correctly the end of the structure.

One possible solution is to reduce the length of the wire associated to one clock region. The analysis therefore focuses on reducing the length of the multi-line wire, in order to see what is the maximum molecular number for which, given the conditions of the structure, binary information can reach the end of the wire. Experimentally, it can be seen that ten molecules per line is the maximum limit for the wire to function properly. Fig. 4.6a and 4.6b show the propagation of the binary value '1' in the absence of an external electric field in two multi-line structures characterized by a different number of molecules per line. While Fig. 4.6a is characterized by eleven molecules per line and fails to propagate the information, Fig. 4.6b shows the structure defined by ten molecules per line: the so-defined structure works.

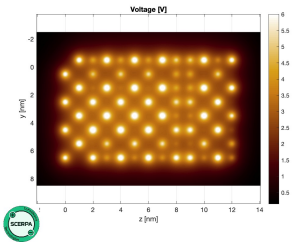

(a) Multi-line wire characterized by eleven molecules per line, with no clock field applied and '1' as an input. The system does not work properly.

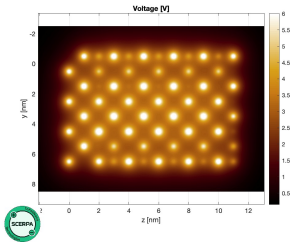

(b) Multi-line wire characterized by ten molecules per line, with no clock field applied and '1' as an input. The system does work properly.

Figure 4.6: Analysis of the propagation of the binary value '1' in multi-line structures characterized by a different number of molecules. No clock field is applied.

At this point, the study focuses on the application of negative electric fields in the initial structure, characterized by 13 molecules per line. From Fig. 4.7a and Fig. 4.7b it can be appreciated how the application of negative field values is sufficient to polarize the charge at Dot 3 even in the presence of a considerable number of molecules. Similarly to the single-line structure, the application of a $-1\,\mathrm{V/nm}$ field does not completely localize the charge on the non-active dot, while the application of $-2\,\mathrm{V/nm}$ corresponds to a complete reset state, denoted by the total absence of bright spots in the figure. It should be noted that the application of negative fields is an effective strategy not only to ensure the reset of the system but also to erase the information previously assumed by the molecules, helping the molecules to vary from a binary value to the other (since the localization of the charges on one of the the active dots corresponds to a stable state).

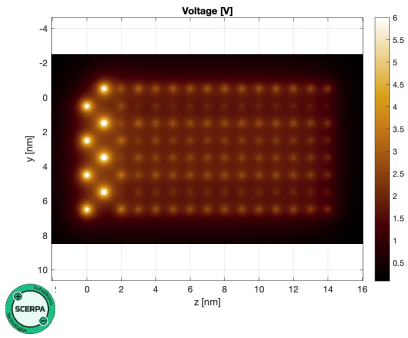

(a) Multi-line system in RESET state, with -1 V/nm clock field applied.

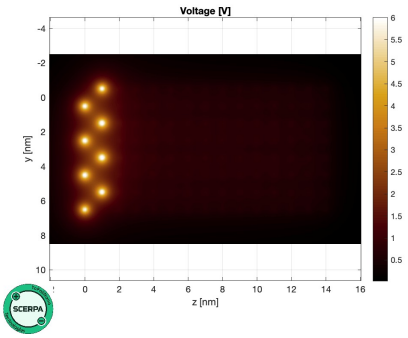

(b) Multi-line system in RESET state, with -2 V/nm clock field applied.

Figure 4.7: Comparison between different negative clock field values in the multi-line system composed by thirteen molecules.

The analysis regarding the multi-line structure conducted so far has considered constant electric field values along the entire trench. However, in order to characterize the MolFCN technology more realistically, it is necessary to explore what happens when non-uniform fields, obtained through simulations with Sentaurus Device, are applied. These field values reflect real operating conditions, where electrostatic potentials vary depending on where they are measured due to the geometric configurations of the trench. The subsequent simulations are therefore of particular interest because they represent a link to real devices that could be created.

The following chapters explore the impact of the variations of geometrical parameters on the multi-line wire functioning. Similarly to the single-line system, the width of the trench, set at 8 nm, is kept constant. Having carried out a preliminary analysis of the field values on SCERPA, it is possible to state that simulations carried out with a molecular length per line of thirteen would result in non-functional systems. Therefore, the length of the structure is reduced with respect to the one studied in Chapter 3: from a 14 nm long wire, this subchapter focuses on a length of 11 nm.
The height of the trench is varied, in order to explore the development of the resulting

electric fields. The height is varied between 3 nm, 6 nm and, finally, 9 nm.
For each of these structures, electric fields are sampled at four distinct points along the trench width: at y = -2.4 nm, y = -0.8 nm, y = 0.8 nm and y = 2.4 nm. This sampling takes into account where the molecules of the multi-line structure could be located. The electrical fields obtained are then sampled, in such a way to obtain a value for each nanometer along the length of the wire. The fields referred to the extremes of the structure, corresponding to z = 1 nm and z = 10 nm, are excluded as the molecules could not be located at the ends of the wire.

4.1.2 Analysis of multi-line single phase wire with 3 nm high trench

The analysis of the one phase wire characterized by a 8 nm wide and 3 nm high trench is here performed.
At first, the upper electrodes are set to -3 V.
The four curves in Fig. 4.8a are the clock fields in the different points of the length of the structure: they exhibit a precise behaviour. Since the structure is symmetrical with respect to the y-axis, the curves relating to the points that are at the same distance from the center of the trench present the same trend. As a result, the curves at y = 2.4 nm and y = -2.4 nm and the curves at y = 0.8 nm and y = -0.8 nm present the same evolution along the length of the structure. This is because at these points the distance between the trench and upper electrodes is the same. Consequently, at y = |2.4| nm there are higher field values while, at y = |0.8| nm, the distance between the electrodes increases, reducing the electric field modulus.
The minimum values of the clock field are obtained at the extremes of the structure, at z = 1 nm, associated to the first molecule of the wire after the driver region, and at z = 11 (referred to the tenth molecule of the wire). The average clock field value is equal to 0.6187 V/nm.

The analysis conducted through SCERPA (Fig. 4.8b) demonstrates how the clock field values are sufficient to help the propagation of the information along the structure.

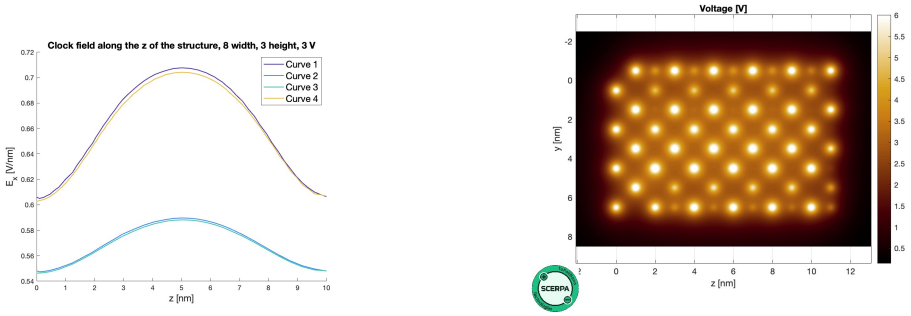

(a) Clock field lines.

(b) SCERPA output.

Figure 4.8: Behaviour of the multi-line structure, characterized by 3 nm high trench, a length of 12 nm and an applied voltage to the upper electrodes equal to -3 V. In 4.8a, Curve 1 refers to y = -2.4 nm, Curve 2 to y = -0.8 nm, Curve 3 to y = 0.8 nm, Curve 4 to y = 2.4 nm. In 4.8b, the propagation of binary value '1' along the multi-line structure can be appreciated.

Furthermore, the transverse electric fields are studied through Sentaurus Device. If the center of the trench is examined, the superposition of the transverse electric fields generated by the two upper electrodes would add up, canceling out as in the case of the single-line structure. But, moving away from the center of the trench, the superposition of the transverse fields no longer results in a null value. This phenomenon occurs because

the distance between the upper electrodes and the points of the trench where the superposition of the fields is analyzed is no longer balanced: the points closer to one of the two upper electrodes are affected more by the field generated by it. Furthermore, in a point nearer to one of the two upper electrodes, the sensed field generated by the other upper electrode is low, given the distance.

Consequently, the transverse fields at points far from the center of the trench do not cancel out.
On the contrary, the greater the distance from the center of the trench, the greater the field values along y. The molecules at the edges of the wire are therefore more affected by this undesirable component: the charge within them could be influenced by the transverse field components, causing the charge to localize in one of the two active dots and influencing the binary information assumed by these molecules.
In Fig. 4.9, the higher transverse fields are therefore associated to the curves referred to y = 2.4 nm and y = -2.4 nm.

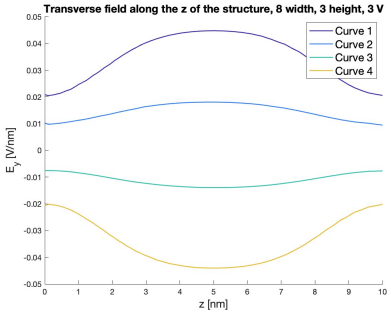

Figure 4.9: Transverse fields of the multi-line structure (-3 V applied voltage). Curve 1 refers to y = -2.4 nm, Curve 4 refers to y = 2.4 nm.

The same simulation is then conducted by applying 6 V to the upper electrodes of the wire. The increase in the applied voltage boosts the sensed clock fields by the molecules (Fig. 4.10a. The system still proves its functionality, as depicted in Fig. 4.10b.

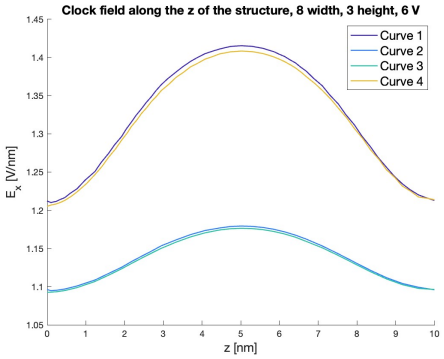

(a) Clock field lines.

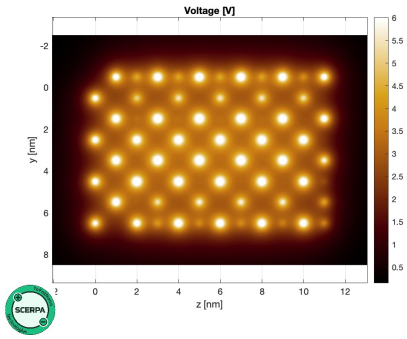

(b) SCERPA output.

Figure 4.10: Behaviour of the multi-line structure, characterized by 3 nm high trench, a length of 12 nm and an applied voltage to the upper electrodes equal to -6 V. In 4.8a, Curve 1 refers to y = -2.4 nm, Curve 2 to y = -0.8 nm, Curve 3 to y = 0.8 nm, Curve 4 to y = 2.4 nm. In 4.8b, the propagation of binary value '1' along the multi-line structure can be appreciated.

In order to provide an analysis as detailed as possible, a simulation is carried out in which the trench length is extended to z = 14 nm, resulting in a wire characterized by thirteen molecules instead of ten. Given the disparity in the number of molecules, an inverting behaviour is expected at the end of the wire with respect to the input provided by the driver molecules. Simulations conducted on SCERPA show that the length of the system thus created is excessive: the binary value fails to reach the end of the wire in the case of both 3 V and 6 V being applied. The clock fields obtained by Sentaurus in both cases are not sufficient to counteract the bi-stability of the bis-ferrocene molecules. The incorrect propagation, predicted by the previous chapter, is reported in Fig. 4.11a and 4.11b

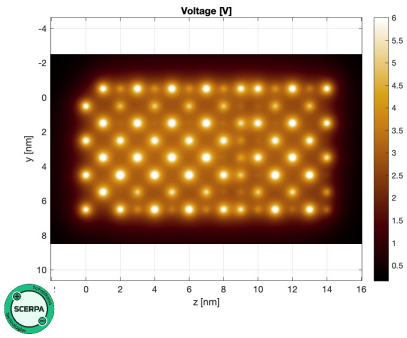

(a) SCERPA output by providing -3 V at the upper electrodes.

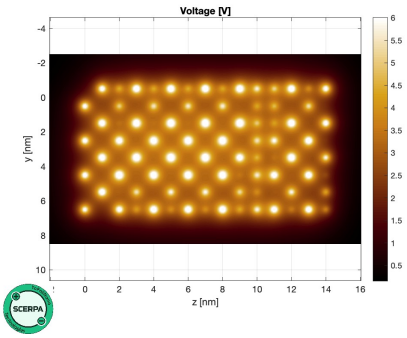

(b) SCERPA output by providing -6 V at the upper electrodes.

Figure 4.11: Behaviour of the multi-line structure, characterized by 3 nm high trench and now a length of 14 nm. The extension of the length of the structure results in a malfunctioning wire.

4.1.3 Analysis of multi-line single phase wire with 6 nm high trench

The increased height of the trench results in lower clock fields with respect to the previous structure. Indeed, the distance between the trench electrode and the upper ones is doubled and, following the parallel-plate capacitor model, the resulting fields must be lower. Nevertheless, the wire still functions properly, as depicted in Figure 4.12c. The transverse fields are reported in Fig. 4.12b.

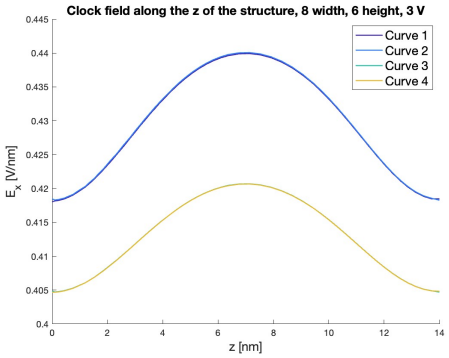

(a) Clock fields.

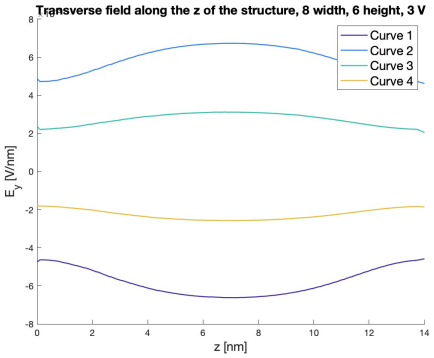

(b) Transverse fields.

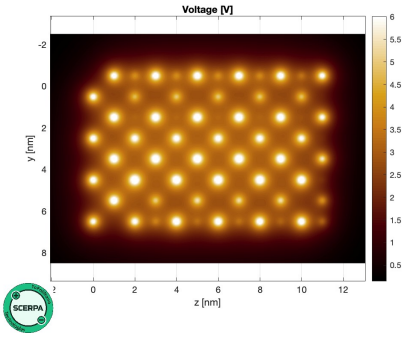

(c) SCERPA output.

Figure 4.12: Behaviour of the multi-line structure, characterized by 6 nm high trench, a length of 12 nm and an applied voltage to the upper electrodes equal to -3 V. In 4.8a, Curve 1 refers to y = -2.4 nm, Curve 2 to y = -0.8 nm, Curve 3 to y = 0.8 nm, Curve 4 to y = 2.4 nm. In 4.8b, the propagation of binary value '1' along the multi-line structure can be appreciated.

The same simulation is then conducted by applying 6 V to the upper electrodes of the wire. The increase in the applied voltage boosts the sensed clock fields by the molecules. Figures are here not reported, avoiding redundancy.

4.1.4 Analysis of multi-line single phase wire with 9 nm high trench

A further increase of the trench height to 9 nm results in an additional reduction of the clock field along the wire. The minimum and maximum values are confirmed at the ends and at the center of the structure, respectively. The same simulation is then conducted by applying 6 V to the upper electrodes of the wire. The increase in the applied voltage boosts the sensed clock fields by the molecule. Figures referred to this last configuration are here not reported, avoiding redundancy.

The bus proves it-self to be a robust structure, given its functioning. The main disadvantage is the reduced length required by the clock regions in order to obtain a functioning circuit.

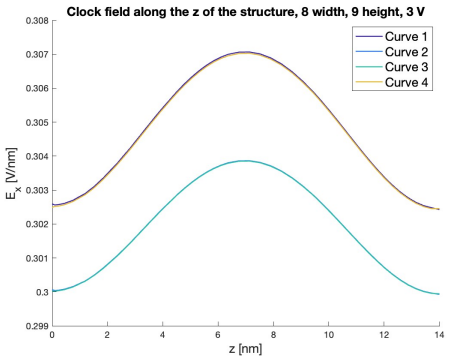

(a) Clock fields.

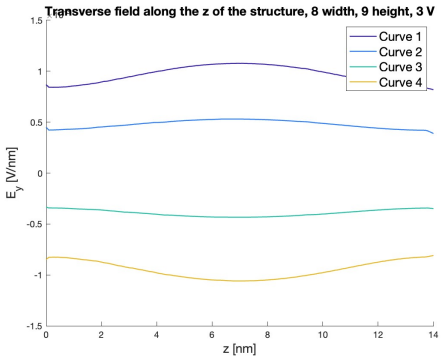

(b) Transverse fields.

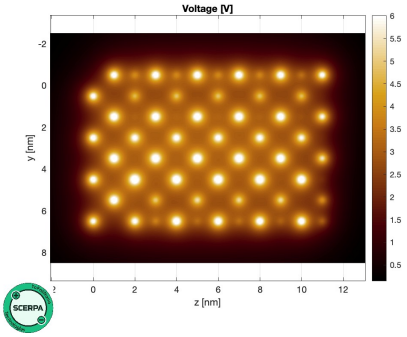

(c) SCERPA output.

Figure 4.13: Behaviour of the multi-line structure, characterized by 9 nm high trench, a length of 12 nm and an applied voltage to the upper electrodes equal to -3 V. In 4.8a, Curve 1 refers to y = -2.4 nm, Curve 2 to y = -0.8 nm, Curve 3 to y = 0.8 nm, Curve 4 to y = 2.4 nm. In 4.8b, the propagation of binary value '1' along the multi-line structure can be appreciated.

4.2 Variation of materials

For the sake of the record, variations at the level of the materials used in the simulations have been analyzed, as it was done in the chapter regarding the single-line system. Particularly, instead of SiO_2, simulations based on Al_2O_3 and HfO_2 are performed. Since the analysis of the electric fields belongs to the trench zone where the medium is air, varying the dielectric does not induce substantial changes in the clock values nor in the transverse field values. As far as the capacitances are concerned, varying the material induces changes in their values. But since the capacitances of interest are those established between the upper electrodes and the trench electrode, and since in the geometric variations the distance between these electrodes does not vary, the capacitance values recorded do not change compared to the single-line case. Varying the distance between the upper electrodes, in fact, varies the capacitance values established between the two upper electrodes themselves. Since the electrodes are placed at the same potential, these capacitances will not charge and discharge during the operation of the device: the values, reported to provide an analysis as complete as possible, are not useful for calculating the power dissipated by the technology. The table therefore shows the capacitance values between the top electrodes, the left column shows the values obtained in the single-line wire, the right column shows the values obtained in the multi-line wire. Obviously, varying the dielectric does not influence the reported capacitance values, given they refer to the air medium which fills the trench.

Single-line one phase wire			
Dielectric	**h = 3 nm**	**h = 6 nm**	**h = 9 nm**
SiO_2	2.7388×10^{-19} F	3.1520×10^{-19} F	3.4633×10^{-19} F
Al_2O_3	2.7350×10^{-19} F	3.1969×10^{-19} F	3.5746×10^{-19} F
HfO_2	2.7246×10^{-19} F	3.2245×10^{-19} F	3.6465×10^{-19} F

Table 4.1: Parasitic capacitances between upper electrodes, single-line one phase wire.

Multi-line one phase wire			
Dielectric	**h = 3 nm**	**h = 6 nm**	**h = 9 nm**
SiO_2	1.2399×10^{-19} F	1.5139×10^{-19} F	1.7235×10^{-19} F
Al_2O_3	1.22836×10^{-19} F	1.5076×10^{-19} F	1.7300×10^{-19} F
HfO_2	1.2222×10^{-19} F	1.5041×10^{-19} F	1.7334×10^{-19} F

Table 4.2: Parasitic capacitances between upper electrodes, multi-line one phase wire.

Chapter 5

Case study: the neural cell

This chapter focuses on the analysis of a more complex system than the wire analyzed previously. The increasing complexity in the systems analyzed is motivated by the desire to better understand the potential of MolFCN technology, evaluating its functionality in different cases. While the previous chapters explored the structure of a wire, linking the simulative environment of Sentaurus with the one of SCERPA, this chapter studies the creation of the main logical structure in the MolFCN technology: the majority voter. To obtain a more practical research and to have terms of comparison with devices presented in literature, a specific case study is chosen to analyze the majority voter: the implementation of an artificial neuron.

The choice to study the neuron as an application case for MolFCN technology is motivated by the interest in artificial neural networks that in recent years has grown. The neuron therefore represent an excellent case study for understanding the potential and limits of MolFCN technology, evaluating its performance.
The neuron of an artificial neural network, as seen in the Introduction, performs a weighted sum of the inputs. The result, filtered by an activation function, is propagated to the output. This mechanism can be achieved through MolFCN technology, in particular by employing the majority voter (MV) as the main logic gate.
Through the MV in fact, molecules containing binary information can be processed: its output will be equal to the logical value assumed by the majority of its inputs. The superposition of the electric fields results indeed in a polarization in the central cell such that a sum of the logical states is obtained.
The mechanism of the sum can be understood by considering a sort of MV with two inputs. If the inputs present polarization P = -1 and P = -1, the polarization of the central cell is equal to P = -1. Vice versa, if the inputs present P = 1 and P = 1, the polarization of the central cell will be equal to 1. Finally, if the polarization of the two inputs is discordant, the output will be equal to 0. The MV implements exactly this dynamic, based on the superposition of the electric fields generated by several neighbouring charges: it can therefore be concluded that this logical structure effectively implements the sum of the inputs.
The result of the sum can also vary depending on the weights assigned to the various

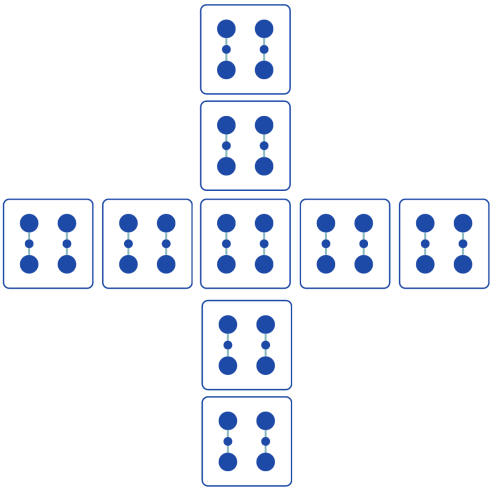

Figure 5.1: Pictorial representation of a majority voter, characterized by the transition region at the center of the cross-shaped structure.

inputs of the MV: it has been shown how the minority input can be output if it is assigned a higher weight. Consequently, the MV is a good tool to implement the weighted sum of the three inputs given to it. This is further proven in the work by G. Beretta et al. (2022), [43].
Therefore, MolFCN technology has a great advantage over other technologies: the sum, so the basis of the neuron's functioning, is linked to the operation of the main logic gate of MolFCN technology, the MV.

In addition to the sum operation, it is also necessary to specify how the weight can be attributed to each input. This concept is intrinsically linked to the nature of molecules which, depending on the voltage they are influenced by, localize more charge on one of the two active dots. This behaviour, well described by VACT, can be exploited to the advantage of neural application. In particular, by varying the saturation voltage (determining the voltage for which charge localizes almost exclusively on one of the two active dots) it is possible to modulate the amount of localized charge in response to a given electric field. In this way it is possible to influence the weight associated to an input. Molecules with different saturation voltages, therefore, simulate different weights: the intensity of the charge localized on a dot, hence the intensity of the logic value they encode, varies as the saturation voltage varies.
MolFCN technology is therefore once again particularly suitable for the implementation of neural networks, whose weights play a key role in determining system learning and operation.

As a consequence, it is necessary to carry out simulations in order to validate the functioning of the neuron based on MolFCN technology. The aim of this thesis, in fact, is to provide a link between the behaviour of the system predicted at a theoretical level and the physical structure of the device. Consequently, the analysis is first conducted

on Sentaurus. This tool is used to model the physical structure (simulating the deposition processes in a realistic manner) and then to analyze the electric fields within it. The analysis is then carried out using SCERPA, in order to verify that the field values, obtained by applying precise voltages to the electrodes of the system, are sufficient to correctly localize the charge of the molecules, propagating the information to the output of the majority voter.

5.1 Definition of structure

The structure that implements the majority voter is based on the one phase wire previously analyzed. The branches constituting the three input and output zones have the same structure as the one phase wire. To create them, therefore, a layer of gold is deposited on the dielectric substrate: it will act as the trench electrode. Dielectric zones are then deposited on it, in such a way as to leave areas of the trench electrode uncovered: the trench is therefore created with a width of 3 nm and a height of 3 nm.
These parameters are chosen in agreement with the results obtained from the one-phase wire. The single-phase wire characterization is expected to be sufficiently robust for the application purposes of the neuron.
The creation of the input and output zones is ended through the deposition of gold electrodes on the sides of the trench. The dimensions of these electrodes are 10 nm in length and 10 nm in width. The analysis is performed by maintaining the trench dimensions set to 3 nm width and 3 nm height. With respect to the on-phase wire, a different mask is used during the deposition steps: the dielectric is deposited in such a way to leave a cross-shaped trench. This shape allows connection to the input and output branches in the so-called transition region. To ensure the correct application of the electric clock field, four electrodes are deposited on either side of the trench where the crossed-branches intersect. In this way, the application of a correct clock in the center of the transition region is guaranteed thanks to the overlap of the electric fields. The dimensions of the electrodes of the transition region are set equal to 10 nm in width and 10 nm in length. Each branch of the transition region is therefore 10 nm long: this ensures that the electrodes correctly influence the entire central MV cell.
Through Sentaurus Process, Fig. 5.2 is so created.

The structure has a surface area of $2209\,\mu m^2$, with the trench that occupies $273\,\mu m^2$. Such a structure can accommodate 85 molecules spaced 1 nanometer one from the other. For each branch, which is 10 nm long plus 2 nm of spacing, eleven molecules can be placed by excluding the ends of the structure. In the transition region area, for each propagation of the cross-shaped trench, 10 molecules are found. To these the contribution of the single molecule placed exactly in the center of the transition region must be added, at the intersection of the two arms of the trench.

The materials used to create the MV are chosen on the basis of specific properties. The electrodes are made of gold, taking advantage of its high conductivity value and excellent chemical stability. As for the dielectric, Al_2O_3 is chosen.
First of all, given the extremely small dimensions required by MolFCN technology, it is

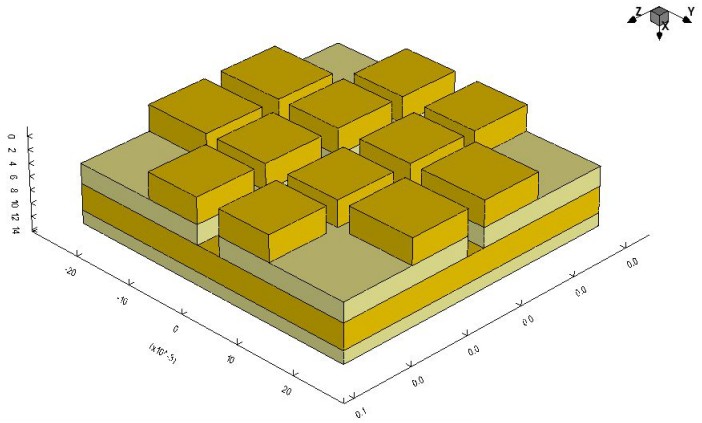

Figure 5.2: Three-dimensional representation of the neuron: the majority voter.

necessary to choose a material that could be deposited with such reduced resolutions. So, a dielectric compatible with the best deposition technique actually available (that is the atomic layer deposition) must be chosen.
Furthermore, the value of the relative permittivity of the dielectric is directly linked to the power consumption of the device. Its dielectric constant indeed influences the value of the parasitic capacitance established between the upper and trench electrodes: these capacitances will charge and discharge during the operation of the device, dissipating a value of power directly proportional to them. As a consequence, in order to minimize the energy dissipation, the dielectric material that minimizes parasitic capacitances should be chosen, hence the one with the lowest dielectric constant. It follows that, compared to the dielectrics previously considered, silicon dioxide would be the best choice: its dielectric constant is 3.9 while the one of Al_2O_3 is 3.9 and the one of HfO_2 is $\varepsilon = 25$. However, the processability of SiO_2 at such small nanometric dimensions is limited. Instead, HfO_2 would significantly easier to use but it would increase the switching power. Al_2O_3, with its dielectric constant of intermediate value compared to the other two materials, is therefore the best compromise between energy performance and ease of deposition due to its compatibility with advanced atomic layer deposition techniques. Consequently, Al_2O_3 is chosen as the main dielectric for the realization of the majority voter.

5.2 Simulation conditions

In the simulations conducted on Sentaurus, precise voltage values are set at the electrodes of the system. These applied voltages must create electric fields between the upper and trench electrodes, varying the location of charge inside the molecules placed on the trench. The trench electrode is always kept connected to ground, to provide a common reference for the entire structure. The voltages applied to the upper electrodes are instead varied according to the type of clock to be applied. In this way, it is possible to vary between two steady-state phases: the **hold** phase, in which the charge is localized in one of the

two active dots by encoding a binary value according to the logical value propagated by the driver molecules, and the **reset** phase. In the reset phase, on the other hand, an electric field is applied in such a way as to localize the charge in the lower part of the molecule, where Dot 3 is found. In this way the molecule is unable to encode any binary value. This phase is essential to avoid spontaneous polarization phenomena and to erase the information previously assumed by the molecule. In order to correctly implement the clock mechanism, the circuit has therefore been divided into different operating zones. Each zone is assigned to a different function, whose duty is to encode a binary value or to remain in a NULL state.

To ensure a link between the electric fields obtained through Sentaurus and SCERPA, two MATLAB code are created. At first, the fields are extracted from the curves obtained through Sentaurus. They are then processed in order to create a matrix where the first column assumes a value referring to a molecule of the circuit, while the second column stores the field value appropriately sampled. In this way, every molecule in the circuit is associated to a clock value.
The second code creates the layout of molecules: in this way, the MV is created in SCERPA too. It is important to notice how a MV in SCERPA is produced by a matrix of numbers where '1' encodes the presence of a molecule and '0' its absence, 'Dr1' and 'Dr2' to the driver molecules. The numbering of the molecules starts at the top of this matrix, proceeding from left to right and from top to bottom. Molecules belonging to the vertical arms of the MV must be placed in pairs, sampled every two nanometers. Once at the horizontal arm of the MV in the array, a row of molecules must be defined. They must be sampled every nanometer and must not be placed in pairs. The MATLAB code takes care of creating this matrix itself for use in SCERPA. An example of the matrix that is created is shown below. The only input to be provided is the number of rows to be included in the matrix, a value provided by the MATLAB code that creates the `.cmd` file of Sentaurus Process.

These MATLAB codes provide an important link between the simulative environment of Sentaurus and the molecular analysis of SCERPA. Their full consultation is in the appendix.

```
circuit.structure = {
    0 0 0 0 0 0 'Dr1' 'Dr2' 0 0 0 0
    0 0 0 0 0 0 '1' '1' 0 0 0 0
    0 0 0 0 0 0 '1' '1' 0 0 0 0
    'Dr1' 'Dr2' '1' '1' '1' '1' '1' '1' '1' '1' '1' '1'
    0 0 0 0 0 0 '1' '1' 0 0 0 0
    0 0 0 0 0 0 '1' '1' 0 0 0 0
    0 0 0 0 0 0 'Dr1' 'Dr2' 0 0 0 0
};
```

5.2.1 First approach to the neuron: the two phase majority voter

Initially, the circuit could be divided into two regions: the transition region and then the input and output zones, so the three branches at the ends of which are the driver molecules and the fourth branch.
This division is intended to optimize circuit operation and reduce overall energy consumption.
The application of voltages to the electrodes in the transition region will remain independent, ensuring a separation of input and output region. This division of input and output is crucial to avoid spontaneous charge polarizations that could occur in a wire characterized by too many molecules. By limiting to two clock regions, the number of voltage sources connected to the circuit can be minimized, considering that each region requires a dedicated one. Since each voltage source requires power, their reduction allows for lower power consumption. In addition, the reduction of required voltage sources facilitates future integration with architectures that do not belong to MolFCN technology but are fundamental to its operation. Given the extremely small size of the technology, reducing the number of connections with larger components greatly simplifies the process of designing and creating devices.

Consequently, the voltages are applied to the two clock regions as follows:

1. At first, the input branches must propagate the information provided by the driver molecules. Hence, the potentials of the first zone must be negative in order to create an electric field that localizes the positive charge in the active dots (remember the use of oxidized bis-ferrocene, characterized by a positive charge that can localize on the redox-centers). Therefore the first clock region is in a **switching** state. The transition region, on the other hand, must prevent binary encoding to its molecules because they, being too distant from the driver molecules, could spontaneously polarize, encoding a logical information that is incorrect with respect to the input information. The upper electrodes of the transition region must therefore be connected to a positive voltage source, so that the generated electric field locates the positive charge of the bis-ferrocene in the lower part of the molecule where Dot 3 is located. The transition region is then in the **reset** state.

2. In the second time step, the binary information has arrived correctly at the estremes of the input branches. At this point, the information must be sustained by these inputs which are in the **hold** state: the potentials in the first clock region must maintain the encoded information so they don't have to be changed. The information maintaining is necessary: the transition region is now released from its **reset** state and assumes the **switching** state. The positive charge, through an application of negative voltage to the upper electrodes, is localized in the active dots, propagating the binary information it receives from the inputs. At this stage, both clock regions have potentials applied to the electrodes of negative value. Consequently, the output region is available for the propagation of the logical information assumed by the transition region.

By observing the clock mechanism applied to a system divided into two regions, however, it can be noted a slight chance to obtain non-functional circuits. The output branch, before receiving information from the transition region, is not forced into a reset state. As a result, the charge localization spontaneously assumed by the output branch is not removed and may conflict with the logical information that has to be propagated in the circuit. Indeed, the output molecules would already be in a stable conformation that maximizes the intermolecular charge spacing. They would therefore require a greater external stimulus to vary their charge localization. Hence, the two phase MV can't be the only configuration to be studied: another approach will therefore be explored to ensure a proper analysis of the structure. This study, concerning a three phase MV, will be performed in Chapter 5.2.2.

For the moment, a detailed analysis regarding the two phase MV will be conducted. Simulations are performed by analyzing different types of structures. First, the case of the MV divided into two clock regions is introduced, setting the voltages at the upper electrodes to a modulus equal to 3 V. Two variations are then studied: first, the structure is analyzed by shrinking the upper electrodes (thus creating shorter clock regions, composed of fewer molecules), then the behaviour of the MV is studied by varying the applied voltages to the electrodes.

At first, the MV is simulated by dividing the MV into two clock regions and applying a modulus voltage of 3 V to the upper electrodes of the system. This value is chosen on the basis of simulations involving the one-phase wire, whereby this clock value is sufficient to guarantee correct propagation of the logic information within the single-line system. The structure simulated through Sentaurus Process is shown in Fig. 5.2.

For the analysis of the system, it is decided to analyze the timing of the most relevant circuit operation, when all regions are active and so in **hold** state. By applying a negative voltage to all electrodes in the circuit, the information encoded by the inputs is propagated within the input branches, arriving at the transition region where it will be processed. Due to the applied clock field, the output of the transition region will then be propagated within the output branch.

First, the trend of the electric fields within the structure is analyzed. The structure is then dissected in order to see how the field values vary along the different points of the structure. The height at which the analysis is performed is 0.4 nm from the trench electrode, consistent with the previous chapters. The points at the center of the trench are then analyzed, making two sections perpendicular to each other that meet at the exact center of the transition region.

These sections are visible in Fig. 5.3, where a top view of the structure can be appreciated. The yellow parts are the dielectric regions while the blue part identifies the trench, whose medium is air. Given the perfectly symmetrical nature of the MV created, the analysis along only one of the two curves is reported below, as the results are perfectly identical. In particular, only the behaviour of C1 is reported, the curve parallel to the z-axis that can be appreciated in Fig. 5.3.

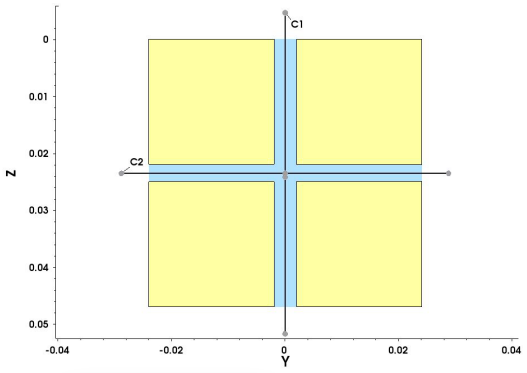

Figure 5.3: Perpendicular sections carried out in the MV.

Fig. 5.4 thus shows how the electric field at the center of the trench is consistent with the sign of the voltages applied to the electrodes. The electric field, having a positive value, will localize the positive charge in the upper pasrt of the bis-ferrocene, where the active dots are.

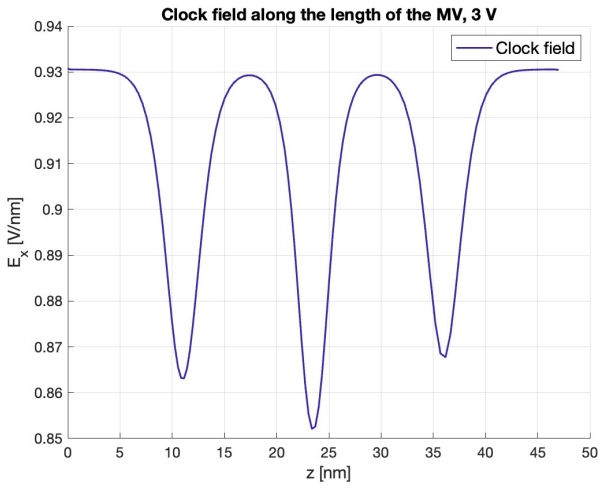

Figure 5.4: Clock field in the two-phase MV when both the first clock region and the second one are set to a hold state. The potential applied to the upper electrodes is in modulus equal to 3 V. The minimum peaks refer to the spacing regions that separate the upper electrodes.

The maximum electric field is equal to 0.9305 V/nm. This value is in agreement with the ideal parallel plate capacitor model, considering the voltage applied to the electrodes and the trench height of 3 nm. The value that can be appreciated in Fig. 5.4 deviates from 1 V/nm, but this behaviour is justified by the distance of the analyzed points from the electrodes.
Lateral minima occur at the spacing points between the upper electrodes. The spacing

is necessary in order to avoid short-circuit phenomena between electrodes that belong to different clock regions. The reduction of the clock field is therefore an unavoidable phenomenon which does not, however, obstacle the propagation of information. Indeed, the spacing value is very low (2 nm) and the reduction in the clock field is not particularly relevant. Furthermore, it must be noted that the molecules placed in the spacing regions will be influenced by the adjacent molecules, which instead belong to different electrodes. The electrostatic interaction will help the molecules of the spacing regions to assume the correct polarization, even if their sensed clock is reduced. This shadow zone, therefore, is not particularly problematic.

In Fig. 5.4, at z = 23.5 nm there is the minimum clock field value displayed by the structure. That point corresponds to the exact center of the transition region. The center of the intersection region between the three inputs represents the point at which the electrodes are furthest from the point of analysis being considered. The reduction in the clock field, therefore, is not unexpected but confirms the results obtained so far: the greater the distance to the electrodes, the lower the influence of the clock field on the molecules.

To evaluate the effectiveness of the system, the values obtained thanks to Sentaurus Device are processed on SCERPA. The two main input configurations of a MV are then analyzed: the *All zeros* configuration (in which the three inputs have a value of '0') and the *All ones* configuration (in which, conversely, the three inputs have a binary value of '1').

In the All zeros configuration (Fig. 5.5a), the system appears to function correctly, propagating the binary value given by the majority of the inputs to the output. However, it must be recalled how the '0' logic configuration is favoured by the asymmetric VACT presented by the bis-ferrocene.
The All ones configuration (Fig. 5.5b), which reveals the fragility of the analyzed structure, is therefore of greater interest. Although the binary information at the beginning appears to propagate correctly, it fails to reach the end of the output region. In fact, the transition region succeeds to assume a correct binary value equal to the majority of the inputs but this value does not reach the end of the output. Indeed, a zone can be seen in the output region where the charge present on the active dots becomes balanced (note the two bright dots per molecule) and no longer encodes any binary value. Consequently, the output region will spontaneously assume the most favoured binary value, '0', propagating it to the far end of the region. The system is therefore unable to correctly propagate the binary information to the output. The applied electric field is therefore not sufficient to help the logical information reach the end of the neuron. This phenomenon can be explained by both noticing the length of the circuit (in this moment, every region is in hold state, therefore the number of active molecules is very high) and by noticing the presence of interference between the ends of the input branches and the initial part of the output branch.

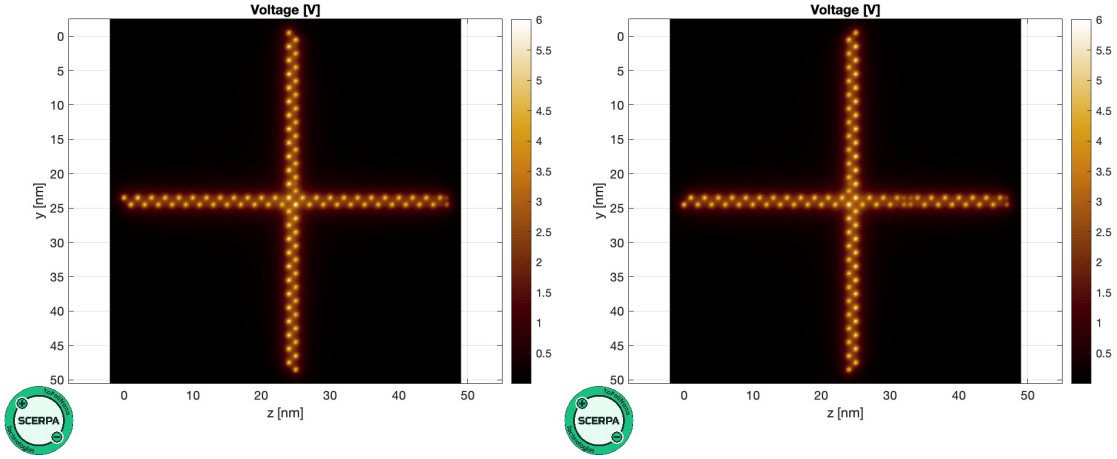

(a) All zeros configuration in the two phase MV. The voltage aplied to the upper electrodes is in modulus equal to 3 V. The system seems to function correctly, propagating the majority of the inputs until the end of the output branch.

(b) All ones configuration in the two phase MV. The voltage applied to the upper electrodes is in modulus equal to 3 V. The system reveals its malfunctioning: an aberration phenomenon can be seen at the beginning of the output branch.

Figure 5.5: Two different configurations of inputs in the two-phase MV.

The other input combinations are not reported, as they confirm the observations concerning the All ones configuration: the MV simulated in this way is not working.

Thus, two possible causes can be identified to justify the absence of proper propagation of information:

- The number of molecules belonging to the individual clock regions is too high. As seen in the case of the multi-line single phase wire, reducing the number of molecules increases the effectiveness of logic propagation;
- The potential applied to the electrodes is too low and cannot generate a sufficient clock field. The localization of the active dots would therefore be insufficient to ensure proper polarization of the molecule.

Consequently, the next two chapters explore the variations that can be implemented in the structure to achieve a neural system that functions correctly.

Two phase MV: variation on the geometry of the electrodes

A possible variation on the structure presented in subchapter 5.2.1 consists in the application of variations regarding the geometric parameters. This sub-chapter reduces the size of the electrodes in such a way that the number of molecules associated with them is reduced. The aim of this sub-chapter is therefore to vary the number of molecules

associated for every clock regions.
A simulation characterized by a 3 nm wide and 3 nm high trench is therefore conducted, as in the previous subsections. The spacing between the upper electrodes is kept at 2 nm: a further reduction would lead to enormous manufacturing difficulties, given the fabrication resolution required. The size of the upper electrodes is shrinked from 10 nm per side to 8 nm. In this way, there are nine molecules per branch. The number of molecules in the transition region changes from 37 to 29.
Voltages in modulus equal to 3 V are applied to the upper electrodes in order to maintain a term of comparison with respect to the structure presented in subchapter 5.2.1.

The electric fields at the center of the trench are analyzed along the section that first runs through the input branch, then the transition region and finally the output region. Fig. 5.6 shows a trend consistent with those obtained previously, with maxima approaching those theorized by the parallel plate capacitor model and minima coinciding with the spacing zones between the electrodes.

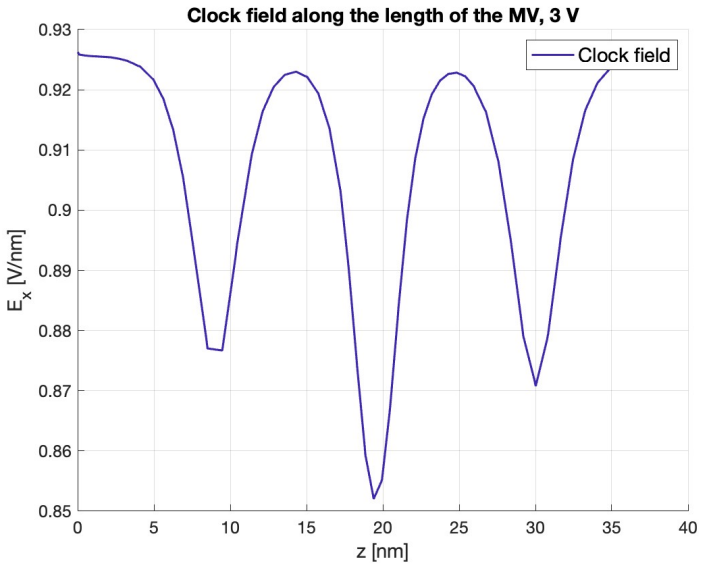

Figure 5.6: Clock fields in the two-phase MV characterized by shrinked electrodes. The voltage applied to the upper electrodes is equal to -3 V.

The maximum values are slightly lower than the one in the subchapter 5.2.1. This decrease is caused by the smaller size of the electrodes: when an electrode is shorter, the electric field does not have enough space to reach its theoretical maximum as it must quickly begin to decrease due to the presence of the spacing zone.

The operation of the structure presenting these charge distributions is verified using SCERPA. A representative result of the simulations is shown in Fig. 5.7. The chosen case study consists of setting the two vertical branches (arranged along the y-axis) at an input of '0'. The horizontal branch, along the z-axis, is instead set to '1'.

An aberration phenomenon can be again appreciated at the beginning of the output wire: the system does not work.
The reason probably lies in the proximity between the molecules of the vertical input and the output branch.

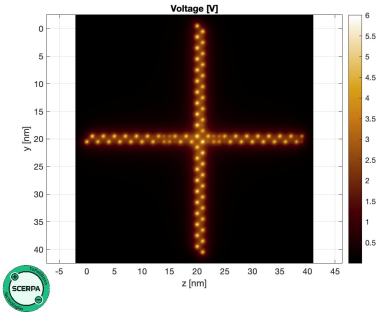

Figure 5.7: '010' input configuration in the two-phase MV characterized by shrinked electrodes. An aberration phenomenon obstacle the correct propagation of the logical value.

Two phase MV: variation on the applied voltage

This subchapter analyzes the MV divided into two clock regions in the presence of higher applied potentials at the electrodes with respect to the ones used the subchapter 5.2.1. If a potential applied to the electrodes of 3 V in modulus was previously analyzed, the potential is now doubled to 6 V in modulus. Such an abrupt increase is justified by the desire to verify whether in extreme conditions the circuit can actually function or whether it is the created structure that presents insuperable limits.

By analyzing only the most relevant instant of time, so the time step at which every region is in the **hold** state, the electric field pattern shown in Fig. 5.8 is obtained. As in the previous subsections, the analysis spatial points remain in the center of the trench, at a height of 0.4 nm with respect to the trench electrode. The electric fields in the horizontal arm of the MV are identical to the fields measured in the vertical arm, due to the perfectly symmetrical nature of the created structure. Fig. 5.8 therefore only shows the field occurring in the trench parallel to the z-axis. To avoid redundancy, the behaviour of the clock field in the trench along the y-axis is not reported. The behaviour of the electric field is similar to the one reported in the previous subchapter. Fig. 5.8 presents significantly higher clock values compared to the case where the voltage applied to the electrodes was equal to -3 V. In this subchapter, the maximum clock value is perfectly doubled with respect to the previous simulation, where the maximum was equal to 0.93 V/nm. This result confirms what is expected from a theoretical point of view: the deviation with respect to the parallel plate capacitor model are negligible.
The minimum values of the clock field are also perfectly doubled with respect to the values shown by the MV with -3 V applied. By recalling the VACT of the bis-ferrocene, it can be noticed that these obtained clock field values induce an optimal charge separation in the active dots.

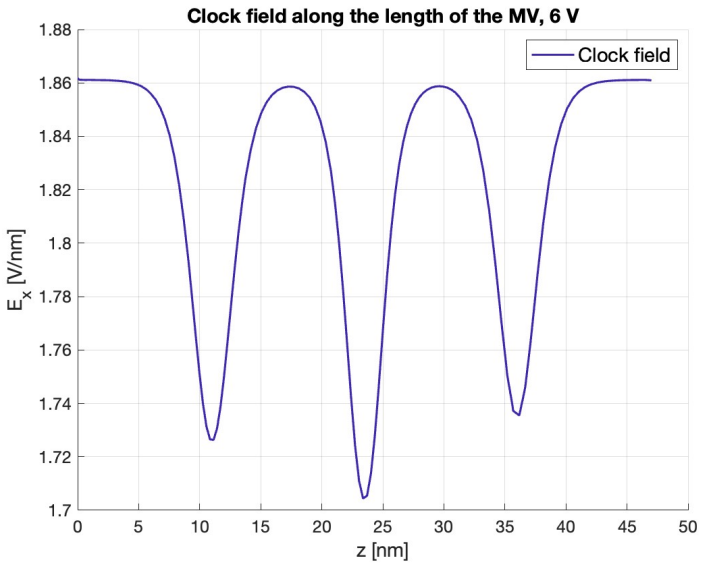

Figure 5.8: Clock field in the two-phase MV, every clock region is set to -6 V.

In order to verify the actual effectiveness of the MV presented in this subchapter, it is necessary to investigate its behaviour through SCERPA. The All ones conditiconfiguration is initially analyzed, as it has been previously shown to be an excellent example for understanding the circuit's functionality.

Fig. 5.9 shows what is obtained through SCERPA by applying '1' to the three inputs. At a glance, the points appear brighter than the MV to which -3 V is applied. Furthermore, although the molecule at the center of the transition region senses the lower clock field, the existence of four molecules surrounding the central one reinforces the propagation of information. The output, displaying a slight fading effect in the last two molecules of the region, is correctly polarized. No phenomena where the charge localizes to both active dots of a molecule are visible (aberration phenomena). It can therefore be said that the MV functions correctly.

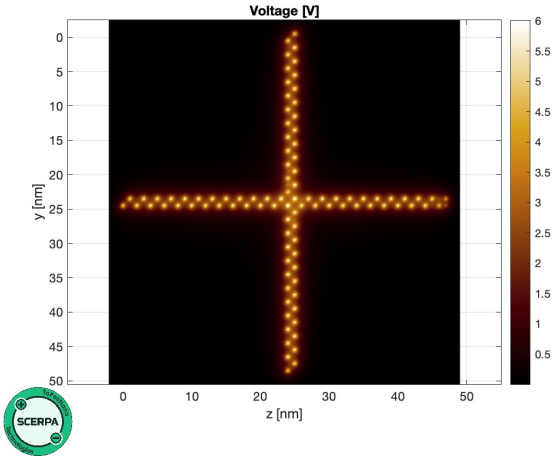

Figure 5.9: Correct propagation by a '111' configuration in the two-phase MV, where the voltage applied to the upper electrodes is equal to -6 V.

Having tested the operation of the MV in its limit and most unfavourable case, the other possible input combinations are then analyzed. Fig. 5.10a shows how, by setting only the input belonging to a vertical arm equal to '0' and keeping the other two inputs at '1', the correct value is obtained at the output. Another alternative is the application of the minority value (in this case '0') as the input of the horizontal input arm. Given the arrangement of the molecules in the center of the transition region, in fact, this input arm is slightly more important in terms of weight than the other two inputs. The structure, shown in Fig. 5.10b, is perfectly functional. In contrast to the other cases, it can be appreciated a phenomenon which reveals the reasons of the functioning. At the end of the horizontal input arm, in fact, there is an area where the molecules do not assume any precise binary value. Instead, the charge in those molecules is distributed between the two active dots, hence it is explained the presence of two bright spots in those molecules. This phenomenon proves the existence of **back-propagation**. Indeed, the information assumed by the charge localization in a molecule influences all adjacent molecules, without favouring any precise direction. Consequently, since the center of the transition region is correctly polarized due to the majority of input molecule, the information assumed by the center of the transition region not only influences the molecules of the output wire but also those of the horizontal arm of the input wire. These molecules will be affected by an intense electric field created by the charge separation at the center of the transition region, an electric field more intense than the one felt by the branch molecules. This phenomenon, therefore, is crucial in order to obtain a correct localization of the output charge.

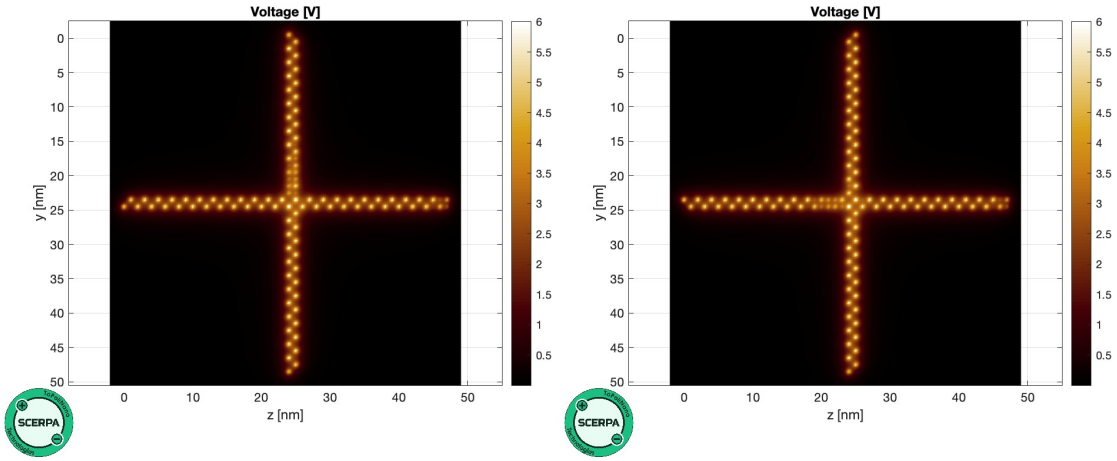

(a) '011' configuration in the two-phase MV.

(b) '011' configuration in the two-phase MV.

Figure 5.10: Two-phase MV with an applied voltage to the upper electrodes equal to -6 V. In both cases, the output correctly reaches the end of the neuron.

Going on with the analysis it is observed that, by varying the voltage value applied

to the upper electrodes, a minimum threshold could be identified to ensure a proper MV operation. After several simulations, not reported here to avoid redundancy, this minimum value is set to 5 V. If a -in modulus- lower potential is applied, the clock field is not sufficient to ensure a correct functioning of the neuron.

It can therefore be concluded that the MV presenting two clock regions proves to be a functioning structure, exceeding the critical voltage threshold of 5 V. The major limitation of this result lies in the high voltage values required at the upper electrodes. Although these fields do not exceed the dielectric strength of the dielectric (equal to approximately 8 MV/cm, [**?**]), which would lead to the destruction of the device, they do heavily influence the power dissipated by the circuit.
It is therefore necessary to think of different solutions, capable of maintaining a correct molecular functioning and ensuring a reduction in the applied voltages.

5.2.2 A more stable configuration: three phase MV

This section regards the exploration of the neuron's functioning by varying the clock application. In particular, while previous subchapters analyzed a neuron in which the clock was applied by partitioning the MV into two regions (input/output and transition region), the circuit is now divided in three different clock regions. In this way, input and output branches are associated to different clock regions and are independent one from the other. Hence, when, for example, the input branch is in **hold** state, the output part can be maintained in the **reset** state.
This mechanism promises a better functioning of the neuron. Indeed, by keeping in reset the output region while the rest of the circuit is transmitting the binary value, it is possible to avoid spontaneous polarization in the molecules placed far from the driver regions. Furthermore, the binary value that has reached the output branch will be sufficiently strong to vary the localization in the active dots of the output wire, given that the output molecules don't present ane binary value already encoded in them.
Consequently, in the MV divided into three clock regions, there is no longer a more critical time instant with respect to the others, when all zones are at the same time active. This configuration is indeed avoided. Therefore, in order to understand if the neuron is actually functioning, it is necessary to analyze all the time instants into which the operation performed by the MV is divided. Consequently, the analysis is divided into four time steps:

1. In the first time step, the input zone is responsible for propagating the logic information provided by the driver molecules. The voltage applied to its electrodes must therefore be negative. Conversely, the transition region and the output region must be in a reset state, preventing spontaneous localization on one of the active dots;

2. In the second time step, the input region must maintain the assumed information to provide correct input to the transition region. The potential at its electrodes continues to be negative. The transition region is activated and enters the **switching** phase: the potential at its upper electrodes is brought to a negative value. The output region continues to encode no binary value: the potential of its upper electrodes continues to be positive;

3. In the third time step, the output region is brought into the **switching** phase. The binary information must now be propagated from the transition region, now in a **hold** state, to the output region, which must now be able to locate the positive charge in its active dots. The input region, on the other hand, must no longer hold the logical information after propagating it to the transition region. The input region can then be reset, erasing the assumed binary information;

4. In the fourth time step, the output region is in the **hold** state, holding the binary information at the output. The transition region no longer has to supply the binary value to the output and can be placed in a reset state. The input wire, which had itself been placed in a reset state, is now free to propagate new input from the driver molecules. It can then be placed in a **switching** state by applying a negative voltage

to its electrodes. The fact that the transition region is in a reset state prevents an overlap between old information (in the output region) and new information (in the input region).

A schematization of the clock system is given in table 5.1.

Time step	**Input Region**	**Transition Region**	**Output Region**
1	Hold (**-V**)	Reset (**+V**)	Reset (**+V**)
2	Hold (**-V**)	Switching (**-V**)	Reset (**+V**)
3	Reset (**+V**)	Hold (**-V**)	Switching (**-V**)
4	Switching (**-V**)	Reset (**+V**)	Hold (**-V**)

Table 5.1: State of the different regions in the three-phase wire during the four time steps of the clocking mechanism.

A pictorial representation of the clock system is then reported in Fig. 5.11, where the yellow electrodes refer to a negative applied voltage (**switching** and **hold** state), while the blue ones refer to a positive applied voltage (**reset** state).

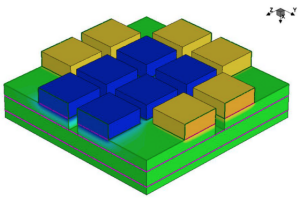

(a) Time step 1.

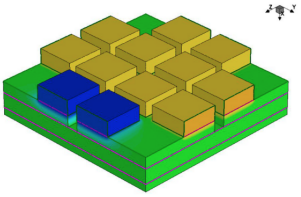

(b) Time step 2.

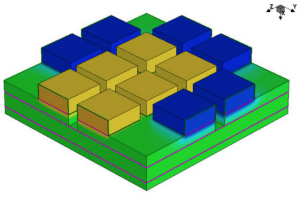

(c) Time step 3.

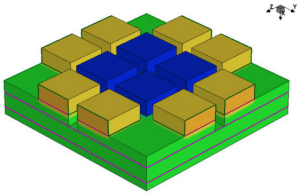

(d) Time step 4.

Figure 5.11: Graphical representation of the different states in the three-phase wire during the four time steps of the clocking mechanism.

The simulation are conducted by varying the applied voltages until the binary information correctly reaches the end of the circuit. This empirical method ensures to find the lowest value of voltage that guarantees the functioning of the neuron.

5.2.3 Three phase MV: 3 V HOLD, 3 V RESET

The analysis of the three phase MV begins by applying symmetrical voltage values to the electrodes, providing to the electrodes in the RESET state an applied voltage of 3 V and to the electrodes in the **hold** and **switching** states an applied voltage of -3 V.

The obtained clock fields are reported in Fig. 5.12a, 5.15b, 5.13a, 5.13b, 5.14a, 5.14b, 5.15a. **??**. Through their analysis, the alternation between positive and negative clock fields can be spotted. The variations with respect to the saturated values are linked to the spacings between the upper electrodes of the structure. Notice the extensions of the axis, given the geometry of the MV that has previously been described: along the z-axis, from z = 0 nm to z = 10 nm, there is an input branch; between z = 12 nm and z = 35 nm there is the transition region; between z = 37 nm and z = 47 nm the output region can be found. Along the y-axis, the other two input branches are placed between y = 13.5 nm and y = 23.5 nm and, similarly, between y = -13.5 nm and y = -23.5 nm. Between them, there is the transition region.
The red spots highlight the center of the structure, where the molecule at the center of the transition region is placed.

All possible input configurations are then tested. The circuit does not function properly for every input combination. Indeed, despite the functioning of some inputs (like the All ones configuration), the MV does not propagate the correct output for every case.

(a) Clock fields along the y-axis.

(b) Clock fields along the z-axis.

Figure 5.12: Clock fields along the different axis of the MV at Time step 1. The maximum field values are observed in the input regions which are set in **hold** state.

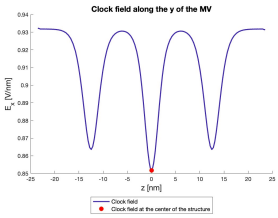

(a) Clock fields along the y-axis.

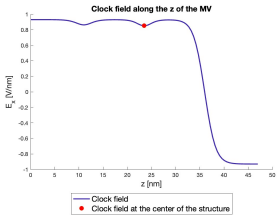

(b) Clock fields along the z-axis.

Figure 5.13: Clock fields along the different axis of the MV at Time step 2. The minimum peaks along the y-axis correspond to the spacings between the upper electrodes of the structure. Only the output region is in RESET state, highlighted by the minimum clock field values at the end of the x-axis.

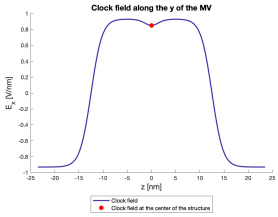

(a) Clock fields along the y-axis.

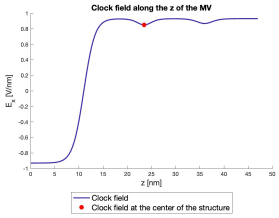

(b) Clock fields along the z-axis.

Figure 5.14: Clock fields along the different axis of the MV at Time step 3. The input region along the y-axis and z-axis are in RESET state, hence the negative values. Maximum clock field values occur in the transition region, visible on both axes, and in the output region, as it can be seen in the z-axis graph.

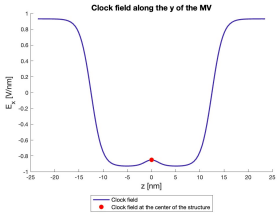

(a) Clock fields along the y-axis.

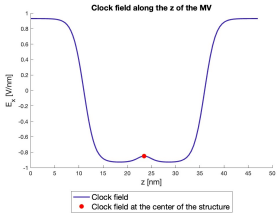

(b) Clock fields along the z-axis.

Figure 5.15: Clock fields along the different axis of the MV at Time step 4. The transition region is now in RESET state, separating a new input that is propagating in the input region from the previous binary value that is still at the end of the output region.

The All zeros configuration is then studied as a case-example. At the first time step, only the input region is in the **hold** state. Transition and output regions, on the other hand, are in the RESET state. The fact that light spots can still be identified in Fig. 5.16 means that the reset state is not complete. The clock electric field does not appear to be sufficient to locate all the charge in Dot 3; consequently, some of the charge will remain evenly distributed on the active dots. This in itself is not an impediment to the propagation of information. It is therefore necessary to analyze the subsequent time steps. During the second time step, the transition region is brought into the **switching** state. The input region remains in the **hold** state while the output region remains in the **reset** state. In this time step, an aberration phenomenon occurs: immediately after the central point of the transition region in Fig. 5.17, molecules can be seen that do not encode any precise binary information: both active dots show bright spots. The information is lost: what is propagated to the output is an erroneous logical value, given by the spontaneous polarization of the molecules of the final branch which, no longer affected by an input, assume the value to which they spontaneously tend. During time steps 3 and 4, therefore, the propagation of this logical wrong information occurs. The alternation of the light spots that makes it appear that there is a correct functioning of the wire should not be misleading: the alternation is due to the electrostatic repulsion that is naturally created between the molecules. The MV with such voltages does not work. This result is not completely unexpected: during the approach to SCERPA, it was noted that molecules affected by a clock field of -1 V did not enter a complete reset state. Slightly glowing spots could be appreciated within the circuit, as can now be seen in the MV. Indeed, such applied voltages induce an average electric field sensed by the molecules lower than -1 V. Therefore, a different value for the application of the RESET state must be looked for.

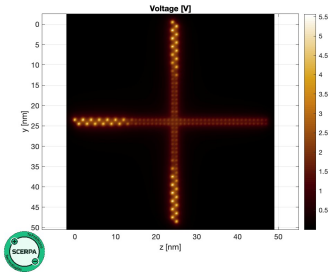

Figure 5.16: All zeros configuration, time step 1.

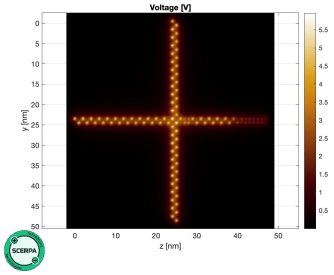

Figure 5.17: All zeros configuration, time step 2.

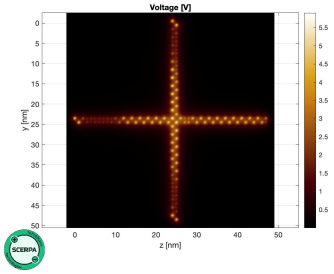

Figure 5.18: All zeros configuration, time step 3.

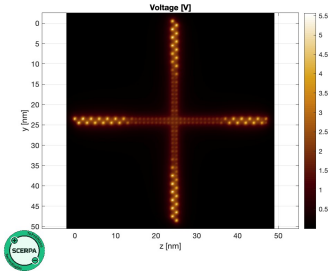

Figure 5.19: All zeros configuration, time step 3.

5.2.4 Three phase MV: 3 V HOLD, 5 V RESET

The combination of applied voltages of -3 V for the **switching** and **hold** state and 5 V for the **reset** state is here tested. As before, images of all input combinations are not shown: Fig. 5.20 only reports one example of input combination, in which the inputs of the highest vertical branch and of the horizontal one are fixed to '0' while the lowest vertical input branch is set to '1'. The combination, from now on referred as '001' configuration, shows how the neuron still does not work.

At the first time step(Fig. 5.20a), the logical value is correctly transmitted along the input branches, while the remaining of the circuit is in the **reset** state.
The problem lies in the region after the central molecule of the transition region, where an aberration phenomenon can be again spotted at the Time step 2 (Fig. 5.20b). It means the the **reset** clock field is not sufficient to correctly localize the predominance of the charge on Dot 3: the molecules of the output region are not enough in a **reset** state, thus their correct polarization is more difficult.
At the Time steps 3 and 4 (Fig. 5.20c and 5.20d), the incorrect logical values reaches the output of the MV.
The neuron still does not work.

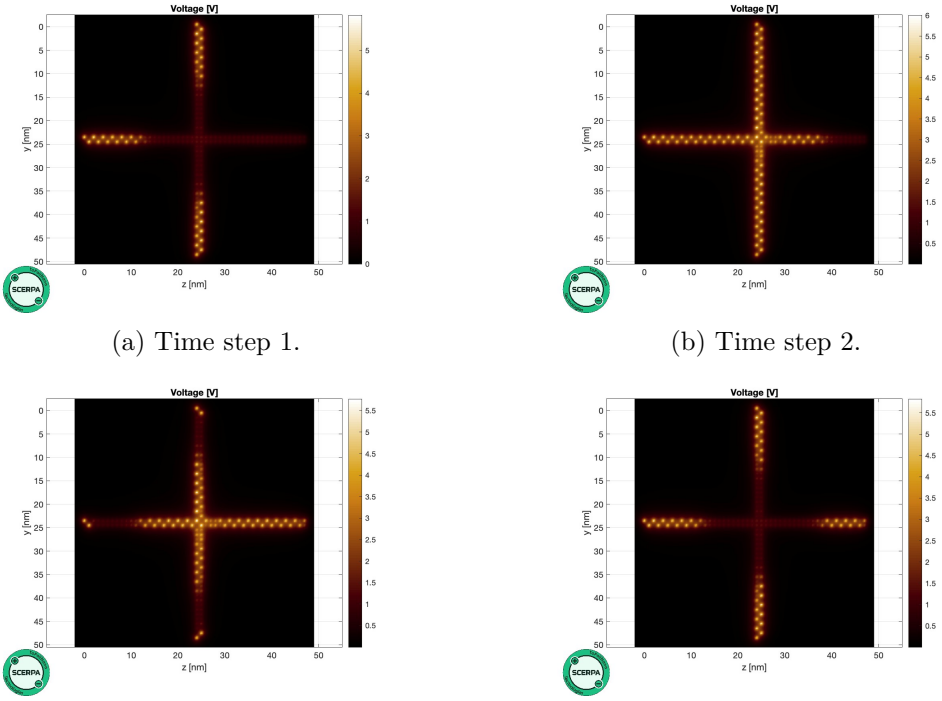

(a) Time step 1.

(b) Time step 2.

(c) Time step 3.

(d) Time step 4.

Figure 5.20: Time steps of the '001' configuration. Applied negative voltage: -3 V, applied positive voltage: 5 V.

5.2.5 Three phase MV: 3 V HOLD, 6 V RESET

A further increase in the **reset** voltage is then tested. While maintaining the negative applied voltage equal to -3 V, the positive voltage rises to 6 V, doubling the initial value tested in the sub-chapter 5.2.3. By recalling the quadratic relation between dissipated power and voltages (and so in an attempt to minimize the power consumed by the neuron as much as possible) the negative voltage remains fixed at -3 V.

Every possible input configuration has been tested, by validating the functioning of the neuron. Such high positive clock field, indeed, ensures a correct localization on Dot 3, putting the correct molecules in a **reset** state. The phenomenon is visible by the nearly complete absence of light spots in the regions where the **reset** is applied.

Two example are therefore reported in Fig. 5.21 and 5.22. Respectively, the All zeros configuration and the '001' configuration are depicted, subdivided in the four time steps needed to correctly apply the clock mechanism.

In both of them, Time step 1 depicts the input transmission from the driver molecules, placed at the extremes of the input branches. In time step 2, the transition region is activated: Fig. 5.21b and 5.22b show how the molecule at the center of the transition region is correctly polarized, assuming the binary value encoded by the majority of the inputs. The molecules of the output branch near the transition region represent the correct binary value. The phenomenon of back propagation can be spotted along the vertical input branch with the minority input (Fig. 5.21b): the influence of the molecule at the center of the transition region is so high that it varies the localization on the branch that does not encode the majority value.
Another interesting phenomenon can be appreciated in Fig. 5.21c, the figure referred to the the Time step 3. At Time step 3, the input region is switched off, by forcing the molecules in a **reset** state. The higher vertical branch, then, presents a slight **skin effect**. There is a partial localization of the charge on the 'wrong' active dot, not fully respecting the alternation in the information assumed by the different molecules. This effect is due to the polarization in the first molecule of the output branch: encoding the correct binary value, the charge is localized near the last molecule of the highest vertical input branch. The proximity between the two molecules induces a slight back propagation phenomenon, favoured by the absence of the driver molecules influence (the input branches are now in **reset** state).
This skin effect does not compromise the information propagation but shows how the interactions between the molecules are delicate. In addition, it reveals the causes behind the MV malfunctioning in the preceding sub-chapters. The presence of molecules close to each other, even diagonally and not in direct concurrence, is a phenomenon that cannot be neglected in order to ensure a proper propagation of information within circuits.

At time step 4 (Fig. 5.21d and 5.22d), the neurons reveal the possibility to implement a kind-of **pipelining** technique: while the output is still inside the circuit, a new logical value can be transmitted through the driver molecules. The separation between input

and output branches by the presence of the transition region permits to avoid waiting that the information is completely outside the system.

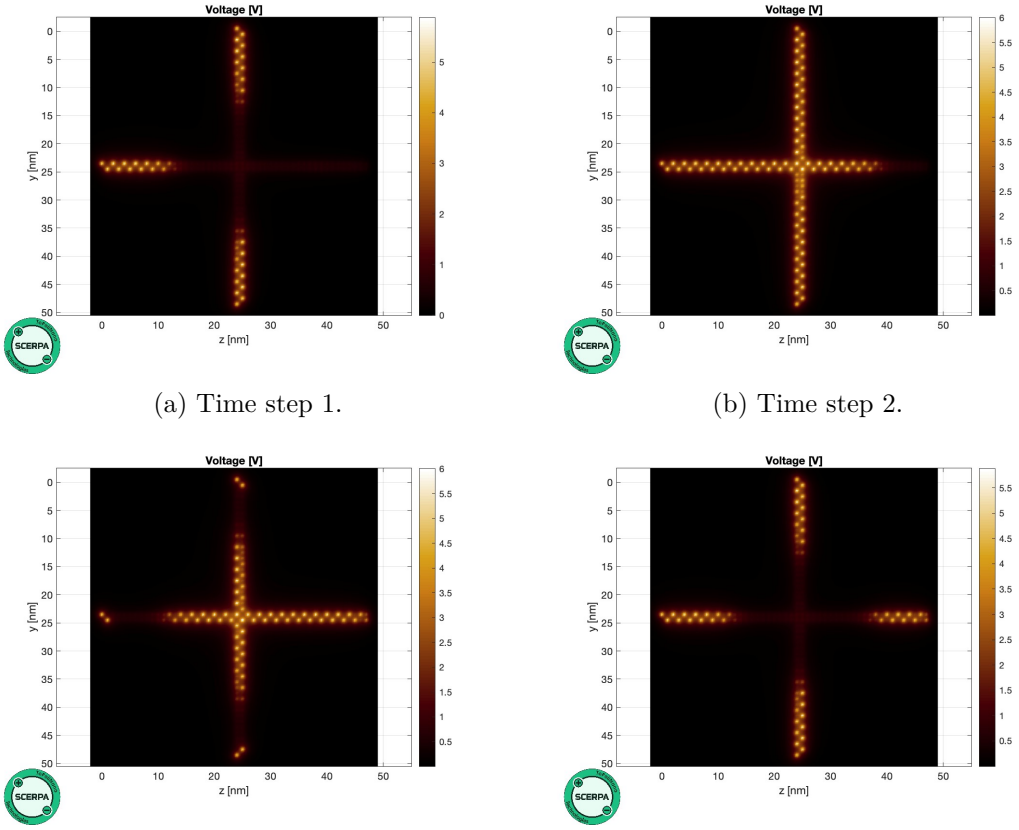

(a) Time step 1.

(b) Time step 2.

(c) Time step 3.

(d) Time step 4.

Figure 5.21: Time steps of the '001' configuration. Applied negative voltage: -3 V, applied positive voltage: 6 V.

The analysis of the different voltage combinations applicable to the electrodes showed how important it is to choose accurately the clock values. While a negative voltage of -3 V is sufficient to aid the propagation of information, it was discovered that to induce the **reset** state, the same value changed by a sign is not sufficient. Simulations with **reset** voltages lower than 6 V, in fact, showed aberration phenomena, resulting in some input cases in the propagation of completely wrong logic information. Conversely, the application of 6 V seems to correspond to the minimum voltage value applicable to the electrodes to induce the molecules in a better **reset** state, characterized by an absence of bright spots in the simulations conducted through SCERPA. The analysis reveals that although the circuit works, there are effects to be taken into account: skin effects and back propagation phenomena seem to be unavoidable. In conclusion, the application of a higher **reset** potential resulted in a functioning neuron.

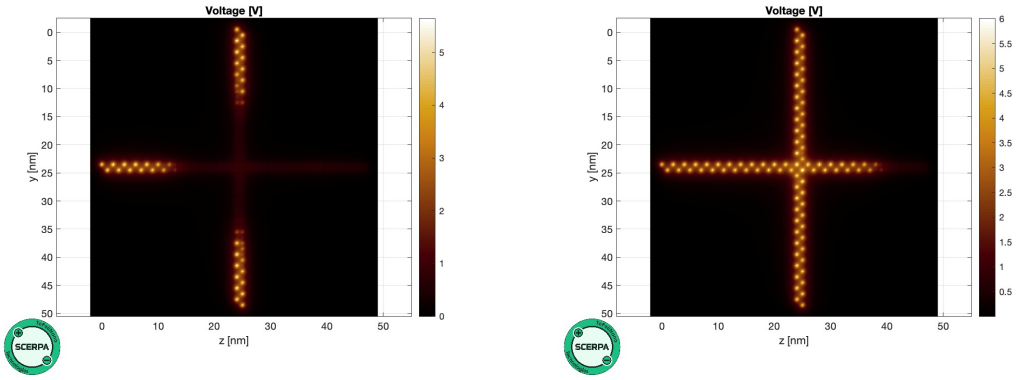

(a) Time step 1.

(b) Time step 2.

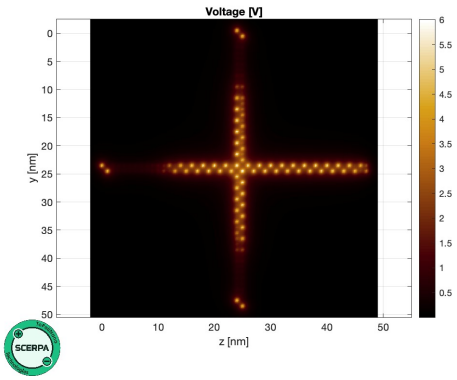

(c) Time step 3.

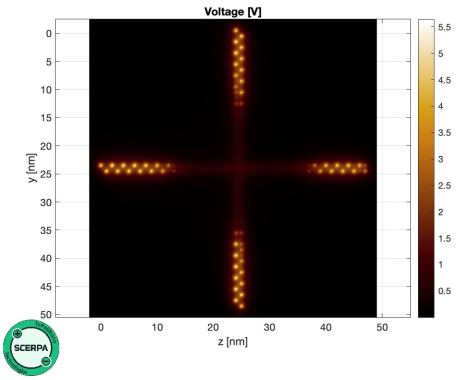

(d) Time step 4.

Figure 5.22: Time steps of the All zeros configuration. Applied negative voltage: -3 V, applied positive voltage: 6 V.

The conclusion of this chapter is the appreciation of the superiority of the three-phase MV over the two-phase MV. Since it is necessary to maintain high reset voltages, the application of a **hold** voltage of -3 V makes permits the minimization as much as possible of the energy dissipated by the circuit. In addition, the three phase MV promises a more stable propagation of information, in which the output branch is placed in **reset** state for as much of the time as possible, avoiding spontaneous polarizations that would obstacle the logical value being propagated and maintaining the molecules ready to assume the correct charge localization.

Chapter 6

Study of dissipated power

In the previous chapters, the behaviour of MolFCN technology was analyzed in detail, varying the structures designed to house the molecules and analyzing the electric fields required for the technology to function properly. The analysis began with a simple structure, a wire characterized by a single clock region, and then moved on to a more complex application case: an artificial neuron. The link made between the simulative environment of Sentaurus and that of SCERPA represented a further step towards a future realization of the device in practice, analyzing how realistic electric field distributions influence logic propagation. But, in order to fully understand the efficiency of the device and to maintain the direction towards a future realization of the device, it is necessary to extend the analysis by studying a very important parameter: power consumption. Understanding how much power the designed devices dissipate is in fact a fundamental aspect to be taken into account when designing a system. Power consumption does not only determine the energy efficiency of the technology but also influences secondary but no less important aspects, such as overheating, lifetime of the systems created and the environmental impact of creating the energy required to operate the devices.

Among the Beyond CMOS technologies, the MolFCN ones is characterized by a reduced occupied surface area an by a good computing speed. However, these two enormous advantages must not be compromised by an excessive power consumption, which would consequently influence the operating frequency and voltage values used, tahr should be therefore reduced, directly affecting the information propagated in the systems. Understanding how much power is dissipated by MolFCN technology, therefore, is not just a theoretical exercise but allows to assess its effectiveness, comparing it with both emerging technological alternatives and well-established devices.

In this chapter, the dissipative contributions of MolFCN technology will be analyzed, starting with the theoretical formulation of dissipated power and then proceeding towards a quantitative analysis, exploring the consumption of previously simulated structures. Particular attention will be paid to the neural case study, comparing the obtained dissipated power values with the ones reported by other technologies that implement artificial neurons.

6.1 Power dissipation in MolFCN devices

Power consumption in a MolFCN device is not based on conductive phenomena. This statement arises from the observation of the fundamental mechanism on which the technology is based: electrostatic repulsion between the molecules in the circuit. This physical phenomenon is based on the localization of charges within the molecules and therefore does not require a shift of electrons from one molecule to another. Consequently, the contribution of power dissipation due to conductive phenomena is minimized, becoming irrelevant. Considering that conductive phenomena are linked to static power (static power is indeed the product of undesired leakage currents and supply voltage), it can therefore be concluded that MolFCN has a negligible static power contribution.

The energy consumption of the technology is mainly related to the dynamic power contribution, so the power used to switch from one state to another.
Whereas in MOSFET technology the dynamic power was related to the power used to vary the binary state, in MolFCN technology it is not imputable to the variation of the binary state it-self. The variation of the logical value occurs spontaneously, to simplify, due to the coulomb repulsions between the charges. Power consumption, on the other hand, is linked to the application of the electric clock field, a mechanism that ensures the functioning of the circuits but at the same time consumes energy.
In fact, when analyzing a system implemented with MolFCN technology, if the molecules don't absorb power, the only remaining elements are the system's electrodes. A time-varying voltage is applied to them, so that they can generate an appropriate clock field. These voltage values are mainly responsible for the power consumption within the MolFCN technology.

A closer look at the system reveals that the arrangement of the electrodes generates a phenomenon that needs to be investigated in more detail. As mentioned in the previous chapters, the upper electrodes are separated from the trench electrode by a dielectric layer, forming an architecture that recalls the parallel plate capacitor model. Similarly to a capacitor, therefore, a build-up of charges is obtained at the interface between the metal and dielectric, proportional to the voltage separating the electrodes themselves. The establishment of these parasitic capacitances is an unintended phenomenon, but one that is inseparable from the very physics of the structure's conformation.
In fact, the need to apply an electric field to the molecules of the structure requires the creation of structures that, when subjected to a potential difference, accumulate charges on the metal surfaces. It is precisely this process that makes it possible to obtain clock fields capable of aiding the propagation of information in the structure. The inevitable disadvantage lies in the energy consumed by the system.
Indeed, when a voltage is applied to the electrodes, the parasitic capacitances become charged, accumulating charge at the interface between metal and dielectric. This accumulation requires energy: the work W needed to move a charge q to one of the two electrodes can be expressed, in infinitesimal terms, as in Eq. 6.1.

$$dW = \Delta V \, dq \tag{6.1}$$

But from the definition of capacitance (equal to the ratio of stored charge with respect to the potential difference applied to the electrodes), the potential difference ΔV can be expressed as in Eq. 6.2.

$$dW = \frac{q}{C} dq \tag{6.2}$$

Overall, the total work that is done to bring a charge value Q to an electrode is obtained by integrating Eq. 6.2. In this integral, the initial charge value can be assumed to be 0: it will be the lower extreme of the integral.

$$dW = \int_0^Q \frac{q}{C}\, dq = \frac{Q^2}{2\,C} = \frac{1}{2}\, C\, V^2 \tag{6.3}$$

The work done coincides with the energy stored in the system. But this contribution, which is obtained during the phenomenon of charging the capacitors is not the only term to be taken into account.

The voltage source to which the electrodes are connected, in fact, provides energy that can be expressed through Eq. 6.4.

$$E = \int_0^T I \cdot V dt = \int_0^T C \frac{dV}{dt} V dt = CV \int_0^V dV = CV^2 \tag{6.4}$$

Half of this energy is stored in the capacitance instaurated between the upper electrodes and the trench electrode. The other half is dissipated through the intrinsic resistance that the parasitic capacitance presents and is therefore trasnformed into heat. In addition it must be considered how, once the applied voltage is removed, the capacitor will present a discharge phenomenon: the amount of stored energy will be released, dissipating it again as heat.

By recalling how energy is related to the concept of power through the period of time in which it is consumed (T), Eq. 6.5 can be obtained. It expresses the concept of power in the MolFCN technology.

$$P = E \cdot T = CV^2 f_{clock} \tag{6.5}$$

The equation presented in 6.5 represents a fundamental result for the analysis of power dissipation by MolFCN devices. Through this equation, it can in fact be established how the power dissipated by MolFCN technology is mainly a dynamic power, related to the switching of the electrodes placed to provide a correct electric field to the molecules in the trench. This dynamic power is also intrinsically related to the charge and discharge phenomena of parasitic capacitances created by the device layout itself.
Eq. 6.5 therefore shows how energy consumption is closely related to the concepts of parasitic capacitance C, the voltage at the upper electrodes V (considering that the trench electrode is connected to ground) and the clock frequency f_{clock}. It is therefore necessary to explore these aspects, at first analyzing the parasitic capacitances within the structure and then appreciating the variations in energy consumption as the voltage and the period for which the electrodes are turned on change.

6.2 Capacitance analysis

In the previous chapter, it was possible to appreciate how the power consumption associated with MolFCN technology is influenced by the charge and discharge phenomenon of the parasitic capacitances in the device. The potential difference established at the electrodes, in fact, generates an electric field, consuming energy. This electric field is not an active part in the logic process; nevertheless it is able to help the information propagation that, in some cases, would not take place without it.
As already mentioned, the system can be analyzed in order to understand the electric fields in it by using the simplification of the parallel-plate capacitor model. This ideal representation provides a theoretical basis for understanding the physical phenomena in the structure.
Using this model, it can be assumed that the electric field established between the electrodes will lead to a build-up of charges on their surfaces, a non-negligible capacitive phenomenon.
In the molecule hosting structure where the molecules will be placed, in fact, the application of a voltage at the upper electrodes -while keeping the trench electrode grounded- creates a parasitic capacitance between the two electrodes, which are separated by a dielectric layer. Using the model of the parallel-plate capacitor, the value of the created capacitances can be appreciated through Eq. 6.6.

$$C = \varepsilon_0 \varepsilon_r \frac{A}{d} \tag{6.6}$$

Where ε_0 and ε_r are, respectively, the vacuum permittivity and dielectric relative permittivity, A refers to the surface area of the two electrodes and d is the distance between them.
The analysis of the capacitance between the electrodes shows how it is directly influenced by the geometry of the device and the material chosen as dielectric. Changing these characteristics changes the capacitance value, directly influencing the energy consumption dissipated by the structure.
Consequently, it is necessary to investigate this phenomenon by studying the capacitances of previously simulated structures in order to be able to provide estimations of the dissipated power.

At first, the simplest simulated structures are analyzed, the ones defined as the one phase wires. These structures are characterized by two upper electrodes and one trench electrode: three parasitic capacitive contributions can be identified in them:

- Capacitance between upper left electrode and trench electrode;
- Capacitance between right upper electrode and trench electrode;
- Capacity between the two upper electrodes.

The first two contributions are identical: the symmetry of the structure involves that the surface area of the electrodes is the same, that the distance between the two capacitances

is identical and that, of course, the material does not change. Regarding the capacitive contribution between the two upper electrodes, the measured values show that in the power analysis it is a negligilbe contribution. Since the two electrodes of the one phase wire belong to the same clock region, the same voltage value will be applied to them. As there is no potential gradient, the capacitance is not charged and discharged, and no energy is dissipated. Consequently, this capacitive value will not be considered in the circuit power calculations.

An analysis of the parasitic capacitances between top electrodes and trench electrode in the structures with various dielectric and trench heights (3 nm, 6 nm and 9 nm) is shown below. The table 6.1 refers to single line one phase wires, characterized by a trench width of 3 nm. The table 6.2, on the other hand, reports the capacitive values in the multi-line one phase wires.
The values shown refer to the capacitance between the upper and trench electrodes. To maintain accurate accuracy in the results, the values in the tables are obtained by averaging the capacitance between the right upper electrode and trench and the capacitance between the left upper electrode and trench. The two capacitance values show differences in the order of zeptofarad, which can be attributed to the numerical simulation conducted by Sentaurus. Nevertheless, to present both values, average values have been calculated and are presented in the tables.

Single line one phase wire			
Dielectric	**h = 3 nm**	**h = 6 nm**	**h = 9 nm**
SiO_2	1.8780×10^{-18} F	1.0935×10^{-18} F	8.0193×10^{-19} F
Al_2O_3	4.0323×10^{-18} F	2.3509×10^{-18} F	1.7385×10^{-18} F
HfO_2	9.3891×10^{-18} F	5.5284×10^{-18} F	4.1055×10^{-18} F

Table 6.1: Parasitic capacitances between upper electrodes and trench electrode, single line one phase wire.

Multi-line one phase wire			
Dielectric	**h = 3 nm**	**h = 6 nm**	**h = 9 nm**
SiO_2	1.9379×10^{-18} F	1.1337×10^{-18} F	8.3195×10^{-19} F
Al_2O_3	4.1016×10^{-18} F	2.3970×10^{-18} F	1.7726×10^{-18} F
HfO_2	9.5801×10^{-18} F	5.5899×10^{-18} F	4.1502×10^{-18} F

Table 6.2: Parasitic capacitances between upper electrodes and trench electrode, multi-line one phase wire.

As it can be seen by comparing the tables, the capacitances as the trench width varies

are not perfectly identical. Increasing the size of the trench results in an increase in the total area of the structure, changing the area occupied by the trench electrode. In the case of the one phase wire, while the trench electrode in the single-line structure has an area equal to $602\,\mu m^2$, the area of the trench electrode in the multi-line structure is equal to $672\,\mu m^2$. This slight discrepancy does not lead to substantial differences in the values obtained.
It should be noted that the values remain in the order of attofarad: the minimum value presented by the single line one phase wire in SiO_2 and the maximum value assumed by the multi-line in HfO_2 are $10.987 \times 10^{-18}\,F$ apart.
For a more immediate understanding of the data, graphical representations of the capacitive values obtained from Sentaurus Device are reported.

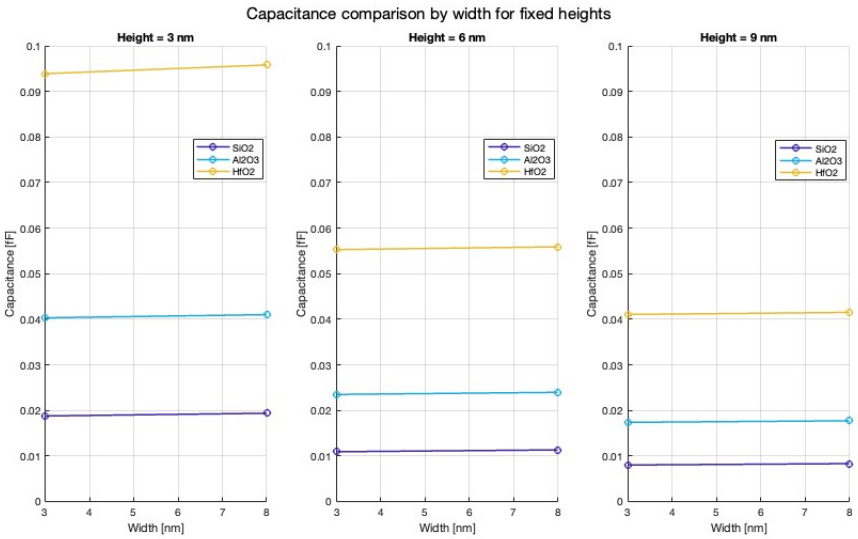

Figure 6.1: Capacitance comparison by trench width, trench height and dielectric adopted.

Fig. 6.1 shows the capacitance values distinguished by trench height (the graph at the lest shows the case where the trench height is fixed at 3 nm, the graph in the right shows the case where the trench height is fixed at 9 nm). It can be seen that the capacitance variations, as the trench width increases, are negligible: the values presented by the 3 nm wide trench and the 8 nm trench show negligible variations.
The capacitance behaviour, at a glance, is inversely proportional to the distance that separates the two electrodes, consistently to the ideal parallel-plate capacitor model. Between capacitance values and dielectric thickness, in fact, there is an inverse relationship that Fig. 6.1 confirms.
From the observation of Fig. 6.1, it should also be noted that the trend of the parasitic capacitances is directly proportional to the dielectric permittivity of the material separating the two electrodes. In fact, the SiO_2 structure, characterized by the lowest permittivity of the three materials considered, shows the lowest values. Accordingly, the

Al_2O_3 structure shows intermediate capacitive values, varying from 0.04 fF to just under 0.02 fF, while the Al_2O_3 structure.
A slight discrepancy must be noted between the values obtained through Sentaurus and those predicted by the parallel-plate capacitor model. For example, if the single-line structure in Al_2O_3 with a trench height of 3 nm is characterized by a capacitive value of 4.0232×10^{-18} F, the case with a trench height of 9 nm is not exactly one third of the initial value.
The fact that the values slightly vary from the ideal parallel-plate capacitor model is caused by the more complex geometry of the simulated structures, compared to the ideal case in which the two electrodes have equal surface area.

Fig. 6.2 better shows the differences obtained when the dielectric material varies. The capacitance values are calculated as the average value between those presented in the single-line system and the multi-line system. The graph again confirms the theoretical predictions, characterized by a capacitive behaviour directly proportional to the permittivity value of each material.

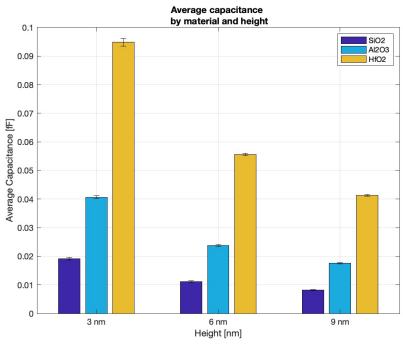

Figure 6.2: Parasitic capacitances values bar chart, obtained by varying the dielectric material and the trench height.

It is therefore concluded that the optimal value of capacitance, the one for which power consumption is directly proportional to it, is obtained by choosing the dielectric characterized by the lowest permittivity and by the highest possible trench height.

6.3 Power analysis: one phase wire

Once the design combinations affecting the parasitic capacitance values have been analyzed, the next step is to actually analyze the power the one phase wire needs to operate correctly. The capacitive values obtained were incorporated into the power equation expressed in the sub-chapter 6.1, where the circuit dissipation is related not only to the system capacitance but also to the clock frequency and, quadratically, to the supply voltage.
First of all, it must be understood how to include the capacitive contributions of the two upper electrodes in the system. The one phase wire is in fact characterized by two upper electrodes, each of which creates a capacitive contribution with the trench electrode, and these values are equal due to the symmetry of the structure. Since the upper electrodes are supplied with the same voltage, there is no potential difference between them: they can therefore be considered as two equipotential points. From a circuitry point of view, since the capacitances have the same ground connection and the same voltage value on

the upper electrode, it can be concluded that the two parasitic capacitances are parallel to each other. It follows that the total capacitance of the one phase wire is equal to the parallel of the two capacitances: the total capacitance will be equal to the sum of the two.
As far as clock frequency and voltage are concerned (they are the two other parameters that appear in the equation to express the circuit's power), the two parameters can be said to be independent of each other. Consequently, in order to appreciate as many cases as possible and understand which power ranges can be consumed, several voltage values and several frequency values were analyzed. For voltage, it is chosen to vary the parameter to analyze its influence on power when it assumes a minimum value of 0.1 V and a maximum value of 6 V. The maximum value was chosen considering the voltage values applied in the previous chapters.
In order to avoid redundancy in the presentation of the results, a structure composed of a dielectric made of Al_2O_3, a wire characterized by a 3 nm wide and 3 nm high trench, was chosen as reference. The material represents a good compromise between electrical permittivity value (more than half of the permittivity value of hafnium dioxide) and production feasibility. As far as the trench width is concerned, it has been shown above that capacitance values do not vary considerably: it is indifferent, at capacitance levels, to choose to study a single-line or a multi-line system. The 3 nm height is the only arbitrarily chosen parameter, since its functionality has been demonstrated in the previous chapters. Furthermore, the MV presented in the chapter 5 presents this identical configuration, confirming its effectiveness.

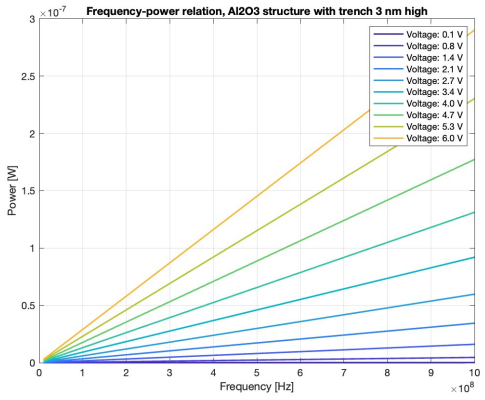

Figure 6.3: Frequency-power relation at various applied voltage. The analyzed structure is characterized by a Al_2O_3 dielectric and a 3 nm high trench.

Fig. 6.3 shows the behaviour of power as the clock frequency varies. The ten curves shown refer to ten different voltage values applied at the upper electrodes. As expected from observing the power equation, the power shows a linear variation as the frequency varies. Therefore, the highest values of dissipated power correspond to the highest values of studied frequency.
As predicted by the theoretical model, where a dependence of power on voltage can be

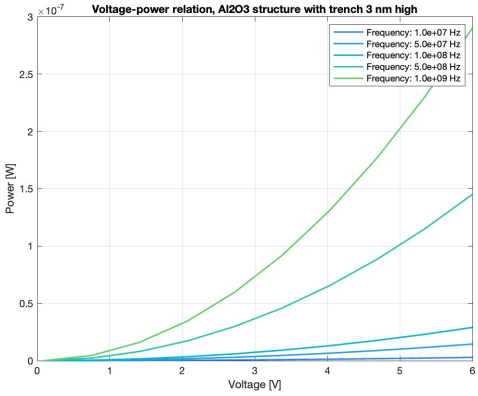

Figure 6.4: Voltage-power relation at various implemented frequencies. The analyzed structure is characterized by a Al_2O_3 dielectric and a 3 nm high trench.

appreciated, as the potential applied to the electrodes increases, more power is dissipated. In Fig. 6.4 it is visible the quadratic trend linking the voltage supplied to the electrodes and the power dissipated by the circuit. This trend shows greater values of power dissipation according to higher values of frequency.
The trends of the curves shown in Fig. 6.3 and 6.4 are identical for all the analyzed structures, regardless of the material used and the height at which the trench was created.
In order to appreciate the variations in energy consumption, comparisons are made by varying the materials implemented. Fig. 6.5 therefore shows the trend in power dissipation in a structure, characterized by a trench height fixed at 3 nm. Fig. 6.5b is the repetition of the previously reported Fig. 6.3. The repetition is due to the necessity to compare more easily the graphs.

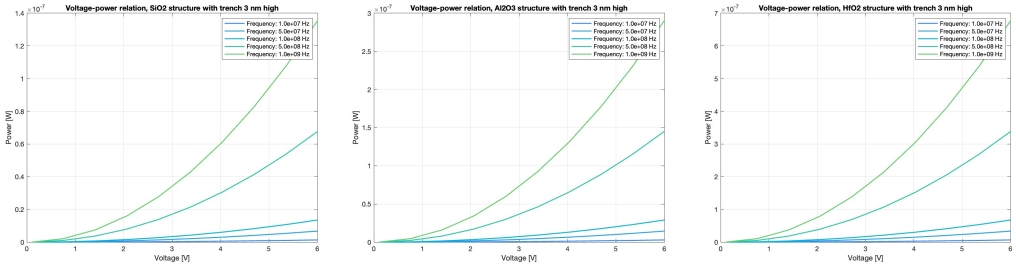

(a) SiO_2 (b) Al_2O_3 (c) HfO_2

Figure 6.5: Voltage-power relation displayed by different dielectrics.

As expected, the lower power consumption values are assumed by the structure with the silicon dioxide dielectric (Fig. 6.5a). With an applied voltage equal to 3 V on the electrodes, for example, the structure in SiO_2 dissipates 0.368×10^{-7} W when the clock frequency assumes the highest considered value (1 GHz). At the same conditions, the

structure with the Al_2O_3 structure requires 0.743×10^{-7} W while the one with the HfO_2 structure needs 1.735×10^{-7} W. Changes in power consumption can also be appreciated in Fig. 6.6 where the linear trend of the clock frequency can be appreciated. Silicon dioxide is the material with the lowest power consumption.

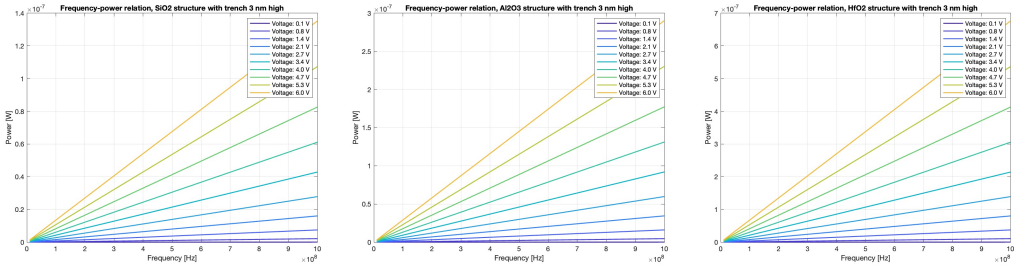

(a) SiO_2 (b) Al_2O_3 (c) HfO_2

Figure 6.6: Frequency-power relation displayed by different dielectrics.

A further comparison can be made by fixing the dielectric material and varying the trench heights. Fig. 6.7 and 6.8 display the relation between the dissipated power and the distance that separates the two electrodes. Given the inverse relation between them, the minimum dissipated power is obtained in the structure characterized by the higher trench height (9 nm, Fig. 6.7c and 6.8c). This phenomenon is directly linked to the variations in the capacitance values.

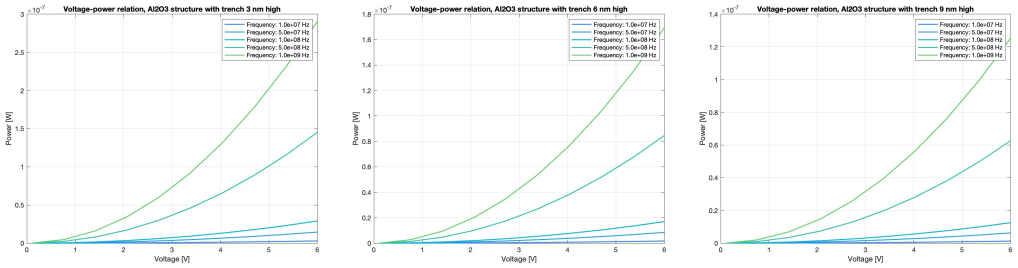

(a) 3 nm trench height. (b) 6 nm trench height. (c) 9 nm trench height.

Figure 6.7: Voltage-power relation displayed by different trench heights in a structure whose dielectric is Al_2O_3.

In this sub-section, the power dissipation of a one phase wire was analyzed in detail. In particular, power consumption values were calculated for various parasitic capacitances, modifying applied electrode voltages and frequencies. The results are in agreement with theoretical models, showing a linear dependence between power and frequency and a quadratic dependence between power and voltage. The results demonstrate the importance that the design of the structure and the clock fields have on power consumption. Indeed, the choice of these parameters, from execution speed to the resolution required during manufacture, directly influences power. The combination that offers the best result, so that consumes the least power, turns out to be the silicon dioxide structure

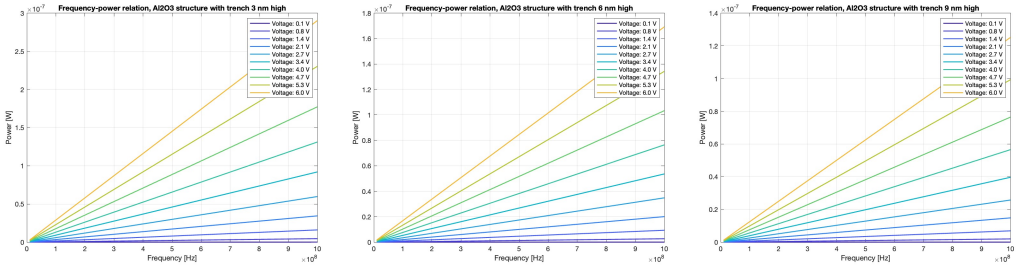

(a) 3 nm trench height. (b) 6 nm trench height. (c) 9 nm trench height.

Figure 6.8: Frequency-power relation displayed by different trench heights in a structure whose dielectric is Al_2O_3.

characterized by a nine-nanometer high trench. But when choosing the best layout, it is not only the power that must be taken into account, but also the feasibility of fabrication and also the combination of geometrical parameters to achieve clock fields capable of operating the circuit correctly. The choice of layout therefore comes down to a series of compromises that seek to optimize operational speed, physical feasibility and power dissipation. A delicate balance that must be explored in even greater detail.

6.4 Power analysis of the case-study: the neural cell

The previous chapter analyzed power dissipation within a very simplified structure, the one phase wire. The delicate balance of trade-offs between power dissipation, operational speed and stability of the propagated information due to the correct application of clock fields was therefore appreciated. Based on these observations, this chapter focuses on the power consumption of a more complex structure: the neuron implemented through a majority voter.

This structure will be implemented through three one-phase wire inputs, a transition region and a one-phase wire output. The dielectric used is aluminium oxide, as it represents a good compromise between deposition feasibility and dielectric permittivity value, on which the value of the parasitic capacitance within the circuit depends. As far as the size of the trench is concerned, it is decided to study the structure characterized by a trench width of 3 nm, in order to ensure the creation of a single line of molecules arranged as neatly as possible. The height is set arbitrarily at 3 nm.

Regarding the capacity of the MV, the input and output branches capacitances must be considered. In addition, the energy input required by the transition region, composed by four upper electrodes, must also be taken into account into the dissipated power by the MV. The capacitance value between an upper electrode and the trench one, provided by Sentaurus Device, is:

$$C_{\text{upper electrode - trench}} = 2.939\,04 \times 10^{-18}\,\text{F}$$

From a circuital point of view, the upper electrodes of a clock region result in two equipotential nodes: the capacitance between them can be neglected.
The total capacitance of each clock region must be doubled, given the existence of two electrodes on either side of the trench (as already done when calculating the power of the one phase wire). For the transition region, however, one must remember to consider all electrodes, so the capacitance value between the upper and lower electrodes must be multiplied by four. Therefore, every electrode of the structure can be seen as a network of circuital nodes connected by capacitances whose values are similar to the ones measured in the one phase wire.

The total capacitance of a neuron composed by one phase inputs and one phase output is equal to:

$$C_{MV} = 4.460\,00 \times 10^{-17}\,F$$

To this value, the contribution of the capacitances between the upper electrodes belonging to different clock regions should be added. Nevertheless, their values are three orders of magnitude smaller with respect to the capacities between an upper electrode and the trench one. Indeed, the capacitance between two upper electrodes of adjacent clock regions is equal to $-2.454\,74 \times 10^{-20}\,F$. This small value is due to the air that separates the electrodes and the small area, given that the surface will be the side of the electrodes. Furthermore, the capacitances between upper electrodes of not neighbouring clock regions will be negligible, given the high distance and its inverse relation to the capacitance values.

A power consumption analysis is therefore conducted. By varying the voltage applied to the electrodes in a range between 0.1 V and 6 V and the clock frequency between 10 MHz and 1 GHz, the results shown in Fig. 6.9a and 6.9b are obtained.

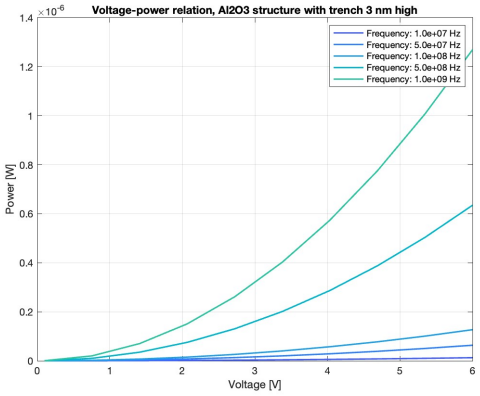

(a) Voltage-power relation in the neuron composed by one-phase input and output branches MV.

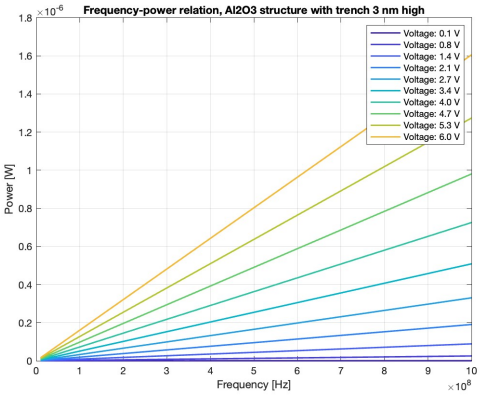

(b) Frequency-power relation in the neuron composed by one-phase input and output branches MV.

Figure 6.9: Figures of merit regarding the power dissipated by the neuron composed by one-phase input and output branches MV.

As in the one phase wire, the dissipated power of the neuron is directly linked to the voltages applied to the electrodes, to the clock frequency and to the geometry of the structure.
Particularly, by modifying the applied voltage the power will quadratically vary while there will be a linear variation if the clock frequency is altered.
The increase of about an order of magnitude compared to the values reported by the one phase wire is due to the increase in the area occupied by the structure. The average dissipated power value is 1.5044×10^{-7} W, at an average clock frequency of 332 MHz. The considered structure covers an area of 2209 nm^2.

By varying the structure of the MV, more data can be collected regarding its power dissipation. For example, by setting the number of clock regions per input and output branch equal to three, a more complex structure can be obtained. This neuron now dissipates 3.5102×10^{-7} W by occupying an area equal to 9025 nm^2.

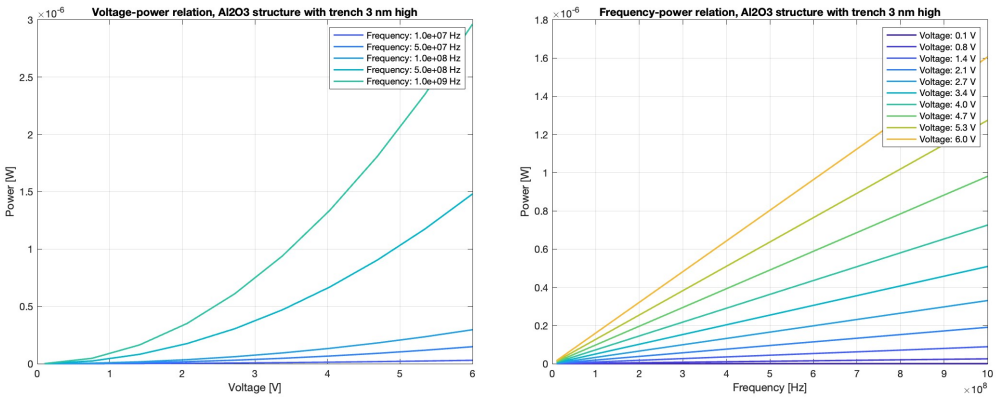

(a) Voltage-power relation in the neuron composed by three-phase input and output branches MV.

(b) Frequency-power relation in the neuron composed by three-phase input and output branches MV.

Figure 6.10: Figures of merit regarding the power dissipated by the neuron composed by three-phase input and output branches MV.

Finally, a comparison with the neural cells reported in literature can be done. The best way to appreciate the competitiveness of MolFCN technology compared to other technologies is to use graphical representations. So, using the graphs defined in chapter 1, the performance of the MolFCN device is compared to neurons implemented through other technologies. In order to select a value among the possible configurations of voltages and frequencies, the average values are used.

From Fig. 7.1, the performance of the MolFCN neuron can be appreciated and compared to other neurons found in literature. The technology, with respect to the proposed other ones, occupies by far less area. Its power consumption shows a competitive value, lower than the average value presented by the others. The ones that show lower values

are spiking neural cells, whose power consumption is directly linked to the frequencies at which the spikings occur. The comparison, therefore, is continued by restricting the competitive technologies to the ones that implement deep neural networks and by selecting the ones that report details concerning the clock frequency. As it can be seen in Fig. 6.12, the MolFCN confirms to be a very efficient solution, characterized by the following value:

$$\frac{P}{A \cdot f_{clock}} = 2.0513 \times 10^{-13} \frac{\mathrm{J}}{\mu\mathrm{m}^2}$$

This thesis finds its conclusion by affirming the efficiency of the MolFCN technology with respect to other Beyond CMOS devices. The promises of MolFCN must be further explored, but they surely promise a bright future.

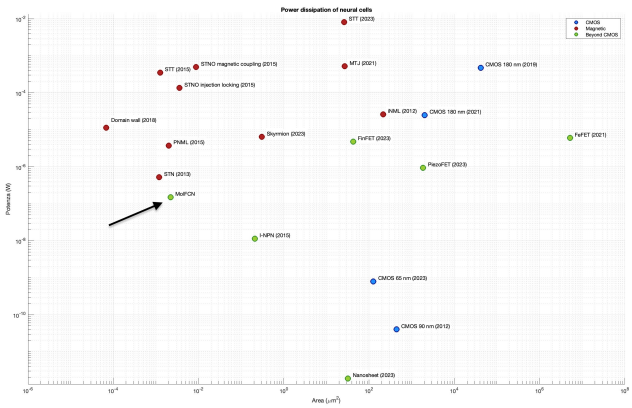

Figure 6.11: Comparison between different technologies implementing a neuron. The black arrow highlights the MolFCN technology.

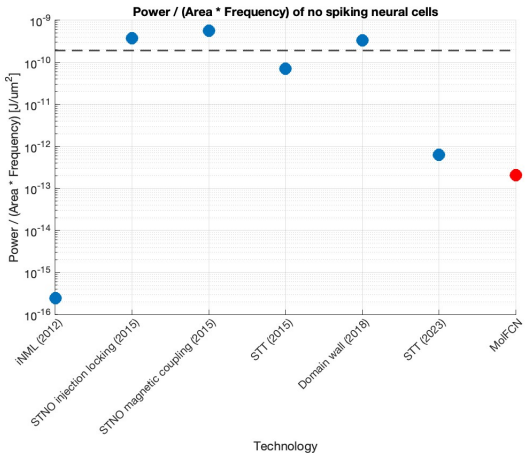

Figure 6.12: Focus on Deep neural networks. The black line refers to the average value of energy consumption related to the occupied area.

Chapter 7

Conclusion

Over the past fifty years, Moore's Law has correctly predicted the technological evolution of electronic devices, characterized by an exponential increase in performance. However, in recent times, this law has become more and more difficult to fulfill: the energy consumption required and the ever smaller dimensions to be manufactured have led to the exploration of new devices, no longer based on silicon and therefore called Beyond-CMOS. Among these technologies, Molecular Field-Coupled Nanocomputing (MolFCN) technology stands out, characterized by an extremely small occupied area and low power operation. This thesis focuses on the analysis and optimization of the structures designed to accommodate molecules, the focal point of the technology. Through the use of TCAD simulation environments such as the Sentaurus framework, devices for MolFCN technology were designed for the first time in a realistic manner, employing deposition techniques and taking into account design choices geared towards future realization. The subsequent electrical simulation showed how the electric field pattern within the structure is inversely proportional to the distance to the electrodes, confirming the theoretical models. Particular attention was paid to the creation of an artificial neuron, which was used as the case study of the thesis. In order to make the structure as parametric as possible, various MATLAB codes have been implemented, ensuring a high degree of flexibility in the variation of the analyzed structures. A link was therefore created between the TCAD environment and SCERPA, a tool that establishes electrostatic interactions between molecules within circuits. The implementation of different types of clock mechanisms was then studied, demonstrating how the division of circuits into clock regions can be implemented from a practical point of view. In this way, it was possible to verify not only the functioning of the designed circuits, but also to characterize them from the point of view of energy consumption. Thus, for the first time, power dissipation values were provided for the devices incorporating MolFCN technology. In particular, having analyzed the case study of the artificial neuron, it was possible to analyze its performance in relation to the values found in the literature referring to other Beyond CMOS technologies.

The next steps involve generalization to more complex circuits, integrating various logic gates and arriving at device-level simulations. Future work, in addition to optimizing the structures created, will analyze interconnections and the integration of more complex

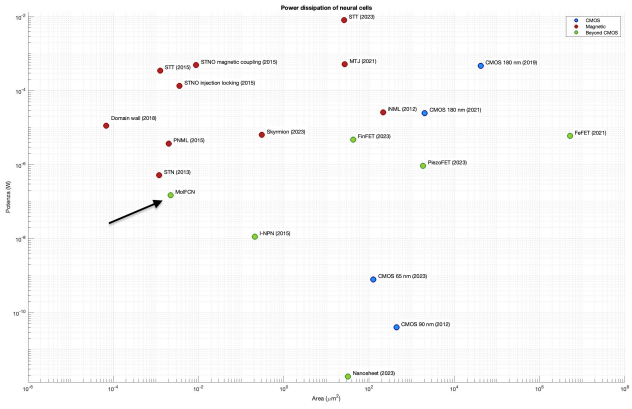

Figure 7.1: Comparison between different technologies implementing a neuron. The black arrow highlights the MolFCN technology.

systems.

In conclusion, the work conducted in this thesis represents an important link between the theoretical models adopted by SCERPA and a future realization of the technology, establishing an approach to unify DFT calculations to practical realization.

Appendix A

MATLAB code for the parametrization of Sentaurus Process

```
clear all
clc
close all

format short

% WARNING: Enter values in micrometers referring to the whole structure
% (ignore the fact that on Sentaurus Process at the beginning we create only half
    of the structure)

% Select the structure:
% 1 = Wire,
% 2 = Wire + transition region,
% 3 = T connection,
% 4 = MV

structure_selection = 4;

% ------------------
% Choice of materials
% ------------------
material_oxide = 'HfO2';

% ------------------
% Number of clock regions
% ------------------

number_clockregions_FirstVerticalWire = 3;
number_clockregions_OutputVerticalWire = 3;
number_clockregions_HorizontalWire = 3;

% ------------------
% Vertical wire
% ------------------

% Widths along Y
width_trench = 8e-3; % um
```

```
width_electrode_top = 10e-3; % "_top" refers to the top electrodes, the ones
    outside the trench electrode
width_oxide_substrate = 2e-3; % it refers to the width of the dielectric arms (on
    which the top electrodes are deposited). This value refers to the width AFTER
    the electrode (so the total dielectric width will be given by the sum of the
    two values)

% Lengths along Z
length_zone = 10e-3; % length of the top electrodes
spacing_between_zones = 2e-3; % spacing between the top electrodes

% Thicknesses along X
depth_trench = 6e-3; % distance between the top of the trench gold electrode and
    the bottom of the adhesion layer in the top electrodes
thickness_adhesion_layer = 0; % if there is no adhesion layer, enter '0'
thickness_gold_electrode = 4e-3;
thickness_oxide_substrate = 2e-3; % thickness of the substrate below the adhesion
    layer/the gold layer of the trench

% ----------------
% Transition region
% ----------------

% Widths along Y
width_electrode_transition = width_electrode_top;
spacing_transition = spacing_between_zones;

% ----------------
% Horizontal wire
% ----------------

% Widths along Y
length_zone_horizontal = length_zone;
spacing_between_zones_horizontal = spacing_between_zones;

% ----------------
% Mesh specs
% ----------------
desired_initial_spacing = 0.0001;
min_spacing_refinementbox = 0.002;



%% From here on, do not edit
%  Just comment on how you want the structure (default: MV. For example, comment
    on the output wire part to have a T-connection)
%  There are five parts: first VerticalWire wire, transition region, right
%  horizontal wire, left horizontal wire, output VerticalWire wire.
%  Be careful on how you apply the reflection command on Sentaurus Process:
%  if you'd like a corner, for example, apply the reflection on the first wire
    and on
%  the transition region: do not reflect the horizontal wire.

FileSentaurus = fopen('Output_Process_MV.txt', 'w');
fprintf(FileSentaurus, 'math  coord.ucs\n\n');

function writeParamsToFile(FileSentaurus, dati)
    for i = 1:size(dati, 1)
        fprintf(FileSentaurus, 'set %s %.3f\n', dati{i, 1}, dati{i, 2});
    end
    fprintf(FileSentaurus, '\n');
end
```

```
%% Desired thicknesses
fprintf(FileSentaurus, '# ------------------------------------ \n# Desired
    Thicknesses\n# ------------------------------------\n');
if thickness_adhesion_layer ~= 0
writeParamsToFile(FileSentaurus, {
    'ThicknessOxideArms', depth_trench;
    'ThicknessAdhesion', thickness_adhesion_layer;
    'ThicknessGold', thickness_gold_electrode;});
else
   writeParamsToFile(FileSentaurus, {
    'ThicknessOxideArms', depth_trench;
    'ThicknessGold', thickness_gold_electrode;});
end


%% First wire
fprintf(FileSentaurus, '# ------------------------------------ \n# First Vertical
    wire\n# ------------------------------------\n');

writeParamsToFile(FileSentaurus, {
    'y_Mid', 0;
    'y_EndTrench_VerticalWire', width_trench/2;
    'y_EndElectrode_VerticalWire', width_trench/2 + width_electrode_top;
    'y_EndRight_VerticalWire', width_trench/2 + width_electrode_top +
        width_oxide_substrate;});

dati_z = {};
start_position = 0;
for i = 1:number_clockregions_FirstVerticalWire
    start_name = sprintf('z_StartZone%d_VerticalWire', i);
    end_name = sprintf('z_EndZone%d_VerticalWire', i);
    dati_z = [dati_z; {start_name, start_position}];
    end_position_first_wire = start_position + length_zone;
    dati_z = [dati_z; {end_name, end_position_first_wire}];
    start_position = end_position_first_wire + spacing_between_zones;
end
writeParamsToFile(FileSentaurus, dati_z);

if thickness_adhesion_layer == 0
        dati_x= {
        'x_TopElectrode', 0;
        'x_TopOxide', thickness_gold_electrode;
        'x_TopTrenchElectrode', thickness_gold_electrode + depth_trench;
        'x_TopTrenchOxide', 2 * thickness_gold_electrode + depth_trench;
        'x_Bottom', 2 * thickness_gold_electrode + depth_trench +
            thickness_oxide_substrate;};
else % if there is an adhesion layer
        dati_x = {
        'x_TopElectrode', 0;
        'x_TopAdhesion',thickness_gold_electrode;
        'x_TopOxide', thickness_gold_electrode + thickness_adhesion_layer;
        'x_TopTrenchElectrode', thickness_gold_electrode +
            thickness_adhesion_layer + depth_trench;
        'x_TopTrenchAdhesion', 2 * thickness_gold_electrode +
            thickness_adhesion_layer + depth_trench;
        'x_TopTrenchOxide', 2 * thickness_gold_electrode + 2 *
            thickness_adhesion_layer + depth_trench;
        'x_Bottom',2 * thickness_gold_electrode + 2 * thickness_adhesion_layer +
            depth_trench + thickness_oxide_substrate;};
end
writeParamsToFile(FileSentaurus, dati_x);

%% Transition region
```

```
if structure_selection > 1

fprintf(FileSentaurus, '# ------------------------------------ \n# Transition
    region\n# ------------------------------------\n');
writeParamsToFile(FileSentaurus, {
    'y_EndRightElectrode_Transition', width_trench/2 + width_electrode_transition;
    'y_EndRightOxide_Transition', width_trench/2 + width_electrode_transition +
        spacing_transition;});
y_EndRightOxide_Transition = width_trench/2 + width_electrode_transition +
    spacing_transition;

writeParamsToFile(FileSentaurus, {
    'z_StartBottomElectrode_Transition', end_position_first_wire +
        spacing_transition;
    'z_StartTrench_HorizontalWire', end_position_first_wire + spacing_transition
        + width_electrode_transition;
    'z_EndTrench_HorizontalWire', end_position_first_wire + spacing_transition +
        width_electrode_transition + width_trench;
    'z_EndTopElectrode_Transition', end_position_first_wire + spacing_transition
        + width_trench + 2 * width_electrode_transition;
    'z_EndTopOxide_Transition', end_position_first_wire + 2 * spacing_transition
        + width_trench + 2 * width_electrode_transition;});
z_StartTrench_HorizontalWire =  end_position_first_wire + spacing_transition +
    width_electrode_transition;
z_EndTopOxide_Transition = end_position_first_wire + 2 * spacing_transition +
    width_trench + 2 * width_electrode_transition;
end
%% Right (horizontal) wire
if structure_selection > 2

fprintf(FileSentaurus, '# ------------------------------------ \n# Right horizontal
    wire\n# ------------------------------------\n');
dati_y_horizontal = {};
start_position = y_EndRightOxide_Transition;
for i = 1:number_clockregions_HorizontalWire
    start_name = sprintf('y_StartZone%d_HorizontalWire', i);
    end_name = sprintf('y_EndZone%d_HorizontalWire', i);
    dati_y_horizontal = [dati_y_horizontal; {start_name, start_position}];
    end_position_horizontal_wire = start_position + length_zone;
    dati_y_horizontal = [dati_y_horizontal; {end_name,
        end_position_horizontal_wire}];
    start_position = end_position_horizontal_wire + spacing_between_zones;
end
writeParamsToFile(FileSentaurus, dati_y_horizontal);

writeParamsToFile(FileSentaurus, {
    'z_Start_HorizontalWire', z_StartTrench_HorizontalWire - width_electrode_top
        - width_oxide_substrate;
    'z_StartElectrode_HorizontalWire', z_StartTrench_HorizontalWire -
        width_electrode_top;
    'z_StartTrench_HorizontalWire', z_StartTrench_HorizontalWire;
    'z_EndTrench_HorizontalWire', z_StartTrench_HorizontalWire + width_trench;
    'z_EndElectrode_HorizontalWire', z_StartTrench_HorizontalWire + width_trench
        + width_electrode_top;
    'z_End_HorizontalWire', z_StartTrench_HorizontalWire + width_trench +
        width_electrode_top + width_oxide_substrate;});
end
%% Output (Vertical) wire
if structure_selection > 3

fprintf(FileSentaurus, '# ------------------------------------ \n# Output Vertical
    wire\n# ------------------------------------\n');
dati_z_output = {};
```

```
start_position = z_EndTopOxide_Transition;
for i = 1:number_clockregions_OutputVerticalWire
    start_name = sprintf('z_StartZone%d_OutputWire', i);
    end_name = sprintf('z_EndZone%d_OutputWire', i);
    dati_z_output = [dati_z_output; {start_name, start_position}];
    end_position_output_wire = start_position + length_zone;
    dati_z_output = [dati_z_output; {end_name, end_position_output_wire}];
    start_position = end_position_output_wire + spacing_between_zones;
end
writeParamsToFile(FileSentaurus, dati_z_output);

elseif structure_selection > 4
    disp('Variabile "structure_selection" is not an allowed number \n')
end

%% Definition of the initial grid

fprintf(FileSentaurus, '# ------------------------------------ \n# Initial grid \n#
    ------------------------------------\n');
fprintf(FileSentaurus, 'line x location= $x_TopElectrode spacing=%.5f
    tag=x_TopElectrode \n', desired_initial_spacing);
if thickness_adhesion_layer ~= 0
fprintf(FileSentaurus, 'line x location= $x_TopAdhesion spacing=%.5f
    tag=x_TopAdhesion \n', desired_initial_spacing);
end
fprintf(FileSentaurus, 'line x location= $x_TopOxide    spacing=%.5f
    tag=x_TopOxide \n', desired_initial_spacing);
fprintf(FileSentaurus, 'line x location= $x_TopTrenchElectrode  spacing=%.5f
    tag=x_TopTrenchElectrode \n', desired_initial_spacing);
if thickness_adhesion_layer ~= 0
fprintf(FileSentaurus, 'line x location= $x_TopTrenchAdhesion   spacing=%.5f
    tag=x_TopTrenchAdhesion \n', desired_initial_spacing);
end
fprintf(FileSentaurus, 'line x location= $x_TopTrenchOxide      spacing=%.5f
    tag=x_TopTrenchOxide \n', desired_initial_spacing);
fprintf(FileSentaurus, 'line x location= $x_Bottom spacing=100<nm>
    tag=x_Bottom \n');

fprintf(FileSentaurus, 'line y location= $y_Mid spacing=%.5f tag=y_Mid\n',
    desired_initial_spacing);
if structure_selection == 1 % Wire
    fprintf(FileSentaurus, 'line y location= $y_EndRight_VerticalWire
        spacing=100<nm> tag=y_EndRight_VerticalWire \n');
elseif structure_selection == 2 % Wire + transition
    fprintf(FileSentaurus, 'line y location= $y_EndRightOxide_Transition
        spacing=100<nm> tag=y_EndRightOxide_Transition \n');
elseif structure_selection == 3 || structure_selection == 4 % T connection or MV
    fprintf(FileSentaurus, 'line y location= $y_EndZone%d_HorizontalWire
        spacing=100<nm>
        tag=y_EndZone%d_HorizontalWire\n',number_clockregions_HorizontalWire,number_clockregions_Hor
end

fprintf(FileSentaurus, 'line z location= $z_StartZone1_VerticalWire spacing=%.5f
    tag=z_StartZone1_VerticalWire \n', desired_initial_spacing);

if structure_selection == 1 % Wire
    fprintf(FileSentaurus, 'line z location= $z_StartZone%d_VerticalWire
        spacing=100<nm> tag=z_StartZone%d_VerticalWire\n',
        number_clockregions_FirstVerticalWire,
        number_clockregions_FirstVerticalWire);
elseif structure_selection == 2 || structure_selection == 3 % Wire + transition
    or T connection
```

```
    fprintf(FileSentaurus, 'line z location= $z_EndTopOxide_Transition
        spacing=100<nm> tag=z_EndTopOxide_Transition\n');
elseif structure_selection == 4 % MV
    fprintf(FileSentaurus, 'line z location= $z_EndZone%d_OutputWire
        spacing=100<nm> tag=z_EndZone%d_OutputWire\n',
        number_clockregions_FirstVerticalWire,
        number_clockregions_FirstVerticalWire);
end

%% Mask definition

% For the trench
if structure_selection == 1 % Wire
    fprintf(FileSentaurus, '\n# ------------------------------------------------\n#Mask
        definition\n# ------------------------------------------------\n');
    fprintf(FileSentaurus, 'mask name=mask_trench left=-1 right=
        $y_EndTrenchVerticalWire front=-1 back= $z_EndZone%d_VerticalWire}\n',
        number_clockregions_FirstVerticalWire);

elseif structure_selection == 2 % Wire + transition
    fprintf(FileSentaurus, '\n# ------------------------------------------------\n# Mask
        definition\n# ------------------------------------------------\n');
    fprintf(FileSentaurus, 'polygon name=pol segments= { $y_Mid
        $z_StartZone1_VerticalWire \\\n' );
    fprintf(FileSentaurus, '$y_EndTrench_VerticalWire $z_StartZone1_VerticalWire
        \\\n' );
    fprintf(FileSentaurus, '$y_EndTrench_VerticalWire
        $z_StartTrench_HorizontalWire \\\n' );
    fprintf(FileSentaurus, '$y_EndRightOxide_Transition
        $z_StartTrench_HorizontalWire \\\n' );
    fprintf(FileSentaurus,  '$y_EndRightOxide_Transition
        $z_EndTrench_HorizontalWire \\\n' );
    fprintf(FileSentaurus, '$y_EndTrench_VerticalWire $z_EndTrench_HorizontalWire
        \\\n' );
    fprintf(FileSentaurus, '$y_EndTrench_VerticalWire $z_EndTopOxide_Transition
        \\\n' );
    fprintf(FileSentaurus, '$y_Mid $z_EndTopOxide_Transition } \n' );
    fprintf(FileSentaurus,  'mask name=mask_trench polygons= { pol }\n');
elseif structure_selection == 3 % T connection
    fprintf(FileSentaurus, '\n# ------------------------------------------------\n# Mask
        definition\n# ------------------------------------------------\n');
    fprintf(FileSentaurus, 'polygon name=pol segments= { $y_Mid
        $z_StartZone1_VerticalWire \\\n');
    fprintf(FileSentaurus, '$y_EndTrench_VerticalWire $z_StartZone1_VerticalWire
        \\\n');
    fprintf(FileSentaurus, '$y_EndTrench_VerticalWire
        $z_StartTrench_HorizontalWire \\\n');
    fprintf(FileSentaurus, '$y_EndZone%d_HorizontalWire
        $z_StartTrench_HorizontalWire \\\n',number_clockregions_HorizontalWire );
    fprintf(FileSentaurus, '$y_EndZone%d_HorizontalWire
        $z_EndTrench_HorizontalWire \\\n', number_clockregions_HorizontalWire);
    fprintf(FileSentaurus, '$y_EndTrench_VerticalWire $z_EndTrench_HorizontalWire
        \\\n');
    fprintf(FileSentaurus, '$y_EndTrench_VerticalWire $z_EndTopOxide_Transition
        \\\n');
    fprintf(FileSentaurus, '$y_Mid $z_EndTopOxide_Transition } \n' );
    fprintf(FileSentaurus, 'mask name=mask_trench polygons= { pol }\n');
elseif structure_selection == 4 % MV
    fprintf(FileSentaurus, '\n# ------------------------------------------------\n# Mask
        definition\n# ------------------------------------------------\n');
    fprintf(FileSentaurus, 'polygon name=pol segments= { $y_Mid
        $z_StartZone1_VerticalWire \\\n');
```

```
    fprintf(FileSentaurus, '$y_EndTrench_VerticalWire $z_StartZone1_VerticalWire
        \\\n');
    fprintf(FileSentaurus, '$y_EndTrench_VerticalWire
        $z_StartTrench_HorizontalWire \\\n');
    fprintf(FileSentaurus, '$y_EndZone%d_HorizontalWire
        $z_StartTrench_HorizontalWire \\\n' ,number_clockregions_HorizontalWire );
    fprintf(FileSentaurus, '$y_EndZone%d_HorizontalWire
        $z_EndTrench_HorizontalWire \\\n', number_clockregions_HorizontalWire);
    fprintf(FileSentaurus, '$y_EndTrench_VerticalWire $z_EndTrench_HorizontalWire
        \\\n' );
    fprintf(FileSentaurus, '$y_EndTrench_VerticalWire $z_EndZone%d_OutputWire
        \\\n', number_clockregions_OutputVerticalWire );
    fprintf(FileSentaurus, '$y_Mid $z_EndZone%d_OutputWire } \n',
        number_clockregions_OutputVerticalWire);
    fprintf(FileSentaurus, 'mask name=mask_trench polygons= { pol }\n');
end
fprintf(FileSentaurus,'\n');
% For the top electrodes
for i=1:number_clockregions_FirstVerticalWire
fprintf(FileSentaurus,'mask name=mask_%d_electrode_verticalwire left=
    $y_EndTrench_VerticalWire right= $y_EndElectrode_VerticalWire
    front=$z_StartZone%d_VerticalWire back= $z_EndZone%d_VerticalWire
    negative\n', i,i,i);
end
fprintf(FileSentaurus,'\n');
if structure_selection > 1 % Wire + transition, T connection, MV
    fprintf(FileSentaurus,'mask name=mask_electrode_transition_bottom left=
        $y_EndTrench_VerticalWire right= $y_EndRightElectrode_Transition front=
        $z_StartBottomElectrode_Transition back= $z_StartTrench_HorizontalWire
        negative\n');
    fprintf(FileSentaurus,'mask name=mask_electrode_transition_top left=
        $y_EndTrench_VerticalWire right= $y_EndRightElectrode_Transition front=
        $z_EndTrench_HorizontalWire back= $z_EndTopElectrode_Transition
        negative\n');
    fprintf(FileSentaurus,'\n');
if structure_selection > 2 % T connection, MV
    for i=1:number_clockregions_HorizontalWire
    fprintf(FileSentaurus,'mask name=mask_%d_electrode_horizontalwire left=
        $y_StartZone%d_HorizontalWire right= $y_EndZone%d_HorizontalWire
        front=$z_StartElectrode_HorizontalWire back=
        $z_StartTrench_HorizontalWire negative \n', i,i,i);
    fprintf(FileSentaurus,'mask name=mask_%dB_electrode_horizontalwire left=
        $y_StartZone%d_HorizontalWire right= $y_EndZone%d_HorizontalWire
        front=$z_EndTrench_HorizontalWire back= $z_EndElectrode_HorizontalWire
        negative \n', i,i,i);
    end
    fprintf(FileSentaurus,'\n');
if structure_selection > 3 %MV
    for i=1:number_clockregions_OutputVerticalWire
    fprintf(FileSentaurus,'mask name=mask_%d_electrode_outputwire left=
        $y_EndTrench_VerticalWire right= $y_EndElectrode_VerticalWire
        front=$z_StartZone%d_OutputWire back= $z_EndZone%d_OutputWire
        negative\n', i,i,i);
    end
    fprintf(FileSentaurus,'\n');
end
end
end

fprintf(FileSentaurus,'\n');

%% Creation of the structure through the deposition steps
```

```
fprintf(FileSentaurus, '\n# ------------------------------------------------\n# Creation
    of the structure\n# ------------------------------------------------\n');

if structure_selection == 1 % Wire
fprintf(FileSentaurus, '# Dielectric substrate definition\nregion %s
    xlo=x_TopTrenchOxide xhi=x_Bottom ylo=y_Mid yhi=y_EndRight_VerticalWire
    zlo=z_StartZone1_VerticalWire zhi=z_StartZone%d_VerticalWire\n',
    material_oxide ,number_clockregions_FirstVerticalWire);
elseif structure_selection == 2 % Wire + transition
fprintf(FileSentaurus, '# Dielectric substrate definition\nregion %s
    xlo=x_TopTrenchOxide xhi=x_Bottom ylo=y_Mid yhi=y_EndRightOxide_Transition
    zlo=z_StartZone1_VerticalWire zhi=z_EndTopOxide_Transition\n', material_oxide
    );
elseif structure_selection == 3 % T connection
fprintf(FileSentaurus, '# Dielectric substrate definition\nregion %s
    xlo=x_TopTrenchOxide xhi=x_Bottom ylo=y_Mid yhi=y_EndZone%d_HorizontalWire
    zlo=z_StartZone1_VerticalWire zhi=z_EndTopOxide_Transition\n', material_oxide
    , number_clockregions_HorizontalWire);
elseif structure_selection == 4 % MV
fprintf(FileSentaurus, '# Dielectric substrate definition\nregion %s
    xlo=x_TopTrenchOxide xhi=x_Bottom ylo=y_Mid yhi=y_EndZone%d_HorizontalWire
    zlo=z_StartZone1_VerticalWire zhi=z_EndZone%d_OutputWire\n', material_oxide
    ,number_clockregions_HorizontalWire, number_clockregions_OutputVerticalWire);
end
fprintf(FileSentaurus, '\n# Requested parameters to perform the simulation\ninit
    !DelayFullD\nAdvancedCalibration\n\n');

if thickness_adhesion_layer ~= 0
        fprintf(FileSentaurus, '# Deposition of adhesion layer everywhere on the
            substrate\n');
        fprintf(FileSentaurus, 'deposit thickness=$ThicknessAdhesion Titanium\n');
end

fprintf(FileSentaurus, '# Deposition of gold everywhere on the substrate\n');
fprintf(FileSentaurus, 'deposit thickness=$ThicknessGold Gold\n');

fprintf(FileSentaurus, '# Deposition of dielectric to obtain the arms\ndeposit
    thickness= $ThicknessOxideArms %s mask=mask_trench\n',material_oxide);

fprintf(FileSentaurus, '# Deposition of electrodes, vertical wire\n');
if thickness_adhesion_layer ~= 0
    for i=1:number_clockregions_FirstVerticalWire
        fprintf(FileSentaurus, 'deposit thickness= $ThicknessAdhesion Titanium
            mask=mask_%d_electrode_verticalwire\n',i);
        fprintf(FileSentaurus, 'deposit thickness= $ThicknessGold Gold
            mask=mask_%d_electrode_verticalwire\n',i);
    end
if structure_selection > 1 % Wire + transition, T connection, MV
    fprintf(FileSentaurus, '# Deposition of electrodes on the arms,
        transition\n');
        fprintf(FileSentaurus, 'deposit thickness= $ThicknessAdhesion Titanium
            mask=mask_electrode_transition_bottom \n');
        fprintf(FileSentaurus, 'deposit thickness= $ThicknessAdhesion Titanium
            mask=mask_electrode_transition_top \n');
        fprintf(FileSentaurus, 'deposit thickness= $ThicknessGold Gold
            mask=mask_electrode_transition_bottom \n');
        fprintf(FileSentaurus, 'deposit thickness= $ThicknessGold Gold
            mask=mask_electrode_transition_top \n');
if structure_selection > 2 % T connection, MV
    fprintf(FileSentaurus, '# Deposition of electrodes on the arms, horizontal
        wire\n');
    for i=1:number_clockregions_HorizontalWire
```

```
        fprintf(FileSentaurus, 'deposit thickness= $ThicknessAdhesion Titanium
            mask=mask_%d_electrode_horizontalwire\n',i);
        fprintf(FileSentaurus, 'deposit thickness= $ThicknessAdhesion Titanium
            mask=mask_%dB_electrode_horizontalwire\n',i);
        fprintf(FileSentaurus, 'deposit thickness= $ThicknessGold Gold
            mask=mask_%d_electrode_horizontalwire\n',i);
        fprintf(FileSentaurus, 'deposit thickness= $ThicknessGold Gold
            mask=mask_%dB_electrode_horizontalwire\n',i);

    end
if structure_selection > 3 % MV
    fprintf(FileSentaurus, '# Deposition of electrodes on the arms, output
        wire\n');
    for i=1:number_clockregions_OutputVerticalWire
        fprintf(FileSentaurus, 'deposit thickness= $ThicknessAdhesion Titanium
            mask=mask_%d_electrode_outputwire\n',i);
        fprintf(FileSentaurus, 'deposit thickness= $ThicknessGold Gold
            mask=mask_%d_electrode_outputwire\n',i);
    end
end
end
end
elseif thickness_adhesion_layer == 0
    for i=1:number_clockregions_FirstVerticalWire
        fprintf(FileSentaurus, 'deposit thickness= $ThicknessGold Gold
            mask=mask_%d_electrode_verticalwire\n',i);
    end
if structure_selection > 1 % Wire + transition, T connection, MV
        fprintf(FileSentaurus, '\n# Deposition of electrodes on the arms,
            transition wire\n');
        fprintf(FileSentaurus, 'deposit thickness= $ThicknessGold Gold
            mask=mask_electrode_transition_top \n');
        fprintf(FileSentaurus, 'deposit thickness= $ThicknessGold Gold
            mask=mask_electrode_transition_bottom \n');
if structure_selection > 2 % T connection, MV
    fprintf(FileSentaurus, '\n# Deposition of electrodes on the arms, horizontal
        wire\n');
    for i=1:number_clockregions_HorizontalWire
        fprintf(FileSentaurus, 'deposit thickness= $ThicknessGold Gold
            mask=mask_%d_electrode_horizontalwire\n',i);
        fprintf(FileSentaurus, 'deposit thickness= $ThicknessGold Gold
            mask=mask_%dB_electrode_horizontalwire\n',i);

    end
if structure_selection > 3 % MV
    fprintf(FileSentaurus, '\n# Deposition of electrodes on the arms, output
        wire\n');
    for i=1:number_clockregions_OutputVerticalWire
        fprintf(FileSentaurus, 'deposit thickness= $ThicknessGold Gold
            mask=mask_%d_electrode_outputwire\n',i);
    end
end
end
end
end

fprintf(FileSentaurus, '\n# Reflection\n');
fprintf(FileSentaurus, 'transform reflect left\n\n');

%% Refinement for Sentaurus Device

fprintf(FileSentaurus, '\n# ------------------------------------------------\n#
    Refinement of the mesh\n# ------------------------------------------------\n');
```

```
fprintf(FileSentaurus, 'refinebox mask=mask_trench extrusion.min=$x_TopElectrode
    extrusion.max=$x_TopTrenchOxide xrefine= { %.3f %.3f %.3f} yrefine= { %.3f
    %.3f %.3f} zrefine= { %.3f %.3f %.3f} extend= 0.010 \n',
    min_spacing_refinementbox,min_spacing_refinementbox,min_spacing_refinementbox,min_spacing_refinen
fprintf(FileSentaurus, 'grid remesh\n\n' );


%% Definition of contacts
fprintf(FileSentaurus, '\n# ------------------------------------------------\n#
    Definition of the contacts\n# ------------------------------------------------\n');
fprintf(FileSentaurus, '#Trench\n');
if thickness_adhesion_layer == 0

if structure_selection == 1 % wire
    fprintf(FileSentaurus, 'contact box xlo=$x_TopTrenchElectrode
        ylo=-$y_EndRight_VerticalWire zlo=$z_StartZone1_VerticalWire
        xhi=$x_TopTrenchOxide yhi=$y_EndRight_VerticalWire
        zhi=$z_EndZone%d_VerticalWire name=TrenchElectrode
        Gold\n',number_clockregions_VerticalVerticalWire);
elseif structure_selection == 2 % wire + transition
    fprintf(FileSentaurus, 'contact box xlo=$x_TopTrenchElectrode
        ylo=-$y_EndRightOxide_Transition zlo=$z_StartZone1_VerticalWire
        xhi=$x_TopTrenchOxide yhi=$y_EndRightOxide_Transition
        zhi=$z_EndTopOxide_Transition name=TrenchElectrode Gold\n');
elseif structure_selection == 3 % T connection
    fprintf(FileSentaurus, 'contact box xlo=$x_TopTrenchElectrode
        ylo=-$y_EndZone%d_HorizontalWire zlo=$z_StartZone1_VerticalWire
        xhi=$x_TopTrenchOxide yhi=$y_EndZone%d_HorizontalWire
        zhi=$z_EndTopOxide_Transition name=TrenchElectrode
        Gold\n',number_clockregions_HorizontalWire,
        number_clockregions_HorizontalWire);
elseif structure_selection == 4 % MV
    fprintf(FileSentaurus, 'contact box xlo=$x_TopTrenchElectrode
        ylo=-$y_EndZone%d_HorizontalWire zlo=$z_StartZone1_VerticalWire
        xhi=$x_TopTrenchOxide yhi=$y_EndZone%d_HorizontalWire
        zhi=$z_EndZone%d_OutputWire name=TrenchElectrode
        Gold\n',number_clockregions_HorizontalWire,
        number_clockregions_HorizontalWire,
        number_clockregions_OutputVerticalWire);
end

fprintf(FileSentaurus, '\n#First vertical wire\n');
for i=1:number_clockregions_FirstVerticalWire
        fprintf(FileSentaurus, 'contact box xlo=$x_TopElectrode
            ylo=$y_EndTrench_VerticalWire zlo=$z_StartZone%d_VerticalWire
            xhi=$x_TopOxide yhi=$y_EndElectrode_VerticalWire
            zhi=$z_EndZone%d_VerticalWire name=Electrode_VerticalWire_%d_Right
            Gold\n',i,i,i);
        fprintf(FileSentaurus, 'contact box xlo=$x_TopElectrode
            ylo=-$y_EndTrench_VerticalWire zlo=$z_StartZone%d_VerticalWire
            xhi=$x_TopOxide yhi=-$y_EndElectrode_VerticalWire
            zhi=$z_EndZone%d_VerticalWire name=Electrode_VerticalWire_%d_Left
            Gold\n',i,i,i);
end

    if structure_selection > 1
        fprintf(FileSentaurus, '\n#Bottom electrodes of the transition region\n');
        fprintf(FileSentaurus, 'contact box xlo=$x_TopElectrode
            ylo=$y_EndTrench_VerticalWire zlo=$z_StartBottomElectrode_Transition
            xhi=$x_TopOxide yhi=$y_EndRightElectrode_Transition
            zhi=$z_StartTrench_HorizontalWire name=BottomElectrodeTransitionRight
            Gold\n');
```

```
    fprintf(FileSentaurus, 'contact box xlo=$x_TopElectrode
        ylo=-$y_EndTrench_VerticalWire zlo=$z_StartBottomElectrode_Transition
        xhi=$x_TopOxide yhi=-$y_EndRightElectrode_Transition
        zhi=$z_StartTrench_HorizontalWire name=BottomElectrodeTransitionLeft
        Gold\n');
    fprintf(FileSentaurus, '#Top electrodes of the transition region\n');
    fprintf(FileSentaurus, 'contact box xlo=$x_TopElectrode
        ylo=$y_EndTrench_VerticalWire zlo=$z_EndTrench_HorizontalWire
        xhi=$x_TopOxide yhi=$y_EndRightElectrode_Transition
        zhi=$z_EndTopElectrode_Transition name=TopElectrodeTransitionRight
        Gold\n');
    fprintf(FileSentaurus, 'contact box xlo=$x_TopElectrode
        ylo=-$y_EndTrench_VerticalWire zlo=$z_EndTrench_HorizontalWire
        xhi=$x_TopOxide yhi=-$y_EndRightElectrode_Transition
        zhi=$z_EndTopElectrode_Transition name=TopElectrodeTransitionLeft
        Gold\n');

if structure_selection > 2
fprintf(FileSentaurus, '\n#Horizontal wire right\n');
for i=1:number_clockregions_HorizontalWire
        fprintf(FileSentaurus, 'contact box xlo=$x_TopElectrode
            ylo=$y_StartZone%d_HorizontalWire
            zlo=$z_StartElectrode_HorizontalWire xhi=$x_TopOxide
            yhi=$y_EndZone%d_HorizontalWire zhi=$z_StartTrench_HorizontalWire
            name=Electrode_HorizontalWire_%d_Right
            Gold\n',i,i,number_clockregions_HorizontalWire+1-i);
        fprintf(FileSentaurus, 'contact box xlo=$x_TopElectrode
            ylo=$y_StartZone%d_HorizontalWire zlo=$z_EndTrench_HorizontalWire
            xhi=$x_TopOxide yhi=$y_EndZone%d_HorizontalWire
            zhi=$z_EndElectrode_HorizontalWire
            name=Electrode_HorizontalWire_%d_Left
            Gold\n',i,i,number_clockregions_HorizontalWire+1-i);
end
fprintf(FileSentaurus, '\n#Horizontal wire left\n');
for i=1:number_clockregions_HorizontalWire
        fprintf(FileSentaurus, 'contact box xlo=$x_TopElectrode
            ylo=-$y_StartZone%d_HorizontalWire
            zlo=$z_StartElectrode_HorizontalWire xhi=$x_TopOxide
            yhi=-$y_EndZone%d_HorizontalWire
            zhi=$z_StartTrench_HorizontalWire
            name=Electrode_HorizontalReflectedWire_%d_Right
            Gold\n',i,i,number_clockregions_HorizontalWire+1-i);
        fprintf(FileSentaurus, 'contact box xlo=$x_TopElectrode
            ylo=-$y_StartZone%d_HorizontalWire
            zlo=$z_EndTrench_HorizontalWire xhi=$x_TopOxide
            yhi=-$y_EndZone%d_HorizontalWire
            zhi=$z_EndElectrode_HorizontalWire
            name=Electrode_HorizontalReflectedWire_%d_Left
            Gold\n',i,i,number_clockregions_HorizontalWire+1-i);
end

if structure_selection > 3
        fprintf(FileSentaurus, '\n#Output vertical wire \n');
for i=1:number_clockregions_OutputVerticalWire
        fprintf(FileSentaurus, 'contact box xlo=$x_TopElectrode
            ylo=$y_EndTrench_VerticalWire zlo=$z_StartZone%d_OutputWire
            xhi=$x_TopOxide yhi=$y_EndElectrode_VerticalWire
            zhi=$z_EndZone%d_OutputWire name=Electrode_OutputWire_%d_Right
            Gold\n',i,i,i);
```

```
            fprintf(FileSentaurus, 'contact box xlo=$x_TopElectrode
                ylo=-$y_EndTrench_VerticalWire zlo=$z_StartZone%d_OutputWire
                xhi=$x_TopOxide yhi=-$y_EndElectrode_VerticalWire
                zhi=$z_EndZone%d_OutputWire name=Electrode_OutputWire_%d_Left
                Gold\n',i,i,i);
    end
    end
    end
    end

else % if there is an adhesion layer

if structure_selection == 1 % wire
    fprintf(FileSentaurus, 'contact box xlo=$x_TopTrenchElectrode
        ylo=-$y_EndRight_VerticalWire zlo=$z_StartZone1_VerticalWire
        xhi=$x_TopTrenchAdhesion yhi=$y_EndRight_VerticalWire
        zhi=$z_EndZone%d_VerticalWire name=TrenchElectrode
        Gold\n',number_clockregions_VerticalVerticalWire);
elseif structure_selection == 2 % wire + transition
    fprintf(FileSentaurus, 'contact box xlo=$x_TopTrenchElectrode
        ylo=-$y_EndRightOxide_Transition zlo=$z_StartZone1_VerticalWire
        xhi=$x_TopTrenchAdhesion yhi=$y_EndRightOxide_Transition
        zhi=$z_EndTopOxide_Transition name=TrenchElectrode Gold\n');
elseif structure_selection == 3 % T connection
    fprintf(FileSentaurus, 'contact box xlo=$x_TopTrenchElectrode
        ylo=-$y_EndZone%d_HorizontalWire zlo=$z_StartZone1_VerticalWire
        xhi=$x_TopTrenchAdhesion yhi=$y_EndZone%d_HorizontalWire
        zhi=$z_EndTopOxide_Transition name=TrenchElectrode
        Gold\n',number_clockregions_HorizontalWire,
        number_clockregions_HorizontalWire);
elseif structure_selection == 4 % MV
    fprintf(FileSentaurus, 'contact box xlo=$x_TopTrenchElectrode
        ylo=-$y_EndZone%d_HorizontalWire zlo=$z_StartZone1_VerticalWire
        xhi=$x_TopTrenchAdhesion yhi=$y_EndZone%d_HorizontalWire
        zhi=$z_EndZone%d_OutputWire name=TrenchElectrode
        Gold\n',number_clockregions_HorizontalWire,
        number_clockregions_HorizontalWire,
        number_clockregions_OutputVerticalWire);
end

fprintf(FileSentaurus, '\n#First vertical wire\n');
    for i=1:number_clockregions_FirstVerticalWire
            fprintf(FileSentaurus, 'contact box xlo=$x_TopElectrode
                ylo=$y_EndTrench_VerticalWire zlo=$z_StartZone%d_VerticalWire
                xhi=$x_TopAdhesion yhi=$y_EndElectrode_VerticalWire
                zhi=$z_EndZone%d_VerticalWire
                name=Electrode_VerticalWire_%d_Right Gold\n',i,i,i);
            fprintf(FileSentaurus, 'contact box xlo=$x_TopElectrode
                ylo=-$y_EndTrench_VerticalWire zlo=$z_StartZone%d_VerticalWire
                xhi=$x_TopAdhesion yhi=-$y_EndElectrode_VerticalWire
                zhi=$z_EndZone%d_VerticalWire name=Electrode_VerticalWire_%d_Left
                Gold\n',i,i,i);
    end

    if structure_selection > 1
        fprintf(FileSentaurus, '\n#Bottom electrodes of the transition region\n');
        fprintf(FileSentaurus, 'contact box xlo=$x_TopElectrode
            ylo=$y_EndTrench_VerticalWire zlo=$z_StartBottomElectrode_Transition
            xhi=$x_TopAdhesion yhi=$y_EndRightElectrode_Transition
            zhi=$z_StartTrench_HorizontalWire name=BottomElectrodeTransitionRight
            Gold\n');
```

```
    fprintf(FileSentaurus, 'contact box xlo=$x_TopElectrode
        ylo=-$y_EndTrench_VerticalWire zlo=$z_StartBottomElectrode_Transition
        xhi=$x_TopAdhesion yhi=-$y_EndRightElectrode_Transition
        zhi=$z_StartTrench_HorizontalWire name=BottomElectrodeTransitionLeft
        Gold\n');
    fprintf(FileSentaurus, '#Top electrodes of the transition region\n');
    fprintf(FileSentaurus, 'contact box xlo=$x_TopElectrode
        ylo=$y_EndTrench_VerticalWire zlo=$z_EndTrench_HorizontalWire
        xhi=$x_TopAdhesion yhi=$y_EndRightElectrode_Transition
        zhi=$z_EndTopElectrode_Transition name=TopElectrodeTransitionRight
        Gold\n');
    fprintf(FileSentaurus, 'contact box xlo=$x_TopElectrode
        ylo=-$y_EndTrench_VerticalWire zlo=$z_EndTrench_HorizontalWire
        xhi=$x_TopAdhesion yhi=-$y_EndRightElectrode_Transition
        zhi=$z_EndTopElectrode_Transition name=TopElectrodeTransitionLeft
        Gold\n');

if structure_selection > 2
fprintf(FileSentaurus, '\n#Horizontal wire right\n');
for i=1:number_clockregions_HorizontalWire
        fprintf(FileSentaurus, 'contact box xlo=$x_TopElectrode
            ylo=$y_StartZone%d_HorizontalWire
            zlo=$z_StartElectrode_HorizontalWire xhi=$x_TopAdhesion
            yhi=$y_EndZone%d_HorizontalWire zhi=$z_StartTrench_HorizontalWire
            name=Electrode_HorizontalWire_%d_Right
            Gold\n',i,i,number_clockregions_HorizontalWire+1-i);
        fprintf(FileSentaurus, 'contact box xlo=$x_TopElectrode
            ylo=$y_StartZone%d_HorizontalWire zlo=$z_EndTrench_HorizontalWire
            xhi=$x_TopAdhesion yhi=$y_EndZone%d_HorizontalWire
            zhi=$z_EndElectrode_HorizontalWire
            name=Electrode_HorizontalWire_%d_Left
            Gold\n',i,i,number_clockregions_HorizontalWire+1-i);
end
fprintf(FileSentaurus, '\n#Horizontal wire left\n');
for i=1:number_clockregions_HorizontalWire
        fprintf(FileSentaurus, 'contact box xlo=$x_TopElectrode
            ylo=-$y_StartZone%d_HorizontalWire
            zlo=$z_StartElectrode_HorizontalWire xhi=$x_TopAdhesion
            yhi=-$y_EndZone%d_HorizontalWire
            zhi=$z_StartTrench_HorizontalWire
            name=Electrode_HorizontalReflectedWire_%d_Right
            Gold\n',i,i,number_clockregions_HorizontalWire+1-i);
        fprintf(FileSentaurus, 'contact box xlo=$x_TopElectrode
            ylo=-$y_StartZone%d_HorizontalWire
            zlo=$z_EndTrench_HorizontalWire xhi=$x_TopAdhesion
            yhi=-$y_EndZone%d_HorizontalWire
            zhi=$z_EndElectrode_HorizontalWire
            name=Electrode_HorizontalReflectedWire_%d_Left
            Gold\n',i,i,number_clockregions_HorizontalWire+1-i);
end

if structure_selection > 3
        fprintf(FileSentaurus, '\n#Output vertical wire \n');
for i=1:number_clockregions_OutputVerticalWire
        fprintf(FileSentaurus, 'contact box xlo=$x_TopElectrode
            ylo=$y_EndTrench_VerticalWire zlo=$z_StartZone%d_OutputWire
            xhi=$x_TopAdhesion yhi=$y_EndElectrode_VerticalWire
            zhi=$z_EndZone%d_OutputWire name=Electrode_OutputWire_%d_Right
            Gold\n',i,i,i);
```

```
            fprintf(FileSentaurus, 'contact box xlo=$x_TopElectrode
                ylo=-$y_EndTrench_VerticalWire zlo=$z_StartZone%d_OutputWire
                xhi=$x_TopAdhesion yhi=-$y_EndElectrode_VerticalWire
                zhi=$z_EndZone%d_OutputWire name=Electrode_OutputWire_%d_Left
                Gold\n',i,i,i);
    end
    end
    end
    end
end

%% Conclusion
fprintf(FileSentaurus, '\n# ------------------------------------------------\n#
    Conclusions: exporting data \n# ------------------------------------------------\n');
fprintf(FileSentaurus, 'struct tdr= n@node@_presimulation;\n');


%% Closure of file
fclose(FileSentaurus);

disp('Done, check the files "Output_Process_MV.txt" :) ')
disp('Copy and paste the updated code into "sprocess_fps.cmd" of Sentaurus
    Process')
disp('replacing the previous one')
```

Appendix B

MATLAB code for the extraction of the field values

```
    clear all
clc
close all

% ------------------------------------------------------------------
% MAJORITY VOTER EXTRACTION OF DATA FROM SENTAURUS
% ------------------------------------------------------------------

% Setup

        FolderNameInput = "...";
        FolderNameOutput = "...";

        for Phase = 1:4
        csv_curve_horizontal =
           sprintf('%d_ExparallelZ.csv',Phase); % In Sentaurus,
           it's the field along the z-axis
        csv_curve_vertical = sprintf('%d_ExparallelY.csv',
           Phase); % In Sentaurus, it's the field along the
           y-axis

        data_curve_horizontal =
           readmatrix(fullfile(FolderNameInput,
           csv_curve_horizontal));
        data_curve_vertical =
           readmatrix(fullfile(FolderNameInput,
           csv_curve_vertical));
```

```
        field_values = [];

% Visualization of the fields

        color_blue = colormap('parula');
        blue = color_blue(3, :);
        sampled_data = [];

        figure;
        hold on
        PLOT_x_horizontal = data_curve_horizontal(:, 1) * 1000;
        PLOT_Field_horizontal = data_curve_horizontal(:, 2) /
           1e7;

        PLOT_x_sampled_horizontal =
           linspace(min(PLOT_x_horizontal),
           max(PLOT_x_horizontal), 1000);
        PLOT_Field_interpolated_horizontal =
           interp1(PLOT_x_horizontal, PLOT_Field_horizontal,
           PLOT_x_sampled_horizontal, 'linear', 'extrap');

        Field_value_center_MV =
           PLOT_Field_interpolated_horizontal(floor(length(PLOT_Field_interpo
           / 2));
        x_center = (min(PLOT_x_sampled_horizontal) +
           max(PLOT_x_sampled_horizontal)) / 2;

        plot(PLOT_x_horizontal, PLOT_Field_horizontal,
           'DisplayName', 'Clock field', 'LineWidth', 2,
           'Color', blue);
        plot(x_center, Field_value_center_MV, 'o',
           'MarkerSize', 8, 'MarkerFaceColor', 'r',
           'DisplayName', 'Clock field at the center of the
           structure');

        legend('show', 'Location', 'southoutside');
        xlabel('z [nm]', 'FontSize', 14)
        ylabel('E_x [V/nm]', 'FontSize', 14)
        titleString = sprintf('Clock field along the z of the
           MV');
        title(titleString, 'FontSize', 14)
        legendHandle = legend();
        set(legendHandle, 'FontSize', 14);
```

```
filenameexport = sprintf('MV Field along the z axis of
    the structure %d.jpg', Phase);
saveas(gcf, filenameexport);
hold off

figure;
hold on
PLOT_x_vertical = data_curve_vertical(:, 1) * 1000;
PLOT_Field_vertical = data_curve_vertical(:, 2) / 1e7;

PLOT_x_sampled_vertical =
    linspace(min(PLOT_x_vertical), max(PLOT_x_vertical),
    1000);
PLOT_Field_interpolated_vertical =
    interp1(PLOT_x_vertical, PLOT_Field_vertical,
    PLOT_x_sampled_vertical, 'linear', 'extrap');

Field_value_center_MV_yaxis =
    PLOT_Field_interpolated_vertical(floor(length(PLOT_Field_interpola
    / 2));
x_center = (min(PLOT_x_sampled_vertical) +
    max(PLOT_x_sampled_vertical)) / 2;

plot(PLOT_x_vertical, PLOT_Field_vertical,
    'DisplayName', 'Clock field', 'LineWidth', 2,
    'Color', blue);
plot(x_center, Field_value_center_MV_yaxis, 'o',
    'MarkerSize', 8, 'MarkerFaceColor', 'r',
    'DisplayName', 'Clock field at the center of the
    structure');
legend('show', 'Location', 'southoutside');
xlabel('z [nm]', 'FontSize', 14)
ylabel('E_x [V/nm]', 'FontSize', 14)
titleString = sprintf('Clock field along the y of the
    MV');
title(titleString, 'FontSize', 14)
legendHandle = legend();
set(legendHandle, 'FontSize', 10);
filenameexport = sprintf('MV Field along the y axis of
    the structure %d .jpg', Phase);
saveas(gcf, filenameexport);
hold off
```

```
% curve 1, horizontal curve for SCERPA. Sample every nm

        x_horizontal = data_curve_horizontal(:, 1) * 1000;  %
           odd column: x value. '* 1000' to change from um to nm
        Field_horizontal =  data_curve_horizontal(:, 2)  / 1e7;
                % evencolumn: y value. '* 0.001' to change from
           V/cm to V/nm

        x_sampled_horizontal =
           min(x_horizontal):1:max(x_horizontal);  % Sample
           every 1 nm
        x_sampled_horizontal = x_sampled_horizontal(2:end-1); %
           remove the extremes
        Field_interpolated_horizontal = interp1(x_horizontal,
           Field_horizontal, x_sampled_horizontal, 'linear',
           'extrap');  % Interpolation

        central_index_horizontal = ceil
           (length(Field_interpolated_horizontal) / 2);

        Field_interpolated_horizontal =
           [Field_interpolated_horizontal(1:central_index_horizontal-1)';
           Field_value_center_MV; Field_value_center_MV;
           Field_interpolated_horizontal(central_index_horizontal+1:end)'];

        x_horiz =
           [x_sampled_horizontal(1:central_index_horizontal-1)';
           Field_value_center_MV; Field_value_center_MV;
           x_sampled_horizontal(central_index_horizontal+1:end)'];

% curve 2, vertical one

        x_vertical = data_curve_vertical(:, 1) * 1000;  % odd
           column: x value. '* 1000' to change from um to nm
        Field_vertical = data_curve_vertical(:, 2)  / 1e7;
           % even column: y value. '* 0.001' to change from
           V/cm to V/nm

        x_sampled_vertical = [min(x_vertical):2:-1,
           1.5:2:(max(x_vertical)+0.5)]';  % Sample every nm,
           curve parallel to y axis
        x_sampled_vertical = x_sampled_vertical(2:end-1);
```

```
        %x_sampled_vertical = [min(x_vertical):2:-1.5,
            1.5:2:max(x_vertical)]';  % Sample every nm, curve
            parallel to y axis

        Field_interpolated_vertical = interp1(x_vertical,
            Field_vertical, x_sampled_vertical, 'linear',
            'extrap');  % Interpolation

        x_sampled_vertical_repeated =
            repelem(x_sampled_vertical, 2, 1);
        Field_interpolated_vertical =
            repelem(Field_interpolated_vertical,2,1);

        central_index_vertical =
            ceil((length(x_sampled_vertical_repeated) / 2 ) );
        x_vert = x_sampled_vertical;

% Assembling

        Field_values =
            [Field_interpolated_vertical(1:central_index_vertical);Field_interp
        x_tot =
            [x_sampled_vertical_repeated(1:central_index_vertical);x_horiz;x_s

% Adding the index for the molecules' identification

        final_matrix = [];
        for index = 1:length(Field_values)
             final_matrix(index,:) = [index,
                Field_values(index)];
        end

% Saving the results

        output_filename = sprintf('%d_Extracted_MV.csv',Phase);
        writematrix(final_matrix, fullfile(FolderNameOutput,
            output_filename));

        end
```

Appendix C

MATLAB code for the layout to insert in SCERPA

```
    clear all
clc
close all


% ------------------------------------------------------------------
% MAJORITY VOTER LAYOUT CREATION FOR SCERPA
% ------------------------------------------------------------------

% Set up

            number_of_zeros_columns = 18; % elettrodi lunghi 10
               mm: 22, elettrodi lunghi 8 mm: 18
            number_of_zeros_rows = number_of_zeros_columns / 2;

            number_rows = number_of_zeros_rows * 2 + 3;
            number_columns = number_of_zeros_columns * 2 + 4;

            circuit_structure = cell(number_rows,
               number_columns); % creation of the structure
            circuit_structure(:) = {0}; % initialization


% First row, where Dr1 and Dr2 are located (given the number of
   0, it must be added up the space occupied by Dr1 and Dr2
   along the first and second column: the position of Dr1 and
   Dr2 on the first column
```

```
            circuit_structure(1, number_of_zeros_columns +
               3:number_of_zeros_columns + 4) = {'Dr1', 'Dr2'};

% Second part, '1' at the center

            for index_row = 2:(number_of_zeros_rows +1)
                circuit_structure(index_row,
                   number_of_zeros_columns +
                   3:number_of_zeros_columns + 4) = {'1', '1'};
            end

% One full row of '1'

            circuit_structure(number_of_zeros_rows+2, 1:2) =
               {'Dr1', 'Dr2'};
            circuit_structure(number_of_zeros_rows+2,
               3:number_columns) = {'1'};

% Third part, '1' at the center

            for index_row = number_of_zeros_rows+3:number_rows-1
                circuit_structure(index_row,
                   number_of_zeros_columns +
                   3:number_of_zeros_columns + 4) = {'1', '1'};
            end

% Last row: like the first one with the driver

            circuit_structure(number_rows,
               number_of_zeros_columns +
               3:number_of_zeros_columns + 4) = {'Dr1', 'Dr2'};

% Show the result and display the number of written '1' in
   order to check the result

            count_ones = 0;
            disp('circuit.structure = {');
            for index_row = 1:number_rows
                fprintf('    ');
                for index_column = 1:number_columns
                    if ischar(circuit_structure{index_row,
                       index_column})
```

```
                fprintf('''%s'' ',
                    circuit_structure{index_row,
                    index_column});
                if strcmp(circuit_structure{index_row,
                    index_column}, '1') % Se la cella
                    contiene '1'
                     count_ones = count_ones + 1;
                end
            else
                fprintf('%d ',
                    circuit_structure{index_row,
                    index_column});
            end
        end
        fprintf('\n');
    end
    disp('};');

    fprintf('The number of written "1": %d\n',
        count_ones);
```

Bibliography

[1] G. E. Moore, "Progress in digital integrated electronics [Technical literature, Copyright 1975 IEEE. Reprinted, with permission. Technical Digest. International Electron Devices Meeting, IEEE, 1975, pp. 11–13]," *IEEE Solid-State Circuits Soc. Newslett.*, vol. 11, no. 3, pp. 36–37, Sept. 2006.

[2] Gordon E. Moore, "Progress in Digital Integrated Electronics," *IEEE International Electron Devices Meeting (IEDM)*, pp. 11-13, 1975.

[3] Mark Bohr and Kaizad Mistry, "Intel's Revolutionary 22 nm Transistor Technology," Intel Corporation, May 2011. Presentation available: https://download.intel.com/newsroom/kits/22nm/pdfs/22nm-Details_Presentation.pdf.

[4] Thomas N. Theis and H.-S. Philip Wong, "The End of Moore's Law: A New Beginning for Information Technology," *Computing in Science and Engineering*, vol. 19, no. 2, pp. 41-50, 2017.

[5] Chris Mack, "The Multiple Lives of Moore's Law," *IEEE Spectrum*, vol.52, no. 4, pp. 31, 2015.

[6] Andreas Tsormpatzoglou, Constantinos A. Dimitriadis, et al., "Threshold Voltage Model for Short-Channel Undoped Symmetrical Double-Gate MOSFETs," *IEEE Transactions on Electron Devices*, vol. 55, no. 9, pp. 2512-2516, 2008.

[7] Kaushik Roy, Saibal Mukhopadhyay, and Hamid Mahmoodi-Meimand, "Leakage Current Mechanisms and Leakage Reduction Techniques in Deep-Submicrometer CMOS Circuits," *Proceedings of the IEEE*, vol. 91, no. 2, pp. 305-327, 2003.

[8] Thomas N. Theis and H.-S. Philip Wong, "The End of Moore's Law: A New Beginning for Information Technology," *Computing in Science and Engineering*, vol. 19, no. 2, pp. 41-50, 2017.

[9] Tianchang Shan, "Advantages of FINFETs over Traditional CMOS: Reasons and Implications," *Theoretical and Natural Science*, vol. 14, pp. 219-223, 2023.

[10] Digh Hisamoto, W. C. Lee, J. Kedzierski, et al., "FinFET—A Self-Aligned Double-Gate MOSFET Scalable to 20 nm," *IEEE Transactions on Electron Devices*, vol. 47, no. 12, pp. 2320-2325, 2000.

[11] International Roadmap Committee, "IRDS," *International Roadmap for Devices and Systems*, 2023.

[12] International Energy Agency, "Net Zero Roadmap: A Global Pathway to Keep the 1.5° C Goal in Reach," IEA Paris, 2023.

[13] International Energy Agency, "Electricity 2024 analysis and forecast to 2026," IEA Paris, 2024.

[14] Energy Institute Statistical Review of World Energy, "Statistical Review of World Energy, energy institute," 2024.

[15] N.H. Weste, D. Harris, " CMOS VLSI Design: A circuits and systems perspective," Pearson Education.

[16] Huang, Liu, Jeng, Ko, Hu, " A physical model for MOSFET output resistance," 1992 International Technical Digest on Electron Devices Meeting, San Francisco, CA, USA, 1992, pp. 569-572.

[17] M. T. Bohr, R. S. Chau, T. Ghani and K. Mistry, "The High-k Solution," *IEEE Spectrum*, vol. 44, no. 10, pp. 29-35, Oct. 2007.

[18] D. J. Frank, R. H. Dennard, E. Nowak, P. M. Solomon, Y. Taur, and Hon-Sum Philip Wong, "Device scaling limits of Si MOSFETs and their application dependencies," *Proceedings of the IEEE*, vol. 89, no. 3, pp. 259-288, March 2001.

[19] Craig S. Lent, Beth Isaksen, and Marya Lieberman, "Molecular Quantum-Dot Cellular Automata," *Journal of the American Chemical Society*, vol.125, no. 4, pp. 1056-1063, 2003.

[20] Y. Ardesi, A. Gaeta, G. Beretta, G. Piccinini, M. Graziano, "Ab initio Molecular Dynamics Simulations of Field-Coupled Nanocomputing Molecules," *Journal of Integrated Circuits and Systems*, vol. 16, pp. 1-8, 2021

[21] J. Timler, and C. S. Lent,"Power gain and dissipation in quantum-dot cellular automata," *Journal of Applied Physics*, vol. 91, pp. 823-831, 2002.

[22] M. Graziano, R. Wiung, M. Ruo Roch, Y. Ardesi, F. Riente, G. Piccinin,"Characterisation of a bis-ferrocene molecular QCA wire on a non-ideal gold surface," *Micro and Nano Letters*, vol. 14, pp. 22-27, 2019.

[23] F. Ravera, G. Beretta, Y. Ardesi, M. Graziano, G. Piccinini, ,"Addressing multi-molecule field-coupled nanocomputing for neural networks with SCERPA," *Journal of Computational Electronics*, vol. 23, pp. 1-10, 2024.

[24] C. Lent, D. Tougaw, et al.,"Quantum Cellular Automata," *Nanotechnology*, vol. 4, p. 49, 1999.

[25] M. Houshmand, S. H. Khayat, and R. Rezaei, "Genetic algorithm based logic optimization for multi-output majority gate-based nano-electronic circuits," *IEEE International Conference on Intelligent Computing and Intelligent Systems*, pp. 584-588, Shanghai, China, 2009.

[26] Y. Ardesi, "Investigation of Molecular FCN for Beyond-CMOS: Technology, design, and modeling for nanocomputing," Politecnico di Torino, 2022.

[27] J. von Neumann, "First draft of a report on the EDVAC," *IEEE Annals of the History of Computing*, vol. 15, no. 4, pp. 27-75, 1993.

[28] M. S. Asghar, S. Arslan, and H. Kim, "A Low-Power Spiking Neural Network Chip Based on a Compact LIF Neuron and Binary Exponential

Charge Injector Synapse Circuits," *Sensors (Basel)*, vol. 21, no. 13, p. 4462, Jun. 2021.

[29] G. Indiveri and S.-C. Liu, "Memory and Information Processing in Neuromorphic Systems," *Proceedings of the IEEE*, vol. 103, no. 8, pp. 1379-1397, Aug. 2015.

[30] S. R. Nandakumar, S. R. Kulkarni, A. V. Babu, and B. Rajendran, "Building Brain-Inspired Computing Systems: Examining the Role of Nanoscale Devices," *IEEE Nanotechnology Magazine*, vol. 12, no. 3, pp. 19–35, Sept. 2018.

[31] G. S. Stent, "A physiological mechanism for Hebb's postulate of learning," *Proc. Natl. Acad. Sci. U.S.A.*, vol. 70, no. 4, pp. 997–1001, Apr. 1973.

[32] T. H. Brown, E. W. Kairiss, and C. L. Keenan, "Hebbian synapses: biophysical mechanisms and algorithms," *Annu. Rev. Neuroscience*, vol. 13, pp. 475–511, 1990.

[33] M.-K. Kim, Y. Park, I.-J. Kim, and J.-S. Lee, "Emerging Materials for Neuromorphic Devices and Systems," *iScience*, vol. 23, no. 12, 2020.

[34] S. Sharma, S. Sharma, and A. Athaiya, "Activation Functions in Neural Networks," *Int. J. Eng. Appl. Sci. Technol.*, vol. 04, pp. 310–316, 2020.

[35] Y. Ito, "Representation of functions by superpositions of a step or sigmoid function and their applications to neural network theory," *Neural Networks*, vol. 4, no. 3, 1991.

[36] J. Schmidt-Hieber, "Nonparametric regression using deep neural networks with ReLU activation function," *Ann. Statist.*, vol. 48, no. 4, pp. 1875–1897, Aug. 2020.

[37] M. S. Asghar, S. Arslan, and H. Kim, "A Low-Power Spiking Neural Network Chip Based on a Compact LIF Neuron and Binary Exponential Charge Injector Synapse Circuits," *Sensors*, vol. 21, p. 4462, 2021.

[38] W. S. McCulloch and W. Pitts, "A logical calculus of the ideas immanent in nervous activity," *Bull. Math. Biophys.*, vol. 5, pp. 115–133, 1943.

[39] I. Yeo, M. Chu, and B.-G. Lee, "A Power and Area Efficient CMOS Stochastic Neuron for Neural Networks Employing Resistive Crossbar Array," *IEEE Trans. Biomed. Circuits Syst.*, vol. 13, no. 6, pp. 1678–1689, Dec. 2019.

[40] D. E. Nikonov and I. A. Young, "Benchmarking Physical Performance of Neural Inference Circuits," 2019.

[41] M. Tanavardi Nasab, A. Amirany, M. Moaiyeri, and K. Jafari, "Hybrid MTJ/CNTFET-based Binary Synapse and Neuron for Process-in-Memory Architecture," *IEEE Magnetics Lett.*, pp. 1–5, 2023.

[42] M. Sharad, C. Augustine, G. Panagopoulos, and K. Roy, "Spin-Based Neuron Model With Domain-Wall Magnets as Synapse," *IEEE Trans. Nanotechnol.*, vol. 11, no. 4, pp. 843–853, Jul. 2012.

[43] G. Beretta, Y. Ardesi, M. Graziano, and G. Piccinini, "Multi-Molecule Field-Coupled Nanocomputing for the Implementation of a Neuron," *IEEE Trans. Nanotechnol.*, pp. 1–1, 2022.

[44] C. Lent and D. Tougaw, “Lines of interacting quantum-dot cells: A binary wire,” *J. Appl. Phys.*, vol. 74, pp. 6227–6233, 1993.

[45] F. Ravera, Y. Ardesi, G. Piccinini and M. Graziano, “Technology-Aware Simulation for Prototyping Molecular Field-Coupled Nanocomputing,” *IEEE Transactions on Nanotechnology*, vol. 23, pp. 521-528, 2024.

[46] H. Huang, Y. Wang, K. -H. Chen and X. -X. Fei, “Leakage Current Behavior in HfO2/SiO2/Al2O3 Stacked Dielectric on 4H-SiC Substrate,” *IEEE Journal of the Electron Devices Society*, vol. 11, pp. 438-443, 2023.

[47] C. E. Glaser, A. T. Binder, L. Yates, A. A. Allerman, D. F. Feezell and R. J. Kaplar, “Analysis of ALD Dielectric Leakage in Bulk GaN MOS Devices,” *2021 IEEE 8th Workshop on Wide Bandgap Power Devices and Applications (WiPDA)*, Redondo Beach, CA, USA, pp. 268-272, 2021.

[48] Milad Tanavardi Nasab; Arefe Amirany; Mohammad Hossein Moaiyeri; Kian Jafari

[49] M. T. Nasab, A. Amirany, M. H. Moaiyeri and K. Jafari, "Hybrid MTJ/CNTFET-Based Binary Synapse and Neuron for Process-in-Memory Architecture," in IEEE Magnetics Letters, vol. 14, pp. 1-5, 2023

[50] K. Yogendra, D. Fan and K. Roy, "Coupled Spin Torque Nano Oscillators for Low Power Neural Computation," in IEEE Transactions on Magnetics, vol. 51, no. 10, pp. 1-9, Oct. 2015, Art no. 4003909

[51] M. Sharad, C. Augustine, G. Panagopoulos and K. Roy, "Spin-Based Neuron Model With Domain-Wall Magnets as Synapse," in IEEE Transactions on Nanotechnology, vol. 11, no. 4, pp. 843-853, July 2012

[52] D. Fan, Y. Shim, A. Raghunathan and K. Roy, "STT-SNN: A Spin-Transfer-Torque Based Soft-Limiting Non-Linear Neuron for Low-Power Artificial Neural Networks," in IEEE Transactions on Nanotechnology, vol. 14, no. 6, pp. 1013-1023, Nov. 2015

[53] Mrigank Sharad; Deliang Fan; Kaushik Roy, "Spin-neurons: A possible path to energy-efficient neuromorphic computers"

[54] Abhronil Sengupta; Sri Harsha Choday; Yusung Kim; Kaushik Roy, "Spin orbit torque based electronic neuron"

[55] I. M. Sheriff and R. Sakthivel, "The Artificial Neuron: Built From Nanosheet Transistors to Achieve Ultra Low Power Consumption," in IEEE Access, vol. 12, pp. 11653-11663, 2024

[56] J. M. Cruz-Albrecht, M. W. Yung and N. Srinivasa, "Energy-Efficient Neuron, Synapse and STDP Integrated Circuits," in IEEE Transactions on Biomedical Circuits and Systems, vol. 6, no. 3, pp. 246-256, June 2012

[57] S. Simmich, M. Yilmaz, R. Ashkrizzadeh, A. Petraru and R. Rieger, "A Piezoelectric Biologically Plausible Spiking Neuron," 2023 IEEE International Symposium on Circuits and Systems (ISCAS), Monterey, CA, USA, 2023, pp. 1-5,

[58] Z. Pajouhi, "Energy efficient neuromorphic processing using spintronic memristive device with dedicated synaptic and neuron terminology," 2018 19th International Symposium on Quality Electronic Design (ISQED),

Santa Clara, CA, USA, 2018, pp. 61-68

[59] V. Ostwal, R. Meshram, B. Rajendran and U. Ganguly, "An ultra-compact and low power neuron based on SOI platform," 2015 International Symposium on VLSI Technology, Systems and Applications, Hsinchu, Taiwan, 2015, pp. 1-2

[60] M. K. Q. Jooq, M. R. Azghadi, F. Behbahani, A. Al-Shidaifat and H. Song, "High-Performance and Energy-Efficient Leaky Integrate-and-Fire Neuron and Spike Timing-Dependent Plasticity Circuits in 7nm FinFET Technology," in IEEE Access, vol. 11, pp. 133451-133459, 2023.